**Contract No:**

This document was prepared in conjunction with work accomplished under Contract No. DE-AC09-08SR22470 with the U.S. Department of Energy (DOE) Office of Environmental Management (EM).

**Disclaimer:**

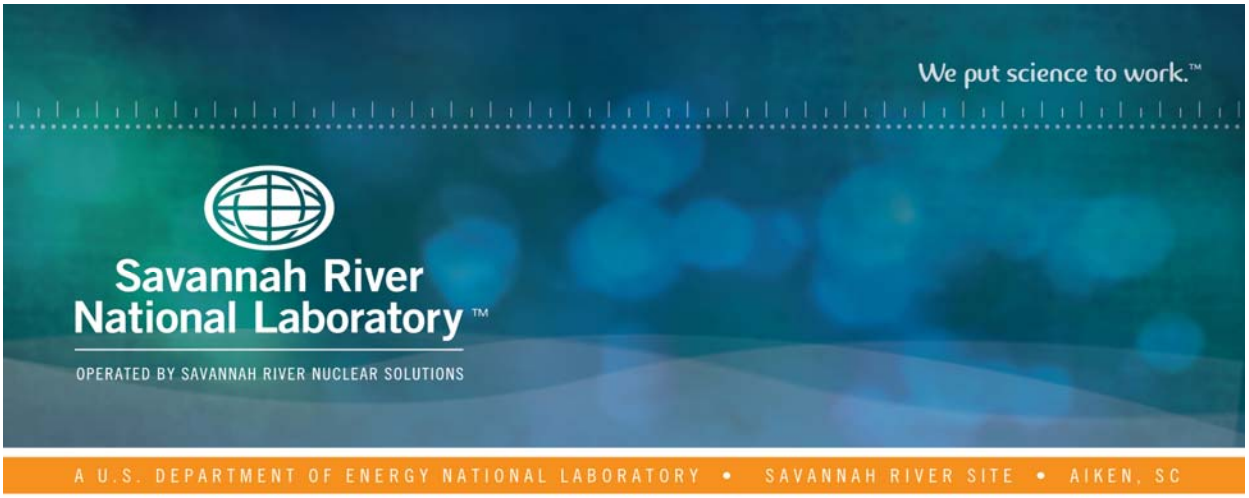


# Investigation of Thermolytic Hydrogen Generation Rate of Tank Farm Simulated and Actual Waste

C.J. Martino
J.D. Newell
W.H. Woodham
J.M. Pareizs
T.B. Edwards
D.P. Lambert
A.M. Howe

February 2019
SRNL-STI-2017-00611, Revision 1

**DISCLAIMER**



**Printed in the United States of America**

**Prepared for**
**U.S. Department of Energy**

SRNL-STI-2017-00611
Revision 1

**Keywords:** *DWPF, Tank Farm, Hydrogen*

**Retention:** *Permanent*

# Investigation of Thermolytic Hydrogen Generation Rate of Tank Farm Simulated and Actual Waste

C.J. Martino
J.D. Newell
W.H. Woodham
J.M. Pareizs
T.B. Edwards
D.P. Lambert
A.M. Howe

February 2019

Prepared for the U.S. Department of Energy under contract number DE-AC09-08SR22470.

Savannah River National Laboratory™
OPERATED BY SAVANNAH RIVER NUCLEAR SOLUTIONS

# REVIEWS AND APPROVALS

AUTHORS:

_____
C.J. Martino, Process Technology Programs Date

_____
J.D. Newell, Process Technology Programs Date

_____
W.H. Woodham, Process Technology Programs Date

_____
J.M. Pareizs, Process Technology Programs Date

_____
T.B. Edwards, Immobilization Technology Date

_____
D.P. Lambert, Process Technology Programs Date

_____
A.M. Howe, Process Technology Programs Date

TECHNICAL REVIEW:

_____
E.K. Hansen, Wasteform Processing Technologies, Reviewed per E7 2.60 Date

_____
M.E. Stone, Wasteform Processing Technologies Date

APPROVAL:

_____

F.M. Pennebaker, Chemical Processing Technologies Date

_____

S. D. Fink, Manager Date
Chemical Processing Technologies

_____

J.E. Occhipinti, Manager Date
Waste Removal & Tank Closure
Tank Farm Facility Engineering

# EXECUTIVE SUMMARY

To support resolution of Potential Inadequacies in the Safety Analysis for the Savannah River Site (SRS) Tank Farm, Savannah River National Laboratory conducted research to determine the thermolytic hydrogen generation rate (HGR) with simulated and actual waste. Gas chromatography methods were developed and used with air-purged flow systems to quantify hydrogen generation from heated simulated and actual waste at rates applicable to the Tank Farm Documented Safety Analysis (DSA). Initial simulant tests with a simple salt solution plus sodium glycolate demonstrated the behavior of the test apparatus by replicating known HGR kinetics. Additional simulant tests with the simple salt solution excluding organics apart from contaminants provided measurement of the detection and quantification limits for the apparatus with respect to hydrogen generation. Testing included a measurement of HGR on actual SRS tank waste from Tank 38. A final series of measurements examined HGR for a simulant with the most common SRS Tank Farm organics at temperatures up to 140 °C. The following conclusions result from this testing.

HGR was measured for an actual-waste Tank 38 sample. The HGR measurements at 80, 90, 100, and 110 °C were $1.7\times10^{-7}$, $4.7\times10^{-7}$, $5.9\times10^{-7}$, and $2.6\times10^{-6}$ $ft^3\ hr^{-1}\ gal^{-1}$, respectively. The Limit of Detection and Limit of Quantification for the HGR measurements were $2.6\times10^{-8}$ $ft^3\ hr^{-1}\ gal^{-1}$ and $5.1\times10^{-8}$ $ft^3\ hr^{-1}\ gal^{-1}$, respectively.

HGR was measured in a high boiling point (HBP) simulant with major known SRS Tank Farm organic compounds. Testing used fresh organics and did not simulate the long-term exposure of these organics already experienced in the waste. Hence, testing is expected to provide high bias to the hydrogen generation rates. The final HGR measurements at 75, 100, and 140 °C were $6.2\times10^{-7}$, $3.0\times10^{-6}$, and $8.1\times10^{-5}$ $ft^3\ hr^{-1}\ gal^{-1}$, respectively. Decreases in the HGR were noted at isothermal conditions with steady gas tracer concentration, which clouds development of a temperature dependent correlation for generation rate. While the simulant contains high concentrations of major SRS organics tested at high temperatures found in the 3H Evaporator, this limited data set may not fully bound values under all possible operating conditions.

The HGR measurement apparatus was successfully employed to replicate hydrogen production rate experiments. Simulant without deliberately added organic carbon was found to contain approximately 200 mg/L of organic carbon from tramp organics in the reagents used to prepare the solution. The tests using such simulant generated hydrogen at rates consistent with, but somewhat lower than, those predicted at equivalent carbon and aluminum loadings by methods used at the Hanford Site. Prior to identifying the organic contaminants, potential sources of hydrogen in simulants without deliberately added organic carbon were examined. Testing determined that this hydrogen is not due to caustic reaction of organic materials of construction within the reaction vessel, electrolysis due to current leak, anode/cathode reactions, corrosion, or the method of heating employed in the experiment.

During the HBP and Tank 38 testing, a peak was identified at a retention time greater than the retention time of the inert tracer of krypton. This peak has been identified as methane, and the data have been reexamined to obtain methane concentrations. For the HBP testing, methane concentration was constant at the highest temperature studied (140 °C) and higher than hydrogen. At the lower temperatures (100 and 75 °C), methane and hydrogen tracked closely, with methane concentration generally lower than hydrogen. For Tank 38, methane concentration was approximately 1/3 of the hydrogen concentration during testing (100 and 110 °C). At lower temperatures for Tank 38 testing (90, 80, and 27 °C), methane fell below the quantification range.

The following recommendations result from this testing.

- Proceed with the planned HGR measurements using a sealed system. The sealed system is designed to measure the low HGR expected for a Tank 50 actual waste sample. The sealed system vessels are constructed of stainless steel in contrast to the glass vessel used in the flow system testing reported here.

- Consider HGR measurements for actual-waste samples of tanks representing other portions of the SRS Tank Farm system. A single test with Tank 38 material may not provide adequate information for the entirety of the liquid waste system. Special consideration should be given to tanks that have a history of high organic content. The need for thermolytic HGR for Tank Farm operations such as aluminum dissolution and oxalic acid cleaning should also be assessed. A test with a sample from the 3H Evaporator system may be appropriate due to the hydrogen and measured in the HBP test.

- If the rates from the HBP and Tank 38 testing prove restrictive when applied to DSA development, additional simulant test to decipher the contributions from individual organic sources in tank waste may be warranted. In such testing, a control test should be performed to establish a baseline HGR without the addition of organics. Use of irradiated organic bearing solutions may be more appropriate to represent the current waste conditions. Additional instrumentation may be warranted on simulant testing if identification and quantification of volatile organic carbon species is to be tested.

- Additional simulant testing should be performed to evaluate the effect of anion concentrations on organic thermolytic HGR, particularly in concentrations ranges relevant to SRS waste.

- Additional measurements should be made with the flow system to examine potential contribution of glass dissolution and aluminosilicate precipitation toward hydrogen generation. Comparison should be made between testing of identical solutions in the glass and stainless steel vessels, preferably at sub-boiling temperature.

- Future testing should include quantification of methane, including establishment of limits of quantification.

# TABLE OF CONTENTS

# LIST OF TABLES

# LIST OF FIGURES

# LIST OF ABBREVIATIONS

| | |
|---|---|
| AA | Atomic Absorption |
| AD | Analytical Development |
| CPC | Chemical Processing Cell |
| CSTR | Continuous Stirred Tank Reactor |
| CVAA | Cold Vapor Atomic Absorption |
| DAC | Data Acquisition and Control |
| DSA | Documented Safety Analysis |
| DWPF | Defense Waste Processing Facility |
| EDTA | ethylenediamenetetraacetic acid |
| FTIR | Fourier Transform Infrared |
| GC | Gas Chromatograph |
| HBP | High Boiling Point |
| HEDTA | N-(2-hydroxy)ethylenediaminetriacetate |
| HGR | Hydrogen Generation Rate |
| HLW | High Level Waste |
| IC | Ion Chromatography |
| ICP-AES | Inductively Coupled Plasma – Atomic Emission Spectroscopy |
| ICP-MS | Inductively Coupled Plasma – Mass Spectroscopy |
| LOD | Limit of Detection |
| LOQ | Limit of Quantification |
| OB | Other Base (excluding carbonate) |
| PID | proportional-integral-derivative |
| PISA | Potential Inadequacy in the Safety Analysis |
| ppmv | parts per million volume |
| PSAL | Process Science and Analytical Laboratory |
| RF | Response factor |
| RSD | Relative Standard Deviation |
| sccm | standard cubic centimeters per minute |
| SEM | Scanning Electron Microscopy |
| SRAT | Sludge Receipt Adjustment Tank |
| SRNL | Savannah River National Laboratory |
| SRR | Savannah River Remediation |
| SRS | Savannah River Site |
| SVOA | Semivolatile Organic Analysis |
| TB | Total Base |
| TC | Total Carbon |
| TIC | Total Inorganic Carbon |
| TOC | Total Organic Carbon |
| TTQAP | Task Technical and Quality Assurance Plan |
| TTR | Technical Task Request |
| VOA | Volatile Organic Analysis |
| VOC | Volatile Organic Compound |
| WTP | Hanford Waste Treatment and Immobilization Plant |
| XEDS | X-ray Energy Dispersive Spectroscopy |
| XRD | X-ray Diffraction |

## 1.0 Introduction

In February 2017, Savannah River Remediation (SRR) declared a Potential Inadequacy in the Safety Analysis (PISA) in each of three Savannah River Site (SRS) Liquid Waste facilities: Tank Farm,[1] Saltstone,[2] and the Defense Waste Processing Facility (DWPF).[3] The PISAs related to how formate and other organics can impact the radiolytic and thermolytic production of hydrogen, which is a flammable gas. Resolution of the PISAs requires research to evaluate the impact of organics including formate on the generation of hydrogen in SRS High-Level Waste (HLW) tanks, processing tanks, and evaporator systems.

This work is governed by a Technical Task Request (TTR)[4] and a Task Technical and Quality Assurance Plan (TTQAP).[5] The work contained in this report partially fulfills Tasks 3 and 4 in the TTR, which are related to testing in support of the SRS HLW Tank Farm. Radioactive sample material from SRS Tank 38 was used for some of the testing, allowing for a measurement of thermolytic Hydrogen Generation Rate (HGR) with the mixture of organics present in the actual waste. The work also included two phases of simulant testing, one to determine the behavior of the equipment prior to HGR measurement in the actual waste material and the other to investigate high temperatures applicable to the SRS Tank Farm evaporator systems.

Three separate run plans were issued for the three separate portions of the work. Initiating prior to the start of actual waste testing and high boiling point (HBP) testing, simulant tests with a simple salt solution (plus sodium glycolate) examined the behavior of the test apparatus by replicating known HGR kinetics.[6] This first group of tests also examined the behavior of the apparatus with respect to hydrogen generation without sodium glycolate. Next, testing included a measurement of HGR on actual SRS tank waste from Tank 38.[7] The third series of measurements examined HGR for a HBP simulant with common SRS Tank Farm organics at temperatures up to 140 °C.[8]

Thermolytic production of gases in radioactive waste media was reported by Delegard in 1980.[9] Using standard laboratory glassware, commercially available reagent-grade NaOH, $NaNO_3$, $NaNO_2$, $Na_2CO_3$, and technical grade $NaAlO_2$, Delegard was able to demonstrate the production of $H_2$, $N_2$, and $N_2O$ gases as products from the thermolysis of N-(2-hydroxy)ethylenediaminetriacetate (HEDTA). It was shown that the production of gases was dependent on the presence of nitrite/nitrate salts and the concentrations of aluminum and hydroxide in solution.

In 1994, Ashby[10] reported the thermolysis of glycolate and HEDTA in simple salt simulants similar to those employed by Delegard. Using Teflon-coated glassware and offgas sampling capabilities, Ashby was able to measure the decomposition rates of glycolate in alkaline media as well as track the production rates of $H_2$, $N_2$, and $N_2O$ gases. Ashby also reported the rates of production of formate and oxalate, both of which are products from glycolate decomposition. Ashby posited the existence of a multi-reaction mechanism for glycolate decomposition and subsequent $H_2$ formation that depended on the presence of nitrite, aluminum, and hydroxide.

Thermolytic production of hydrogen from organic compounds was also described by Hu in 2004.[11] In work designed to support flammability calculations at the Hanford Waste Treatment and Immobilization Plant (WTP), Hu developed an empirical model describing the thermolytic production of $H_2$ from organic molecules as a function of temperature, organic carbon content, and aluminum content. This model is given in Equation 1 below:

$$HGR_{thm} = a_{thm} \cdot r_f \cdot [TOC] \cdot [Al]^{0.4} \cdot L_f \cdot e^{-E_{thm}/RT} \qquad \text{Equation 1}$$

where,

$HGR_{thm}$ = thermolytic hydrogen generation rate, mo1e $kg^{-1}$ $day^{-1}$
$a_{thm}$ = pre-exponential factor, $3.94\times10^{9}$ mo1 $kg^{-1}$ $day^{-1}$
$r_f$ = reactivity coefficient
$[TOC]$ = concentration of total organic carbon in the liquid, wt%
$[Al]$ = concentration of aluminum, wt%
$L_f$ = mass fraction of waste present as liquid
$E_{thm}$ = thermolytic activation energy, 89,600 J $mole^{-1}$
$R$ = gas constant, 8.314 J $mole^{-1}$ $K^{-1}$
$T$ = temperature, K

Both the activation energy and the pre-exponential factor are values regressed from hydrogen generation measurements specific to Hanford actual waste samples at temperatures between 60 and 120 °C. Thus, the values are representative of the specific blend of organics present in that waste. The reactivity factor was used to improve the fit of the data, with recommended values varying between 0.15 and 1. Data generated in this report is compared to the most conservative recommendation, using Equation 1 and a value of reactivity factor of $r_f$ = 1. This treatment is consistent with methodologies applied at the SRS Defense Waste Processing Facility (DWPF) and Saltstone.[12-13] Note that the use of a reactivity factor equal to 1 is more conservative than the values recommended by Hu for Hanford waste tanks (0.3 or 0.6).

The advantage of the empirical model developed by Hu is that exact knowledge of the concentrations for each organic species present is not needed. Rather, a composite measurement (i.e., Total Organic Carbon, TOC) is employed such that hydrogen generation from organic thermolysis can be predicted within a factor of 3 for Hanford organics without the need for extensive sampling and characterization campaigns. This approach is especially useful in the context of evaluating SRS wastes, where hundreds of organics are known to exist in trace amounts.[14]

In 2017, Crawford and King used observations and data generated by Ashby to develop a rate expression for hydrogen generation due to glycolate thermolysis.[15] This rate equation was generated by assuming that the rate of destruction of glycolate is the maximum $H_2$ production rate (i.e., one mole of glycolate can make one mole of hydrogen). Using this assumption, Ashby's kinetic data for glycolate degradation, and an observed hydrogen generation activation energy (113,000 J/mol), a rate expression derived from the Crawford and King model can be developed, given in Equation 2 below:

$$HGR_{thm}^{gly} = k\frac{[Al]\left[NO_2^-\right][gly]}{\left[OH^-\right]}e^{\frac{-E_A}{R}\left(\frac{1}{T}-\frac{1}{393.15}\right)} \qquad \text{Equation 2}$$

where,

$HGR_{thm}^{gly}$ = rate of hydrogen production by glycolate thermolysis, moles $L^{-1}$ $hr^{-1}$
$k$ = rate constant for glycolate degradation at 120 °C, L $mole^{-1}$ $hr^{-1}$
$[Al]$ = aluminum concentration, M
$\left[NO_2^-\right]$ = nitrite concentration, M
$[gly]$ = glycolate concentration, M
$\left[OH^-\right]$ = hydroxide concentration, M

$E_A$ = activation energy for hydrogen generation, 113,000 J mole$^{-1}$
$R$ = gas constant, 8.314 J mole$^{-1}$ K$^{-1}$
$T$ = temperature, K

The analyses and kinetic studies performed by Ashby comprise a matrix of tests to validate and benchmark simulant experimental data generated at SRNL.

There are significant differences between the solution compositions used by Hu and the waste at SRS. Similar differences exist between the experiments performed by Ashby and the waste at SRS. Among these deviations, aluminum concentration differences may have the greatest influence on application of the equations given the relationship described by both Hu and Ashby between HGR and soluble aluminum concentration. Furthermore, the prior studies for Hanford did not consider temperatures as high as those experienced in the SRS evaporators. Therefore, in addition to benchmarking tests based on Ashby's work, additional experiments used a HBP simulant with organics representative of SRS waste, as well as testing with radioactive material from SRS tank waste.

## 2.0 Experimental Procedure

2.1 Simulant Preparation

*2.1.1 Simulant Preparation Setup*

All simulants used in this study were prepared by dissolving predetermined amounts of sodium salts into heated ASTM D1193-Type I deionized water. A 4-L glass or stainless-steel beaker was placed onto a heating stir plate equipped with a thermocouple and temperature control capability. A magnetic stir bar provided agitation while adding simulant components. Deionized water was generated using an Aries deionizing station equipped with a dual bed for organics removal (VP-17-4210) and a mixed bed for high purity (VP-17-4010). Reagent grade 50 wt% sodium hydroxide solution, sodium nitrate (>99%), sodium nitrite (99.9%), and sodium carbonate (>99.9%) were purchased from Fisher Chemicals and used as received. Technical grade sodium aluminate trihydrate was purchased from Spectrum Chemical Manufacturing Corporation and used as received.

While the compounds used and sequence of addition varied between each simulant type, sodium hydroxide was regularly added before sodium aluminate. This approach enhanced aluminum solubility and helped to mitigate the formation of insoluble aluminum hydroxide solids. The addition of sodium hydroxide evolved a significant amount of heat, as expected. Once this exothermic release of energy subsided, simulants were heated to 60 °C during preparation to facilitate complete dissolution. Despite this measure, a small amount of white solids was typically observed at the end of the simulant preparation step.

*2.1.2 Simple Salt Solution Simulant*

To benchmark the designed HGR measurement technique and demonstrate the adequacy of the equipment used, a salt solution simulant was prepared based on the SY1-SIM-91B simulant used by Ashby. Since SY1-SIM-91B included the use of organic compounds, a modified recipe was selected. The modified recipe of this simulant, designated SY1-SIM-91B-NG, follows (in order of addition).

- 0.42 M sodium carbonate
- 2.00 M sodium hydroxide
- 1.54 M sodium aluminate
- 2.24 M sodium nitrite
- 2.59 M sodium nitrate

Preparation of SY1-SIM-91B-NG departed from the method employed by Ashby to prepare SY1-SIM-91B in that components of SY1-SIM-91B-NG were added to a heated beaker of DI water and diluting to volume, whereas SY1-SIM-91B was prepared by dissolving each component in a glass volumetric flask, diluting to volume, and filtering.

*2.1.3 High-Boiling Point Simulant*

HBP simulant testing was designed to incorporate multiple chemical components found in SRS waste (e.g., soluble salts, noble metals, mercury, and organic species). The HBP simulant was prepared by first generating 3.6 L of a base salt solution simulant based on concentrations of hydroxide, aluminate, nitrite, and nitrate measured in Sample 200638582 on September 11th, 2013 from Tank 42 (given below in order of addition).[16]

- 5.48 M sodium hydroxide
- 0.52 M sodium aluminate
- 2.14 M sodium nitrite
- 2.12 M sodium nitrate

1.2 L of this solution was charged to the HGR measurement apparatus. A solution of trim metal nitrates was added such that the final metal concentrations in the kettle were:

- 450 mg/L mercury (added as mercuric nitrate),
- 1 mg/L ruthenium (added as ruthenium nitrosyl nitrate),
- 0.2 mg/L rhodium (added as rhodium nitrate),
- 0.2 mg/L palladium (added as palladium nitrate monohydrate), and
- 0.4 mg/L silver (added as silver nitrate).

After trim addition, the simulant was heated to boiling and continuously evaporated by boiling off excess water while adding approximately 0.7 additional liters of fresh base simulant. The feed rate of base simulant was monitored to maintain the liquid volume of solution in the kettle. While heating the solution, the following organic species were added to the specified concentrations:

- 3000 mg/L formate (added as sodium formate, near maximum concentration in SRS waste),
- 88 mg/L oxalate (added as sodium oxalate, near solubility limit at Tank Farm conditions),
- 1000 mg/L ion exchange resin (added as IONAC A641),
- 1000 mg/L antifoam (added as Antifoam 747),
- 1000 mg/L tributyl phosphate (near maximum concentration in SRS waste), and
- 78 mg/L MCU solvent (Waste Acceptance Criteria limit).

The collection of organic species were chosen on the basis of identification as the largest organic contributions to SRS liquid waste processing.[17] Concentrations of these organic species were decided by discussion between SRR and SRNL personnel. One quarter of the antifoam and all other organic compounds were added before the initial boiling was achieved. The remaining three quarters of the antifoam were added as three separate additions when boiling was achieved. Continuous evaporation was performed by dewatering in the HGR measurement apparatus and adding fresh base simulant until a boiling point of 140.5 °C was achieved (removing approximately 0.9 L of water via evaporation). This solution was cooled to 100 °C, sampled, heated to 140.1 °C, and used in HBP testing.

Note that in some cases during high boiling-point testing, an increased purge rate of air was used to prevent accumulation of hydrogen to levels higher than 25% of the Lower Flammability Limit (LFL). In these cases, it is assumed that the hydrogen present in air (nominally 0.5 ppm)[18] has a negligible effect on the measured concentrations of hydrogen. This is expected because the relatively high generation rate of hydrogen necessary to warrant additional purge gas is significantly higher than the addition rate of hydrogen added as air.

## 2.2 Flow System Set-up

### *2.2.1 Simulant Rig – with Heating Rods*

HGR simulant tests were performed in an approximately 1.2 L borosilicate glass vessel with an additional approximately 0.6 L of headspace, for a total system volume of approximately 1.8 L. Heating was provided using two 0.375-inch diameter Inconel Alloy 800 heating rods powered by an automated direct current power supply (TDK-Lambda Genesys, GEN150-10). Use of a borosilicate glass vessel flow through system with minimal headspace is consistent with the HGR measurement apparatus recommended and developed for qualification of actual-waste feeds for the Hanford WTP.[19-20] The WTP system, however, used a water-blanketed vessel for heating rather than heating rods and has a smaller capacity (nominally 100 mL).

Mixing was controlled using a mixer system consisting of a Servodyne mixing head coupled to an agitator shaft via a Parr high torque magnetic drive. A one inch diameter, 4-blade, 45° pitched turbine stainless steel impeller was welded to the stainless-steel agitator shaft. Purge gas was controlled using a MKS Model 647 Multi Gas Controller.

An offgas condenser allowed the condensate to reflux back to the HGR vessel or be collected in a sample bottle for concentration of the slurry. Offgas exiting the condenser was sampled by a dedicated Agilent/Inficon 3000A dual column micro gas chromatograph (GC), as described in Section 2.3.2.

A schematic depicting the equipment used during testing is presented in Figure 2-1. Figure 2-2 shows the heavily insulated system used during 140 °C measurements. The rig with heating rods originally had a drain valve at the bottom of the vessel, but this feature was removed in later testing.

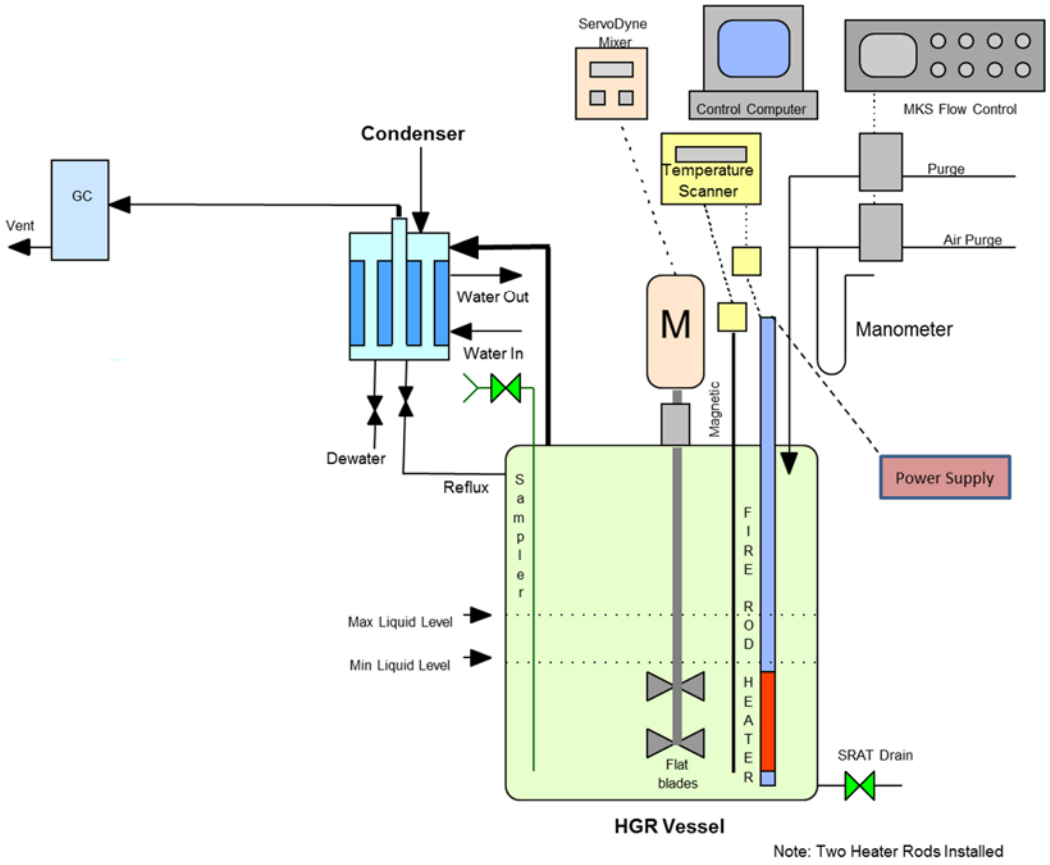


**Figure 2-1. HGR Process Equipment**


**Figure 2-2. Insulated HGR Process Equipment (without drain) Used for HBP Simulant Test**

*2.2.2 Simulant Rig – with Heating Mantle*

Initial HGR results from simulant testing without added glycolate resulted in the unexpected generation of hydrogen gas. To evaluate the possibility that hydrogen gas was produced as a result of galvanic corrosion of the Inconel heating rods, stainless steel agitator shaft, or Inconel thermocouple, the heating rods were removed and heat was provided by an external heating mantle (Glas-Col® TM614) controlled using a variable autotransformer. The thermocouple was inserted inside a borosilicate glass thermowell. This system is shown in Figure 2-3. An additional test was performed without agitation after removal of the agitator shaft from the system and using an external heating mantle.

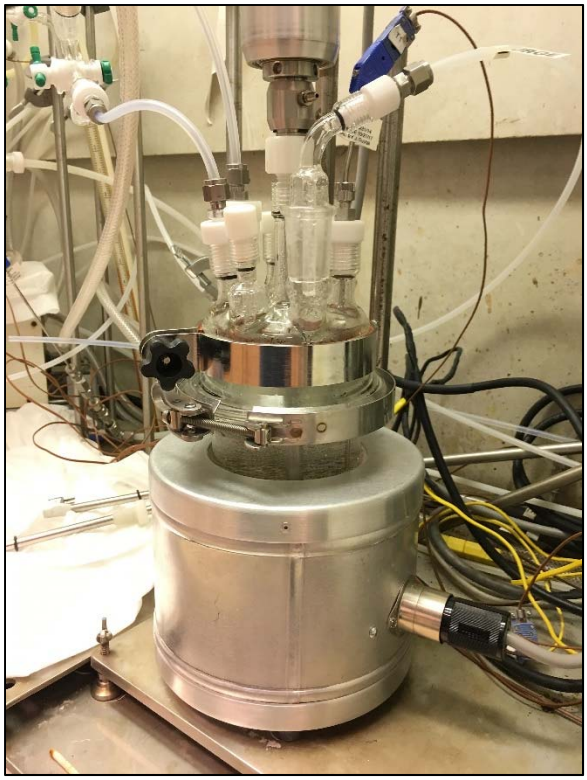

**Figure 2-3. HGR Measurement Apparatus with a Heating Mantle**

*2.2.3 Shielded Cells Rig*

Design elements from equipment used for 1-L and 4-L sludge batch qualification Chemical Process Cell (CPC) testing were combined to create the HGR measurement apparatus for actual waste tests [21-22]. A 1.2 L insulated glass vessel was mounted to the stand used for 4-L testing (Figure 2-4). Aside from manometer design, agitator motor, and the use of specially designed stand, the equipment used in simulant and actual waste tests was the same.

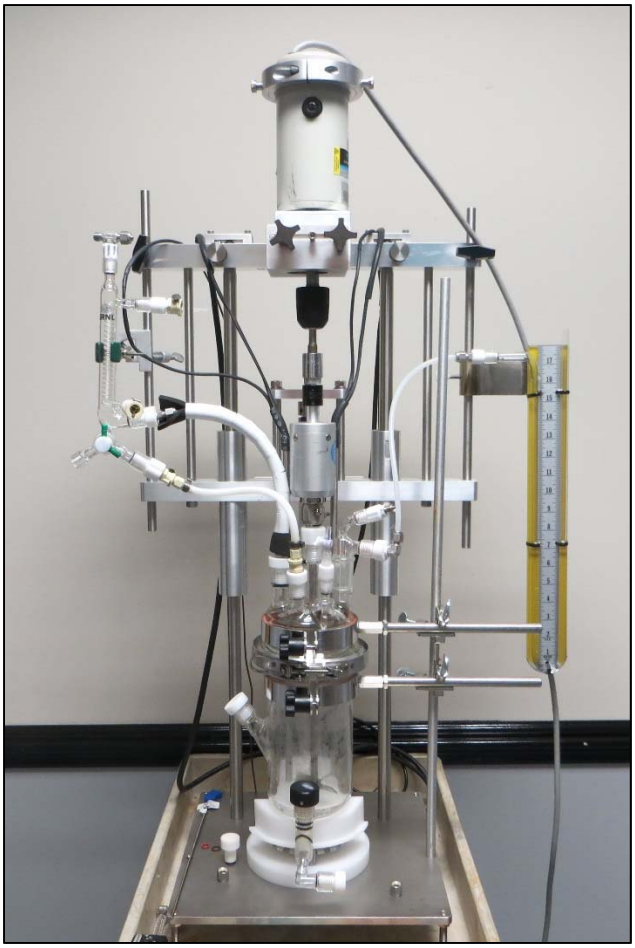

**Figure 2-4: Shielded Cells Process Equipment[a]**

*2.2.4 Data Acquisition Software Description*

A Data Acquisition and Control (DAC) application was programmed using National Instruments LabVIEW software. The software that controlled the process parameters for both the simulant and actual waste tests was developed by adapting the DAC recently used in Sludge Batch 9 qualification. The DAC logged process data and controlled mixing speed, purge gas flow rate, and heating rod temperature.

## 2.3 Data Collection

*2.3.1 HGR Measurement Process*

Vessel designs were chosen to minimize the headspace volume and decrease the time required for each test. The volume of the reactor pot was decreased to 1.2 L, and a condenser with a smaller internal volume was used. Given the final vessel headspace and offgas equipment volume of about 600 mL and the low purge rates necessary to achieve sufficiently-low limits of detection for hydrogen (i.e., 3 standard cubic centimeters per minute, or sccm), it was predicted that sub-boiling experiments would require at least 10 hours (or three volume turnovers) before achieving steady-state conditions.

[a] The glass vessel seen in Figure 2-4 was fabricated with a side wall port. This design was used only for water testing, while the vessel used for actual waste testing was being fabricated. The final design did not include the side wall port. The vessel insulation was removed for photographing.

Assuming a GC detection limit of 2 volumetric parts per million (ppmv) of hydrogen, a sample volume of 1.2 L, and a purge rate of 3 sccm, the method detection limit for the flow system would be expected to be approximately 4 x $10^{-8}$ $ft^3$ $hr^{-1}$ $gal^{-1}$.

For DWPF simulations, SRNL has used 0.5% helium[21] in the purge gas as an inert tracer during processing to evaluate system performance (e.g., in-leakage of air and response time of the system) and total gas generation. However, helium interferes with GC quantification of hydrogen at ppmv levels. Therefore, krypton, which is assumed to be inert in the process and doesn't interfere with the hydrogen signal, was substituted for helium as the tracer.

A proportional-integral-derivative (PID) control algorithm governs the amount of power supplied to the heating rods by comparing the bulk process temperature to the process temperature setpoint. To prevent the rods from overheating, a control limit is defined ("rod dT limit") that prevents the heating rods from exceeding the bulk temperature by the specified amount. Given that HGR is expected to be temperature dependent, efforts were made to eliminate localized hot regions in the process vessel by minimizing the differential temperature between the heating rods and the process temperature and by insulating the process vessel. Rod dT limits for these tests were constrained to 20 ºC while at boiling except where noted.

HGR measurement is reported in the unit $ft^3$ $hr^{-1}$ $gal^{-1}$ to match the units used by the SRS Tank Farm, DWPF, and Saltstone facilities. The gas volume basis ($ft^3$) for data in this report is at standard conditions of 1 atm and 21.1 °C (70 °F). The liquid volume basis ($gal^{-1}$) for Tank 38 and SY1-SIM-91B-NG simulant data is evaluated at ambient temperature (approximately 22 °C). Conversely, the liquid volume basis for the HBP simulant data is evaluated at 140 °C.

### *2.3.2 Gas Handling and Analysis*

Offgas from the flow through tests was characterized using Agilent/Inficon[b] series 3000 micro GCs. Column-A collected data related to He, $H_2$, $O_2$, $N_2$, and Kr, while column-B collected data related to $CO_2$, and $N_2O$. Due to low GC sensitivity, other oxides of nitrogen and carbon were not analyzed. The GC methods were modified to quantify low quantities of hydrogen. The instruments have previously used to quantify offgas from DWPF CPC demonstrations which generally have significantly higher gas generation rates. To quantify the expected low concentrations of hydrogen, sample injection times were increased relative to DWPF simulations. For the Tank 38 sample, injection time was increased from 50 ms to 150 ms. For the non-radioactive tests, injection time was increased from 50 ms to 100 ms. The difference in the inject times for the two tests is because each GC is a little different, and settings for one GC may be different to attain similar results. To improve sensitivity, the GC sensitivity mode was changed from normal to high. Because of these changes, the ability to accurately quantify oxygen and nitrogen has been sacrificed, though even with previous settings, nitrogen results were not very repeatable or useful. Raw chromatographic data were acquired by the GC from the offgas stream samples using a separate computer interfaced to the data acquisition computer. Sampling frequency was approximately one chromatogram every four minutes.

In DWPF CPC demonstrations, additional gasses can be detected via Fourier Transform Infrared (FTIR) spectroscopy and mass spectroscopy. However, these techniques cannot be used with the low flow rates necessary to quantify low hydrogen concentrations.

For all tests, the GCs were calibrated with a gas mixture containing nominally 50 ppmv hydrogen, 20 vol% oxygen, 0.5 vol% krypton, 1 vol% carbon dioxide, 0.5 vol% nitrous oxide, and the balance nitrogen. It is assumed that the GC response (peak area) is linear and proportional to gas concentration. This assumption was checked for hydrogen with several other hydrogen-bearing gas standards – 2.68 ppmv, 10.6 ppmv, 52

[b] Inficon purchased Agilent's micro GC business unit. While the GCs used in the simulant runs was an Inficon GC and the Tank 38 demonstration utilized an Agilent GC, the instruments are essentially the same.

ppmv, and 10,000 ppmv. A chart showing linearity from 2.68 to 52 ppmv is given in Figure 2-5. Samples of the 10,000 ppmv gas yielded results of approximately 10,500 ppmv, biased high by approximately 5%. The calibration was verified prior to testing and after completing each HGR non radioactive experiment. For the Tank 38 series of tests, calibration was checked at the end of all the testing.

The primary purge gas contained 0.5 vol% krypton, 20 vol% oxygen, and 79.5 vol% nitrogen. Overall purge rate could be significantly increased with a separate air purge to ensure hydrogen concentration remained below flammability limits. The Kr-bearing purge gas (as compared to air) served several purposes. First, by using the measured krypton concentration, one could determine if the headspace of the reaction vessel had been purged of air. Second, using the measured krypton concentration allowed for calculation of flow rate out of the vessel, particularly when the Kr-bearing purge gas was supplemented with air. Third, Kr was used to confirm absence of gross in-leakage or gas generation (i.e., essentially that flow rate into the vessel was equal to flow rate out of the vessel). Fourth, unlike air, the purge had no helium and hydrogen, which can interfere with quantification of hydrogen produced from thermolysis or radiolysis.

The calibration and purge gases were produced by Praxair and purchased from Nexair.

In calculating hydrogen generation rates, the following equations were used. Equation 3 was used for most of the experiments. With the use of this equation, it was assumed that flow out of the vessel was equal to flow in to the vessel. The validity of this assumption was confirmed by checking that the measured Kr concentration was the same as the Kr concentration in the purge to the reaction vessel. It should also be noted that typical peak hydrogen generation rates ($4\times10^{-5}$ $ft^3$ $hr^{-1}$ $gal^{-1}$) are equal to approximately 0.004 cc/min, 0.1% of the typical purge rates of 3 cc/min.

Equation 4, Equation 5, and Equation 6 were used for the HBP simulant tests, where an estimate of volume at 140 °C of 1.19 L was used instead of a measurement of mass and density since the simulant was prepared by adding additional salt solution as the vessel contents were heated and water removed to attain the target boiling point. Equation 4 was used when the vessel was being purged with only the Kr-bearing purge gas. Equation 5 was used when air was added to the Kr-bearing purge. Equation 6 was used when only dry air was being used as the purge.

$$H_2gen = H_{2area} \times \frac{H_{2stdconc}}{H_{2stdarea}} \times F_{in} \times \frac{\rho_{sample}}{m_{sample}} \times 8.020 \times 10^{-6} \quad \text{Equation 3}$$

$$H_2gen = H_{2area} \times \frac{H_{2stdconc}}{H_{2stdarea}} \times F_{in} \times \frac{1}{V_{sample}} \times 8.020 \times 10^{-6} \quad \text{Equation 4}$$

$$H_2gen = H_{2area} \times \frac{H_{2stdconc}}{H_{2stdarea}} \times \frac{Kr_{stdarea} \times Kr_{bottle}}{Kr_{stdconc} \times Kr_{area}} \times F_{in} \times \frac{1}{V_{sample}} \times 8.020 \times 10^{-6} \quad \text{Equation 5}$$

$$H_2gen = H_{2area} \times \frac{H_{2stdconc}}{H_{2stdarea}} \times F_{air} \times \frac{1}{V_{sample}} \times 8.020 \times 10^{-6} \quad \text{Equation 6}$$

where,

$H_2gen$ = $H_2$ generation rate, $ft^3 \cdot gal^{-1} \cdot hr^{-1}$ at standard conditions of 21.1 °C and 1 atmosphere

$H_{2area}$ = GC $H_2$ response for a gas sample

$H_{2stdconc}$ = Concentration of $H_2$ calibration gas, ppmv

$H_{2stdarea}$ = Average of five GC responses from the $H_2$ calibration gas

$F_{in}$ = flow of Kr-bearing purge gas into the reaction vessel, sccm

$F_{air}$ = flow of dry air into the reaction vessel, sccm

$\rho_{sample}$ = density of sample, g·mL$^{-1}$

$m_{sample}$ = mass of sample, g

$V_{sample}$ = volume of sample, mL

$8.020\times10^{-6}$ = conversion factor, ft$^3$·min·mL·cc$^{-1}$·gal$^{-1}$·ppmv$^{-1}$·hr$^{-1}$

$Kr_{bottle}$ = Concentration of Kr in the purge gas, not including any supplemental air, vol%

$Kr_{area}$ = GC Kr response for a gas sample

$Kr_{stdconc}$ = Concentration of Kr calibration gas, vol%

$Kr_{stdarea}$ = Average of five GC responses from the Kr calibration gas

The software package GUM workbench[23] was used to determine the partial derivatives used to calculated the overall uncertainty for the above equations. The overall uncertainty (using these derivatives) and one sigma uncertainties in the variables was then used to calculate uncertainties for all the data points using the software package JMP Pro Version 11.2.1.[24]

In the Shielded Cells test with Tank 38, nitrous oxide ($N_2O$) was detected in the first 2.5 hours of boiling. Nitrous oxide was also observed in the first half of the HBP test at 140 °C. The calibration gas was adequate for $N_2O$ quantification but was not suitable to support a rigorous statistical determination of the limit of detection (LOD) and limit of quantification (LOQ). However, chromatograms where small quantities of $N_2O$ were detected were examined. Peaks with areas above 500 μV·s were greater than three times the baseline noise, suggesting an area of 500 or greater reliably represents presence of $N_2O$. Based on a calibration gas of 0.5% $N_2O$ and an area of approximately 51,000 μV·s (or 0.5%/51,000 μV·s = $9.8\times10^{-6}$%/ μV·s) for that calibration gas, the $N_2O$ detection limit is estimated to be 500 μV·s × $9.8\times10^{-6}$% / μV·s = 0.005% or 50 ppmv. A corresponding generation rate is discussed in the Tank 38 results section. In SRNL testing supporting DWPF, other nitrogen oxides are not routinely quantified by GC. Nitric oxide (NO) may be observed after nitrogen on GC Column-A. However, the protocol used in this testing was not designed to ensure analysis of samples for presence of NO (i.e., no calibration for NO and no determination to ensure elution time fell within sampling period).

The analysis of other miscellaneous volatile organic compounds (VOCs) was outside of the scope of this testing, although, methane could be detected, along with hydrogen, during testing. The low detection limit requirement for HGR measurement required low purge rates, which precluded the use of other analytical instruments (i.e., Mass Spectrometry and Fourier Transform Infrared Spectroscopy). However, it is unlikely that one of these online instruments would be able to measure additional VOCs with detection limits as low as the current hydrogen detection limit attained in this report.

*2.3.3 Limits of Detection for Hydrogen*

LOD and LOQ were determined for hydrogen measured by GC in the Tank 38 testing[c] using a methodology outlined in the text "Quality Assurance of Chemical Measurements."[25] In summary, the LOD is when a measured value becomes believable – that is, when the measured value exceeds the uncertainty of the measurement. The LOQ is the point where measurements become quantifiably meaningful. Typically, the LOD is set at $3 \times s_0$ and the LOQ is set at $10 \times s_0$, where $s_0$ = the standard deviation of the measurement noise.

To estimate $s_0$, three concentrations of hydrogen were used. Results are shown in Table 2.1.

**Table 2.1. Results of Gas Standard measurements for Hydrogen Detection Determination**

| $H_2$ Concentration (ppmv) | N (samples)s | Mean( $H_2$ area) | Std Dev( $H_2$ area) | %RSD ($H_2$ area) |
|---|---|---|---|---|
| 2.68 | 34 | 650 | 39.4 | 6.07 |
| 10.8 | 26 | 2552 | 60.4 | 2.37 |
| 52.0 | 32 | 12571 | 88.4 | 0.704 |

The standard deviation of interest may be reasonably well estimated by the smallest standard deviation in the above table, then $s_0 = 39.4$. This value yields, in terms of GC response, an LOD of $3 \times s_0 = 118$ and LOQ of $10 \times s_0 = 394$.

In trying to understand how these estimated "areas" should be utilized, a statistical interpretation is utilized. The regression of the area responses of the GC as it is used to measure the standards is shown in Figure 2-5.

[c] Detection limits are instrument specific and may change. While a rigorous analysis of the GC used in the simulant work was not completed, results of 2.68 ppmv calibration gas suggest similar LOD and LOQ. Note also that for all testing, except the water test, hydrogen levels were well above 2.68 ppmv.

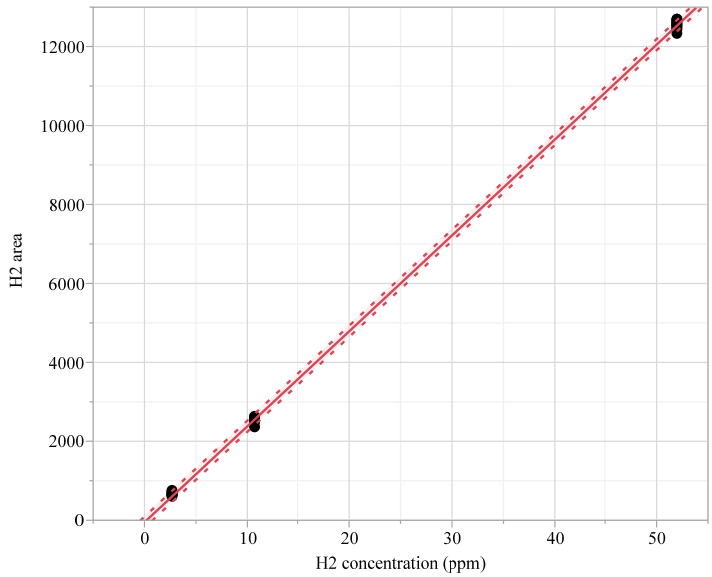


**Linear Fit**
H2 area = -23.70818 + 242.11077*H2 concentration (ppm)

**Summary of Fit**

| | |
|---|---|
| RSquare | 0.99983 |
| RSquare Adj | 0.999828 |
| Root Mean Square Error | 70.35437 |
| Mean of Response | 5334.098 |
| Observations (or Sum Wgts) | 92 |

**Analysis of Variance**

| Source | DF | Sum of Squares | Mean Square | F Ratio |
|---|---|---|---|---|
| Model | 1 | 2623186554 | 2.6232e+9 | 529964.8 |
| Error | 90 | 445476.365 | 4949.7374 | **Prob > F** |
| C. Total | 91 | 2623632030 | | <.0001* |

**Parameter Estimates**

| Term | Estimate | Std Error | t Ratio | Prob>\|t\| |
|---|---|---|---|---|
| Intercept | -23.70818 | 10.39074 | -2.28 | 0.0249* |
| H2 conc (ppm) | 242.11077 | 0.332576 | 727.99 | <.0001* |

**Figure 2-5. Regression of Hydrogen Standards for Estimation of $s_0$**

Using the 95% confidence interval for individual predictions, the following graph (Figure 2-6) can be used to introduce the LOD and LOQ values for area results on the y-axis, and to map those values into $H_2$ concentration values, respectively, on the x-axis. The $H_2$ concentration value for LOD is 1.17 ppmv and the LOQ value is 2.31 ppmv. With a purge rate of 3 sccm and a liquid volume of 1.2 L, the corresponding HGR measurement will have a LOD of $2.6\times10^{-8}$ $ft^3$ $hr^{-1}$ $gal^{-1}$ and a LOQ of $5.1\times10^{-8}$ $ft^3$ $hr^{-1}$ $gal^{-1}$.

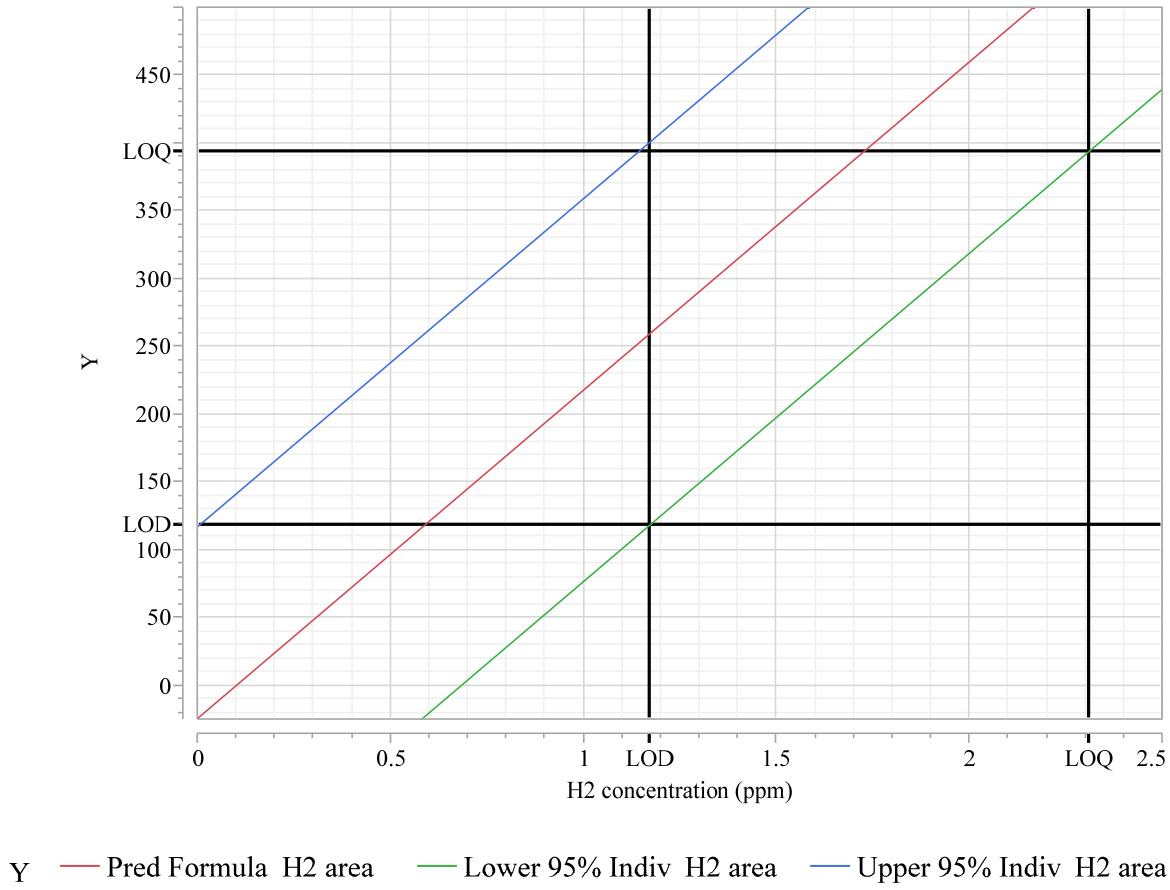


**Figure 2-6. Regression of $H_2$ area versus QC Standards $H_2$ concentration (ppmv) Values**

*2.3.4 Methane*

In both the Tank 38 and the HBP tests, a peak on the chromatograms with a retention time greater than the retention time of the inert tracer of krypton was noted and identified as methane. A discussion of how the peak was identified can be found in the report, "Evaluation of the Current State of Knowledge for Thermolysis of Organics within SRS Waste Forming Volatile Organic Compounds (VOCs)."[26] In that initial identification of the peak, relatively high concentrations of methane gas were used (in separate cylinders containing 500 ppmv and 1 vol% methane). Since then, additional calibration gases were used to estimate the limits of detection. The compositions were:

- 2 ppmv methane, balance air,
- 10 ppmv methane, balance air,
- 50 ppmv methane, balance air, and
- 100 ppmv methane, 50 ppmv hydrogen, 0.5 vol% krypton, 1 vol% carbon dioxide, 0.5 vol% nitrous oxide, balance air.

This last calibration gas is SRNL's current gas for calibrating the GCs for the hydrogen generation rate program. Also, the results of running this gas utilizing the same methods used in this test showed that there was adequate separation between the krypton and methane peaks, and sample data collection time was long enough to not cut off the methane peak at 100 ppmv methane concentrations. See Figure 2-7 for sample chromatograms.

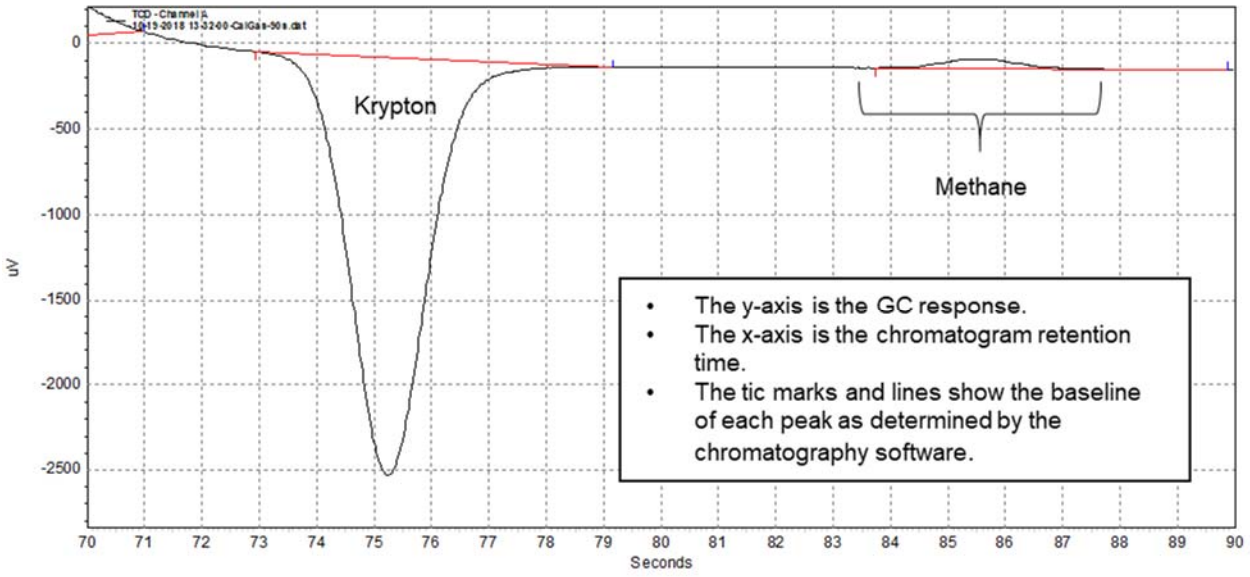


(a) Chromatogram from GC used in HBP testing

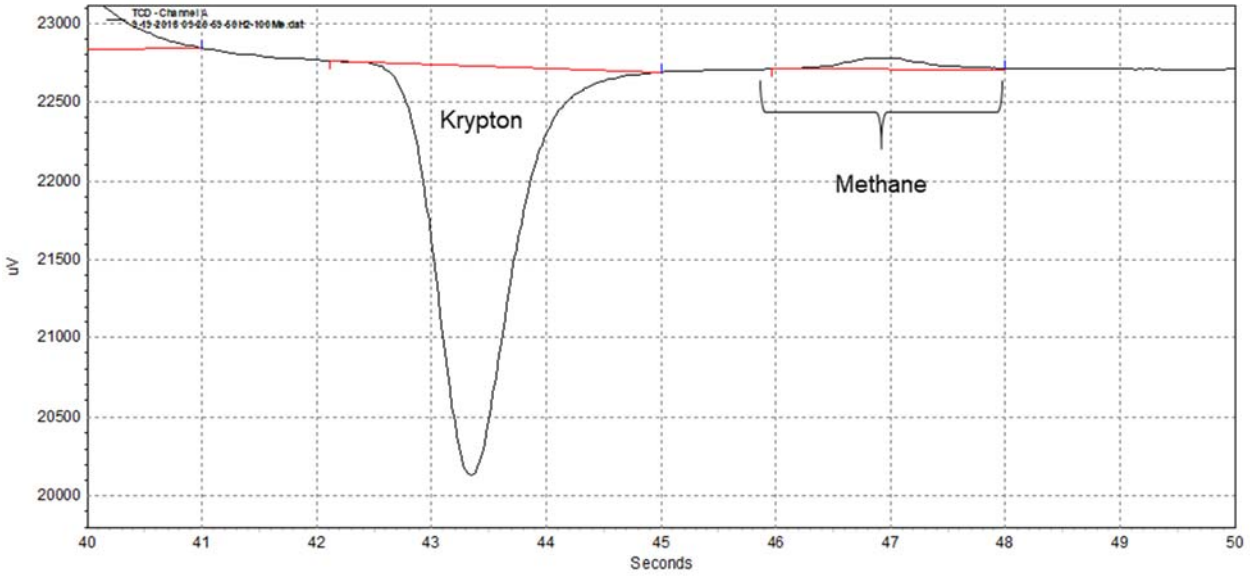


(b) Chromatogram from GC used in Tank 38 testing

**Figure 2-7. Chromatograms Showing Good Separation Between Krypton and Methane**

For Tank 38 testing, the 2, 10, 50, and 100 ppmv methane gases were analyzed on the GC utilizing the same method as used in the testing. For the HBP testing, only the 100 ppmv methane gas was analyzed. A summary of results is given in Table 2.2. As can be seen, the 2 ppmv methane standard was not detected by the GC used in Tank 38 testing while the other standards were each detected. Therefore, the limit of detection is less than 10 ppmv. In comparing the responses of the two GCs for the 100 ppmv methane standard, the GC used for HBP testing has a response of nearly twice that of the GC used for Tank 38 testing, suggesting the limit of detection on the HBP GC is slightly better than the Tank 38 GC.

**Table 2.2. GC Response (Area) for several Methane concentrations**

| | Methane Concentration (ppmv) | GC Response (Area) | |
|---|---|---|---|
| | | Average | %RSD (n=7) |
| HBP | 100 | 9209 | 1.4 |
| Tank 38 | 2 | NA | NA |
| | 10 | 378 | 11 |
| | 50 | 2448 | 3.1 |
| | 100 | 5540 | 2.6 |

Because the original experiments were completed many months before these standards were obtained and analyzed, a rigorous determination of the limit of quantification was not performed; the methane results presented in this report should be used for comparisons and trends only. Methane concentrations were calculated from the GC responses. The 100 ppmv calibration gas results were used to calculate a response factor (RF) to be applied to the integrated areas. This gas was chosen because it contained krypton, which was used as an inert tracer in the testing, and hydrogen, which was observed in the testing. In general, calibration gases should be as similar as possible to the gas to be analyzed.

The methane RF was calculated from the following equation for each GC:

$$RF = \frac{100\ ppmv}{average\ methane\ area}$$

The average areas in Table 2.2 were used to calculate response factors of $1.09\times10^{-2}$ for the HBP testing and $1.81\times10^{-2}$ for Tank 38. The response factors were then applied to the areas in the GC output to calculate methane concentration.

*2.3.5 Analytical Methods for Sample Analysis*

Sample analyses for the radioactive actual waste materials were performed by SRNL Analytical Development (AD) Department. Sample analyses for simulant materials were performed by a combination of AD and SRNL Process Science and Analysis Laboratory (PSAL).

Samples of one batch of the five component simulant SY1-SIM-91B-NG and the four component HBP simulant were submitted to AD for Ion Chromatography (IC) for anions; Volatile Organics Analysis (VOA); Semivolatile Organics Analysis (SVOA); Total Base (TB), free hydroxide, and Other Base excluding carbonate (OB); and Total Inorganic Carbon (TIC) and Total Organic Carbon (TOC). Hydroxide ion ($OH^-$) is reported from the free hydroxide measurement. Carbonate ion is determined from TIC measurement. These simulants were also measured at PSAL for density.

Fluid samples from the SY1-SIM-91B-NG simulant tests were taken after the test completed and the salt solution had been removed to the product container. Samples were taken after each steady state condition measurement during the HBP simulant testing. These samples were taken at elevated temperature (70 to 100 °C) because sampling after this material had cooled to ambient lab temperature would lead to precipitation of solids from the supersaturated solution. In the case of the HBP simulant, materials that deposited on surfaces would not be fully represented in these samples.

Products of the SY1-SIM-91B-NG simulant tests were submitted undiluted to PSAL for measurement by IC and Inductively Coupled Plasma – Atomic Emission Spectroscopy (ICP-AES). Products from the HBP simulant tests were diluted nominally three-times with deionized water and submitted to PSAL for

measurement by IC and to AD for measurement by SVOA, TIC/TOC, and TB/$OH^-$/OB. Water diluted HBP simulant was further diluted nominally ten-times with 2M nitric acid and submitted to PSAL for measurement by ICP-AES.

Solids that were removed from the vessel after the SY1-SIM-91B-NG simulant tests were rinsed with deionized water and analyzed at Aiken County Technology Laboratory (ACTL) by Scanning Electron Microscopy (SEM) with X-ray Energy Dispersive Spectroscopy (XEDS). Solids that were removed from the vessel after the HBP simulant tests were rinsed with deionized water and analyzed by AD using X-ray Diffraction (XRD) and SEM/XEDS. Washed solids from the HBP simulant test were also analyzed at ACTL by SEM/XEDS.

A portion of the actual-waste Tank 38 sample was split from the original sample and used for chemical characterization. The density was measured in quadruplicate on this analytical sample using 2mL volumetric flasks. Subsequently the density was measured in quadruplicate on the split of sample remaining after HGR measurement samples were prepared. The follow-up measurements were performed in quadruplicate using 8.5 mL plastic test tubes whose volumes were determined by weight of water. All density measurements were performed at ambient cell temperature.

Three preparations were performed for most of actual-waste Tank 38 sample analysis. Firstly, the Tank 38 material including insoluble solids was diluted nominally 10-times with 2M nitric acid and analyzed by ICP-AES, Inductively Coupled Plasma – Mass Spectroscopy (ICP-MS), IC, Atomic Absorption (AA), Cold Vapor Atomic Absorption (CVAA) digested for mercury, TIC/TOC, and gamma scan. Secondly, the Tank 38 material was filtered using a 0.45-micron nylon filter, diluted nominally 10-times with deionized water, and analyzed by IC, TIC/TOC, TB/$OH^-$/OB, CVAA digested, ICP-AES, ICP-MS, and gamma scan. Thirdly, the Tank 38 material including insoluble solids was diluted nominally 25-times with DI water and analyzed by IC and TIC/TOC.

The analyses for Tank 38 were performed for triplicate preparations with the following exceptions. For the acid diluted slurry, AA for arsenic and selenium and gamma scan were performed on single aliquots. SVOA and TOC were measured for single aliquots undiluted Tank 38 material.

Results are preceded by "<" when the analyte is below the limits of quantification. The average values and the RSDs are reported for the replicate sample preparations and measurements. The RSD values are not reported when all measurements are below the limits of quantification. When there is a combination of results both above and below the limits of quantification, only the results above the limits of quantification are used in the average. An analytical method "1σ unc." (one sigma uncertainty; i.e., standard deviation) is reported for each analyte and is usually dominated by the uncertainty in the instrument calibration.

### 2.4 Quality Assurance

Requirements for performing reviews of technical reports and the extent of review are established in manual E7 2.60.[27] This document, including all calculations (e.g., hydrogen generation rates and uncertainties), was reviewed by Design Verification by Document Review. SRNL documents the extent and type of review using the SRNL Technical Report Design Checklist contained in WSRC-IM-2002-00011, Rev. 2.[28] Data are recorded in the electronic laboratory notebook system as notebook/experiment numbers A6583-00142-15, A6583-00142-16 , A6583-00142-17, c7605-00021-14, L3293-00100-30, L3293-00100-31, L3293-00100-32, and L3293-00100-33.

## 3.0 Results and Discussion

### 3.1 Results from Testing with SY1-SIM-91B-NG

#### *3.1.1 Analysis of Prepared Simulant*

Table 3.1 contains the results of the measurement of the simulant SY1-SIM-91B-NG. The target recipe concentration is also given for reference. Good agreement is noted for most cases except for aluminum, which was higher than the recipe target. A TOC concentration of 192 mg carbon/L was measured, though no organic carbon was intentionally added in this simulant. Appendix A discusses additional studies to examine the source of the TOC. No volatile or semivolatile organics were identified or measured above the detection limit.

**Table 3.1. Analysis of the Salt Simulant SY1-SIM-91B-NG**

| analyte | method | units | 1σ unc. | Measurement | RSD | Target |
|---|---|---|---|---|---|---|
| Al | ICP-ES | M | 10% | 1.72 | 0.4% | 1.54 |
| Na | ICP-ES | M | 10% | 9.00 | 0.7% | 8.79 |
| $OH^-$ | TB/OH/OB | M | 10% | 2.18 | -- | 2.00 |
| $NO_2^-$ | IC | M | 10% | 2.28 | -- | 2.24 |
| $NO_3^-$ | IC | M | 10% | 2.44 | -- | 2.59 |
| $CO_3^{2-}$ | TIC/TOC | M | 10% | 0.53 | -- | 0.42 |
| | | mg C/L | | 6,400 | -- | 5,000 |
| $CHO_2^-$ | IC | M | -- | < 0.002 | -- | 0 |
| | | mg C/L | | < 27 | -- | 0 |
| $C_2O_4^{2-}$ | IC | M | -- | < 0.001 | -- | 0 |
| | | mg C/L | | < 27 | -- | 0 |
| $PO_4^{3-}$ | IC | M | -- | < 0.001 | -- | 0 |
| $SO_4^{2-}$ | IC | M | -- | < 0.001 | -- | 0 |
| $F^-$ | IC | M | -- | < 0.005 | -- | 0 |
| $Cl^-$ | IC | M | -- | < 0.003 | -- | 0 |
| $Br^-$ | IC | M | -- | < 0.001 | -- | 0 |
| TOC | TIC/TOC | mg C/L | 10% | 192 | -- | 0 |
| SVOA | SVOA | mg/L | -- | < 1.0 | -- | 0 |
| VOA | VOA | mg/L | -- | < 0.25 | -- | 0 |
| density | Densitometer | g/mL | 2% | 1.4206 | -- | N/A |

#### *3.1.2 Testing Parameters and Descriptions*

In total, seven experiments have been conducted using SY1-SIM-91B-NG to measure HGR. Table 3.2 lists the experimental parameters used for each test including the mass of solution added, the concentration of glycolate added, the purge rate employed, and the temperature achieved. Additional information is given to

delineate differences in equipment configuration between each test (e.g., heating method, agitation, and thermowell use).

**Table 3.2. Run Parameters for Simulant Testing with SY1-SIM-91B-NG**

| Test ID | Mass (g) | Purge Rate (sccm[a]) | Glycolate (M) | Temperature (°C) | Heating Method | Agitation Status | Thermowell Status |
|---|---|---|---|---|---|---|---|
| HGR-ASH-1 | 1706 | 3 | 0.21 | 90 | Heating Rods | Mixed | None |
| HGR-ASH-2 | 1704 | 3 | $9.6\times10^{-5}$ | 114[b] | Heating Rods | Mixed | None |
| HGR-ASH-3 | 1708 | 3 | $1.9\times10^{-5}$ | 114[b] | Heating Rods | Mixed | None |
| HGR-ASH-4 | 1515 | 3 | 0 | 114[b] | Heating Rods | Mixed | None |
| HGR-ASH-5 | 1552 | 3 | 0 | 114[b] | External Mantle | Mixed | Glass |
| HGR-ASH-5b[c] | 1552 | 9 | 0 | 75 | Heating Rods | Mixed | Glass |
| HGR-ASH-6 | 1558 | 3 | 0 | 114[b] | External Mantle | Unmixed | Glass |

[a] Standard Conditions of 1 atmosphere, 21.11 °C (70 °F).
[b] Boiling
[c] Test HGR-ASH-5b used the same solution from HGR-ASH-5.

Tests HGR-ASH-1 and HGR-ASH-2 were designed as benchmarking experiments to establish the capabilities of the designed HGR apparatus. HGR-ASH-1 was performed as an attempt to replicate an experiment reported in the literature by Ashby, while HGR-ASH-2 was performed as a modification of the literature experiment designed to demonstrate the ability to measure low concentrations of hydrogen (<10 ppm). Data from these tests led to the observation of an unexplained hydrogen generation in the absence of added organic molecules, which was further explored in tests HGR-ASH-3 through HGR-ASH-6. An additional test (HGR-ASH-4b) was performed at 90 °C; however, this run was not carried out to completion, and is therefore not reported here.

### *3.1.3 Benchmarking Tests (HGR-ASH-1 & HGR-ASH-2)*

Figure 3-1 gives the measured HGR for test HGR-ASH-1 in units of standard cubic feet of $H_2$ per hour per gallon of simulant ($ft^3\ hr^{-1}\ gal^{-1}$) as a function of time since achieving the target temperature (90 °C).

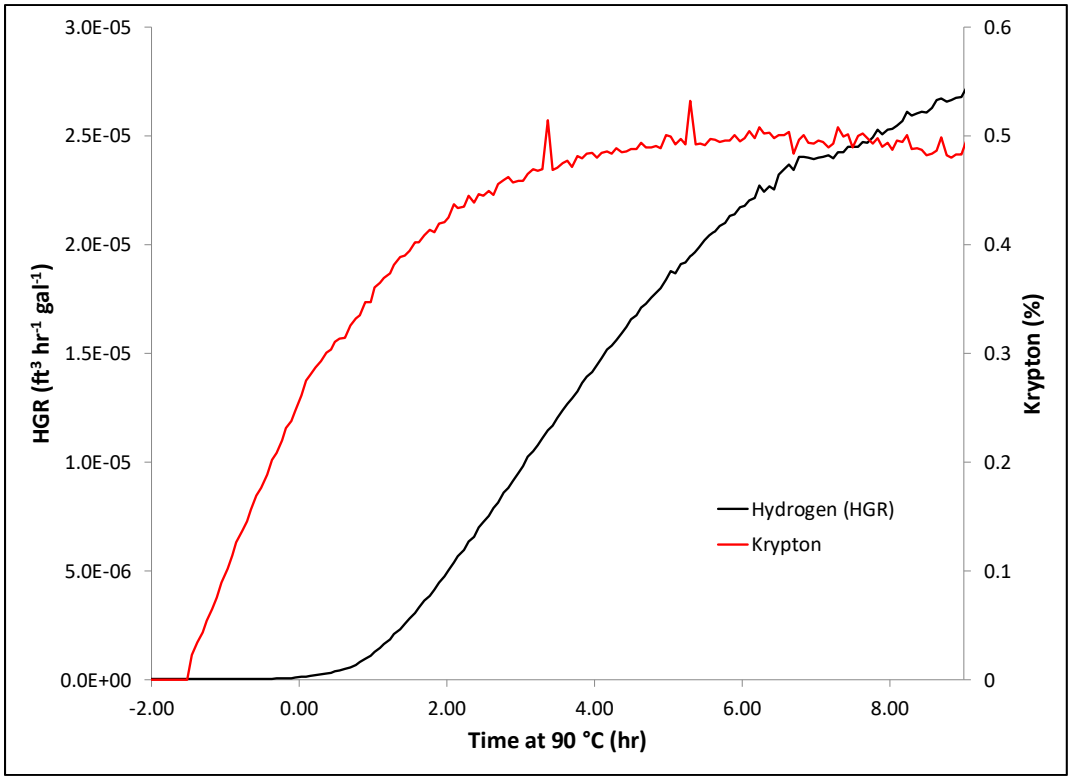


**Figure 3-1. Hydrogen Generation Rate as a Function of Time for Test HGR-ASH-1. Red Line indicates krypton concentration as a function of time.**

The maximum HGR measured in HGR-ASH-1 is $2.7\times10^{-5}$ $ft^3$ $hr^{-1}$ $gal^{-1}$. This value is in good agreement with the HGR predicted using the relationship derived by Crawford and King[15] ($2.7\times10^{-5}$ $ft^3$ $hr^{-1}$ $gal^{-1}$) and the rate reported by Ashby[10] at 24 hours ($2.7\times10^{-5}$ $ft^3$ $hr^{-1}$ $gal^{-1}$). Note that the increasing HGR observed in HGR-ASH-1 suggests a higher HGR may have been observed at longer reaction times. The fact that this increase appears to be decelerating within 6 hours combined with the fact that most of the data reported by Ashby exhibits constant generation rates at longer time scales suggest that the HGR profile follows exponential behavior consistent with that seen in continuously stirred-tank reactor (CSTR) kinetics. Extrapolation of the HGR trend in the deceleration region suggests that a "final" HGR of $3.0\times10^{-5}$ $ft^3$ $hr^{-1}$ $gal^{-1}$ was likely.

While a direct comparison between the dynamic HGR apparatus used here and the static apparatus employed by Ashby is not necessarily justifiable, the HGR observed in HGR-ASH-1 suggests that an order of magnitude comparison is satisfactory. Given the reasonable success with literature replication (and considering the technical differences between the HGR apparatus and the experimental method employed by Ashby), the HGR apparatus was deemed adequate and subsequent testing proceeded.

As mentioned earlier, HGR-ASH-2 was performed at a greatly reduced glycolate concentration relative to HGR-ASH-1 ($9.6\times10^{-5}$ M vs. 0.21 M, or 0.05%) and a higher temperature (114 °C, boiling) to demonstrate the capability of the HGR apparatus to measure lower concentrations of hydrogen and to explore equipment performance at boiling. According to the glycolate thermolysis relationship described by Crawford and King,[15] the predicted HGR for the conditions employed in HGR-ASH-2 is $2.1\times10^{-7}$ $ft^3$ $hr^{-1}$ $gal^{-1}$. Figure 3-2 gives the measured HGR for HGR-ASH-2 as a function of time spent at boiling.

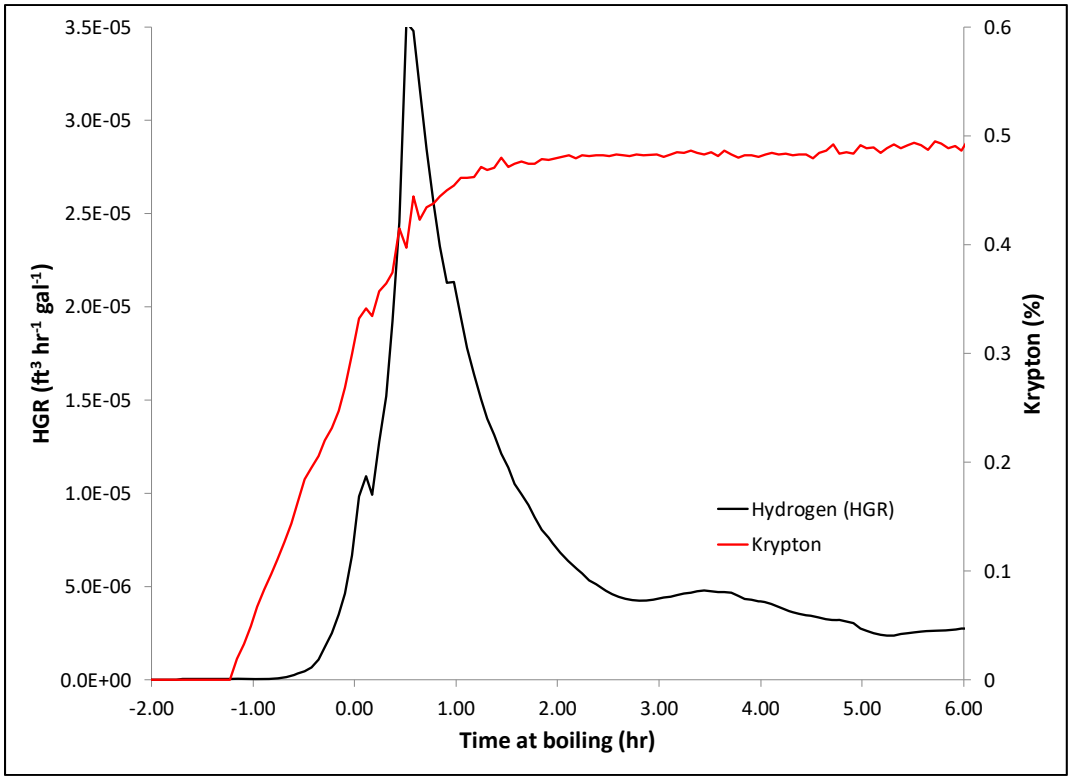


**Figure 3-2. Hydrogen Generation Rate as a Function of Time for Test HGR-ASH-2. Red Line indicates krypton concentration as a function of time.**

As shown in Figure 3-2, the measured HGR from test HGR-ASH-2 was significantly higher than the value expected ($2.1\times10^{-7}$ $ft^3$ $hr^{-1}$ $gal^{-1}$). A peak rate of approximately $3.5\times10^{-5}$ $ft^3$ $hr^{-1}$ $gal^{-1}$ is observed immediately following boiling. This rate then rapidly diminishes to a more persistent rate of $2.7\times10^{-6}$ $ft^3$ $hr^{-1}$ $gal^{-1}$. Both rates of hydrogen production are incongruous with the glycolate destruction rates reported by Ashby. This observation suggests that a non-glycolate mechanism for hydrogen generation is active in these tests.

Sample analysis for test HGR-ASH-1 was inconclusive and is not included in this report. Formate and oxalate were detected in the salt solution product from test HGR-ASH-1 but were below the instrument calibration curve and thus cannot be quantified. Glycolate quantification was not repeatable and reanalysis of the sample after significant time has passed would not be applicable to the test.

### *3.1.4 Glycolate-Free Hydrogen Generation Mechanism Investigation*

Test HGR-ASH-3 was conducted to measure the HGR in the presence of a negligibly small amount of glycolate. Figure 3-3 gives the HGR measured in HGR-ASH-3 as a function of time at boiling.

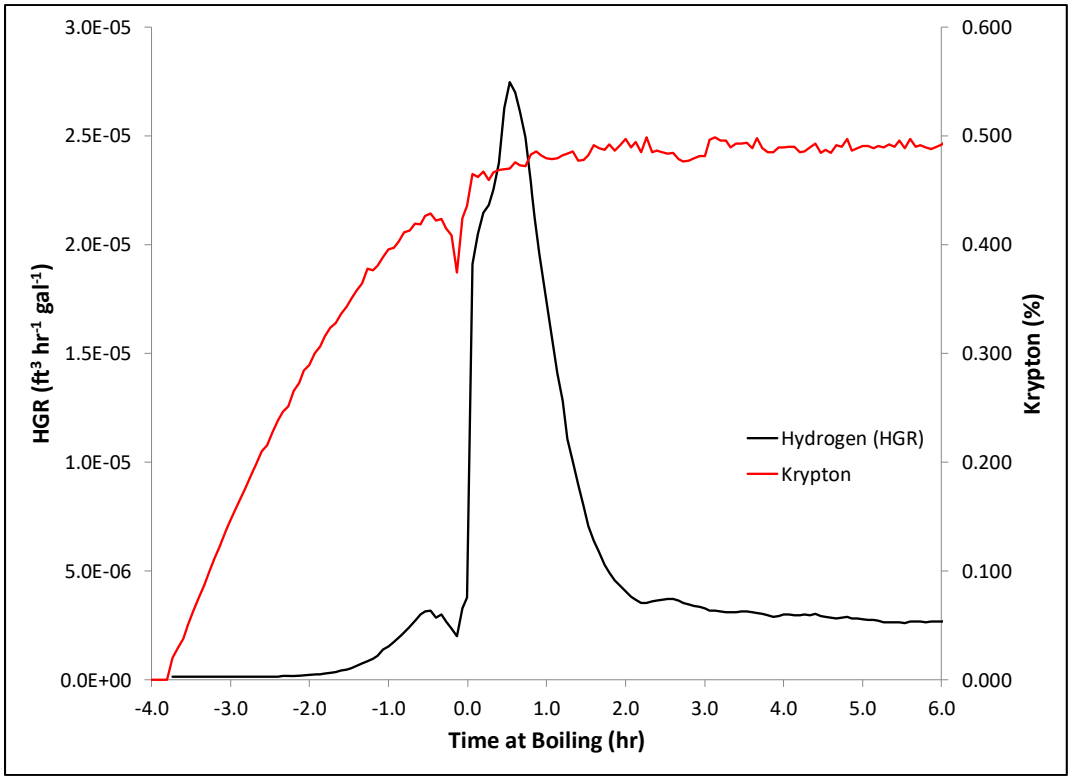


**Figure 3-3. Hydrogen Generation Rate as a Function of Time for Test HGR-ASH-3. Red Line indicates krypton concentration as a function of time.**

As shown in Figure 3-3, HGR-ASH-3 exhibited similar behavior to that of HGR-ASH-2, with a peak generation rate of $2.7\times10^{-5}$ $ft^3$ $hr^{-1}$ $gal^{-1}$ which rapidly declined to a persistent rate near $2.5\times10^{-6}$ $ft^3$ $hr^{-1}$ $gal^{-1}$. Within 12 hours, HGR-ASH-3 produced approximately 36 µmol of hydrogen atoms as hydrogen gas. This amount of generated gas constitutes a significant fraction of the hydrogen atoms added to the solution as glycolate (91 µmol of hydrogen atoms total, 61 µmol capable of undergoing hydrogen gas formation) and suggests a rapid degradation of glycolate in caustic solutions, which is refuted by glycolate destruction rates reported in the literature.[10] The fact that the hydrogen generation behavior seen in HGR-ASH-3 closely mimics that seen in HGR-ASH-2, combined with the fact that the theoretical glycolate destruction rates required to sustain these hydrogen generation rates are in vast excess of glycolate destruction rates reported in literature adds further evidence to the notion that an alternative "glycolate-free" hydrogen generation mechanism must be responsible for the measured HGR.

Following the results of HGR-ASH-3, several glycolate-free tests were performed using the same salt simulant to determine the hydrogen production mechanism(s) responsible for the measured HGR. Test HGR-ASH-4 was conducted by utilizing the same apparatus employed in HGR-ASH-3 and a smaller volume of simulant. This volume reduction was performed to minimize solution contact with the Viton® O-ring and siloxane resin (described in Section 2.2), therefore mitigating the possibility of significant hydrogen generation due to reaction of the simulant with these organic components. Figure 3-4 gives the measured HGR for HGR-ASH-4 as a function of time at boiling.

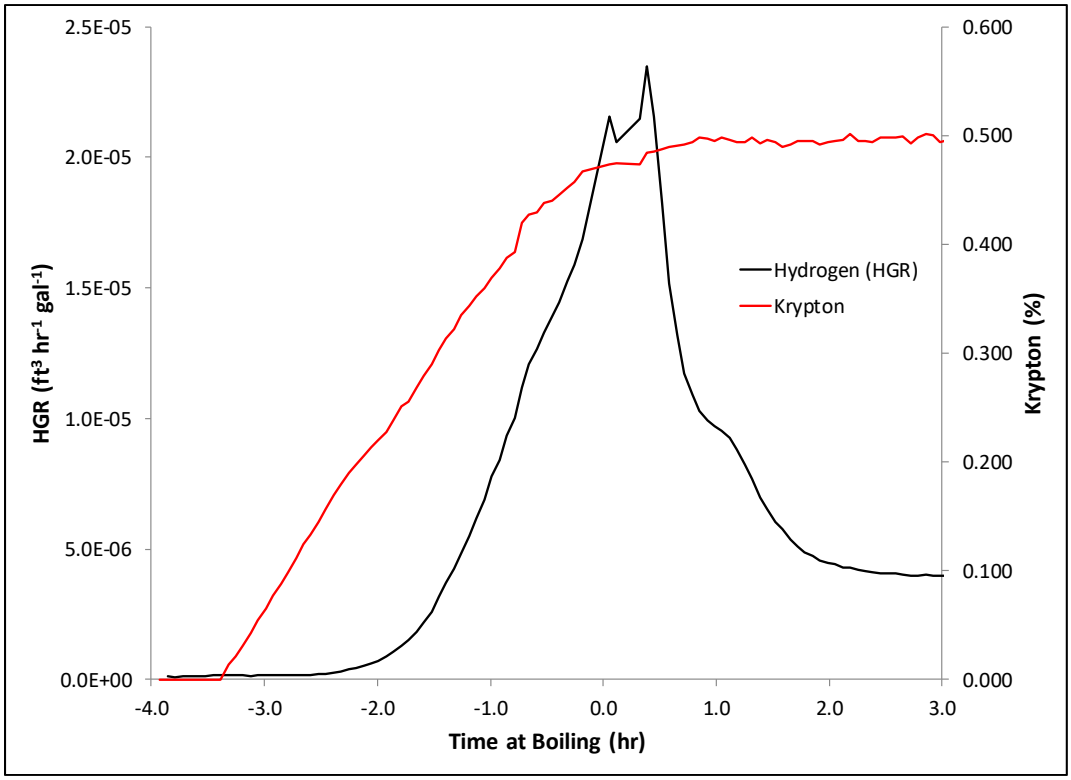


**Figure 3-4. Hydrogen Generation Rate as a Function of Time for Test HGR-ASH-4. Red Line indicates krypton concentration as a function of time.**

Again, an initial peak of hydrogen generation is observed immediately following boiling, achieving a maximum HGR of approximately $2.3\times10^{-5}$ $ft^3$ $hr^{-1}$ $gal^{-1}$. Shortly thereafter, the HGR from HGR-ASH-4 rapidly decreases to an apparently stable value of $4.0\times10^{-6}$ $ft^3$ $hr^{-1}$ $gal^{-1}$. Offgas data from HGR-ASH-4 shows behavior is similar to that of HGR-ASH-2 and HGR-ASH-3, suggesting that any hydrogen produced by reaction of simulant SY1-SIM-91B-NG with the O-rings and resins employed in this study is not the dominant source of the unexpected higher hydrogen generation.

HGR-ASH-5 was conducted by removing the Inconel heating rods and placing the thermocouple within a borosilicate glass thermowell. These changes were made to eliminate the possibility of electrolytic hydrogen generation caused by stray current from the heating rods and thermocouple or from cathode-anode (i.e., galvanic) interactions between the Inconel heating rods, Inconel thermocouple, and stainless-steel agitator. Figure 3-5 gives the measured HGR for HGR-ASH-5 as a function of time at boiling.

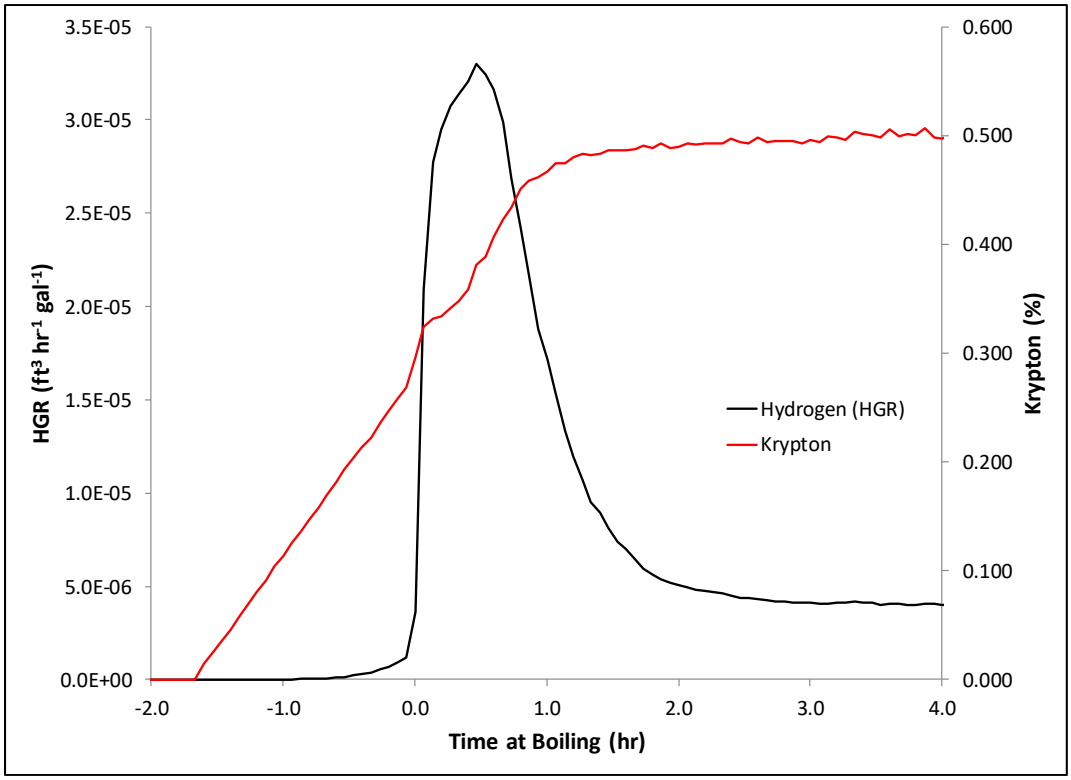


**Figure 3-5. Hydrogen Generation Rate as a Function of Time for Test HGR-ASH-5. Red Line indicates krypton concentration as a function of time.**

As was seen in HGR-ASH-2, 3, and 4, a peak of $3.3\times10^{-5}$ $ft^3$ $hr^{-1}$ $gal^{-1}$ is seen in the hydrogen generation rate of HGR-ASH-5 immediately following boiling, followed by a rapid decrease to approximately $4.2\times10^{-6}$ $ft^3$ $hr^{-1}$ $gal^{-1}$. The fact that the behavior of HGR-ASH-5 mirrors the behavior of HGR-ASH-2, 3, and 4 suggests that most of the generated hydrogen is not caused by electrolytic mechanisms due to the presence of metallic components in contact with the solution.

HGR-ASH-6 was conducted by placing the borosilicate glass vessel into the same heating mantle employed in HGR-ASH-5 and removing the Inconel heating rods. Furthermore, HGR-ASH-6 was performed in the absence of an agitator, thereby removing the last source of metal in the reaction vessel. Note that this modification led to an absence of forced convection in HGR-ASH-6, possibly leading to localized overheating. Figure 3-6 gives the measured HGR for HGR-ASH-6 as a function of time at boiling.

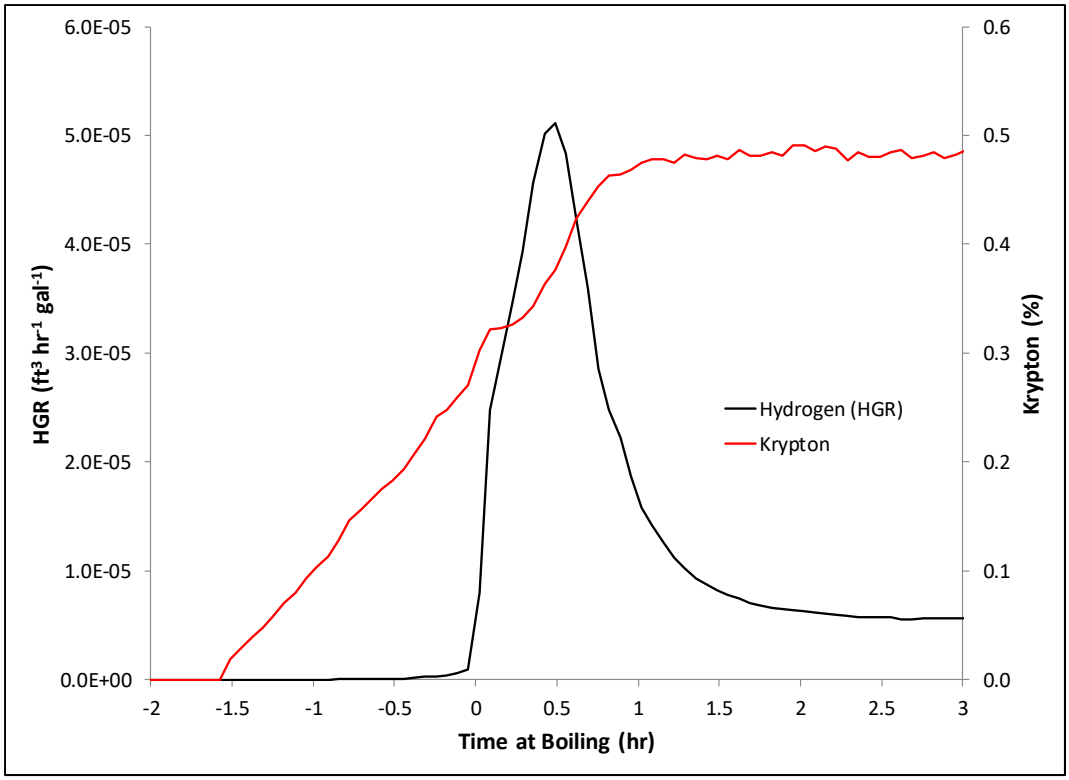


**Figure 3-6. Hydrogen Generation Rate as a Function of Time for Test HGR-ASH-6. Red Line indicates krypton concentration as a function of time.**

The HGR trend shown in Figure 3-6 matches well with the behavior exhibited in HGR-ASH-2, 3, 4, and 5, yielding an initial peak HGR of $5.2\times10^{-5}$ $ft^3$ $hr^{-1}$ $gal^{-1}$ and a persistent, final HGR of $5.6\times10^{-6}$ $ft^3$ $hr^{-1}$ $gal^{-1}$. While the apparent HGR measured in HGR-ASH-6 is higher than those observed in HGR-ASH-2, 3, 4, and 5, it is not clear if this increase is due to physical changes in the test (e.g., additional chemistries present in the test, localized heating caused by a lack of forced convection, etc.) or if it is comparable to the previous runs within experimental error. However, given the absence of metal in HGR-ASH-6, it seems clear that corrosion of metal is a negligible contributor to the HGR observed in this testing.

To date, an insufficient number of tests have been performed to determine and quantify all of the sources of hydrogen generation in the glycolate-free tests described above. However, a number of possible sources of hydrogen have been eliminated, leaving a few possible candidates (some of which have been confirmed as active in these systems, see Appendix A). Testing with water (HGR-WATER) demonstrated that the hydrogen production is not a function of experimental apparatus alone. Figure 3-7 gives the measured HGR for HGR-WATER as a function of time at boiling.

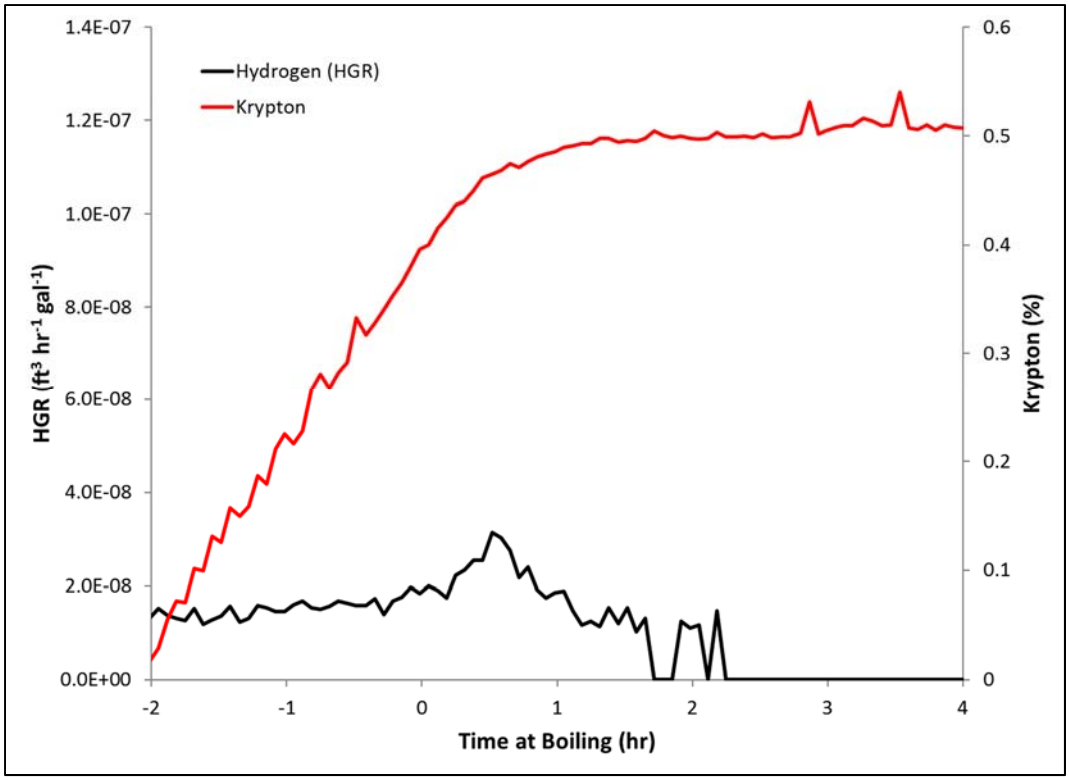


**Figure 3-7. Hydrogen Generation Rate as a Function of Time for Test HGR-WATER. Red Line indicates krypton concentration as a function of time.**

The trends shown in Figure 3-7 show that no appreciable hydrogen is generated from operation of the HGR apparatus alone, but rather is dependent on the use of materials included in the simulant. A small peak in HGR is observed immediately after boiling ($3.1\times10^{-8}$ $ft^3$ $hr^{-1}$ $gal^{-1}$); however, it is likely that this peak is a relic of boiling and not a chemical reaction. The hydrogen observed in HGR-WATER appears to be solely due to hydrogen dissolved in the air initially present in the vessel, gradually disappearing with displacement by hydrogen-free purge gas. Several untested hydrogen generation mechanisms remain and are currently under investigation. Some of these mechanisms are listed below:

- thermolysis of organic impurities in simulant components,
- reaction with glass components,
- reaction due to inorganic impurities in simulant components, or
- unexpected / unknown inorganic reactions.

Of these suggested mechanisms, the first two offer the most evidence for support. Formation of white solids was observed in each test conducted at boiling (see Appendix B). Literature reports of solids generated in similar conditions designate these solids as aluminosilicates, formed from reaction of sodium aluminate and silica dissolved by contacting the glass surface with sodium hydroxide. While there is no known chemistry that the authors are aware of describing hydrogen generation from these components, there is not enough data to completely rule out such contributions to HGR.

The approximately 200 mg/L TOC concentration (see Table 3.1) measured in SY1-SIM-91B-NG suggests the presence of an organic impurity in at least one of the chemical components used during the preparation of SY1-SIM-91B-NG. Additional testing (see Appendix A) investigated this possibility and concluded that hydrogen generation can be observed in simple sodium hydroxide solutions (possibly due to corrosion of

wetted surfaces in the presence of NaOH) and that sodium aluminate seems to bear a relatively large organic carbon impurity which appears to significantly affect the measured HGR in the glycolate-free testing described above.

The Hu model (shown in Equation 1) may be used to evaluate the potential contribution of TOC impurities toward hydrogen generation in SY1-SIM-91B-NG testing. Using a measured TOC concentration of 192 mg/L, the measured aluminum concentration of 1.72 M, and the measured density of SY1-SIM-91B-NG (1.4206 g/mL), weight percentages of TOC and aluminum can be calculated to evaluate the Hu model at the conditions employed in this testing. Doing so yields a Hu-predicted HGR of $1.3\times10^{-5}$ $ft^3$ $hr^{-1}$ $gal^{-1}$. This calculated rate is, in general, lower than the initial peak HGRs observed in the glycolate free experiments and an order of magnitude above the persistent rates observed in this testing. For convenient comparison, the observed rates of HGR-ASH-2,3,4,5, and 6 are listed in Table 3.3.

**Table 3.3. Peak and Persistent HGR for Tests HGR-ASH-2, 3, 4, 5, & 6.**

| Test ID | Peak HGR ($ft^3$ $hr^{-1}$ $gal^{-1}$) | Persistent HGR ($ft^3$ $hr^{-1}$ $gal^{-1}$) | Estimated Uncertainty of the Persistent HGR (95% confidence interval) * |
|---|---|---|---|
| HGR-ASH-2 | $3.5\times10^{-5}$ | $2.7\times10^{-6}$ | 11% |
| HGR-ASH-3 | $2.7\times10^{-5}$ | $2.6\times10^{-6}$ | 10% |
| HGR-ASH-4 | $2.3\times10^{-5}$ | $4.0\times10^{-6}$ | 10% |
| HGR-ASH-5 | $3.3\times10^{-5}$ | $4.2\times10^{-6}$ | 10% |
| HGR-ASH-6 | $5.2\times10^{-5}$ | $5.6\times10^{-6}$ | 9% |
| **AVERAGE** | **$3.4\times10^{-5}$** | **$3.8\times10^{-6}$** | **NA** |

* The uncertainties for these results were calculated by inserting the inputs for Equation 3 (see Section 2.3.2) into the software package, GUM workbench [23], to derive a formula for the overall uncertainty. This formula was then used to calculate uncertainty using the software package JMP™ Pro, Version 11.2.1[24].

The observation that persistent HGR from these glycolate-free tests consistently falls below the generation rates expected by organic thermolysis according to the application of the Hu equation at similar conditions suggests that the TOC impurity measured in SY1-SIM-91B-NG is fully capable of explaining the hydrogen seen in this testing.

### *3.1.5 Evaluation of Hydrogen Generation Rate at 75 °C*

To determine the effect of temperature on the hydrogen generation rate measured in these tests, the product from test HGR-ASH-5 was reheated to 75 °C and monitored for hydrogen production. This test was designated HGR-ASH-5b. Figure 3-8 gives the measured HGR from HGR-ASH-5b as a function of time at 75 °C.

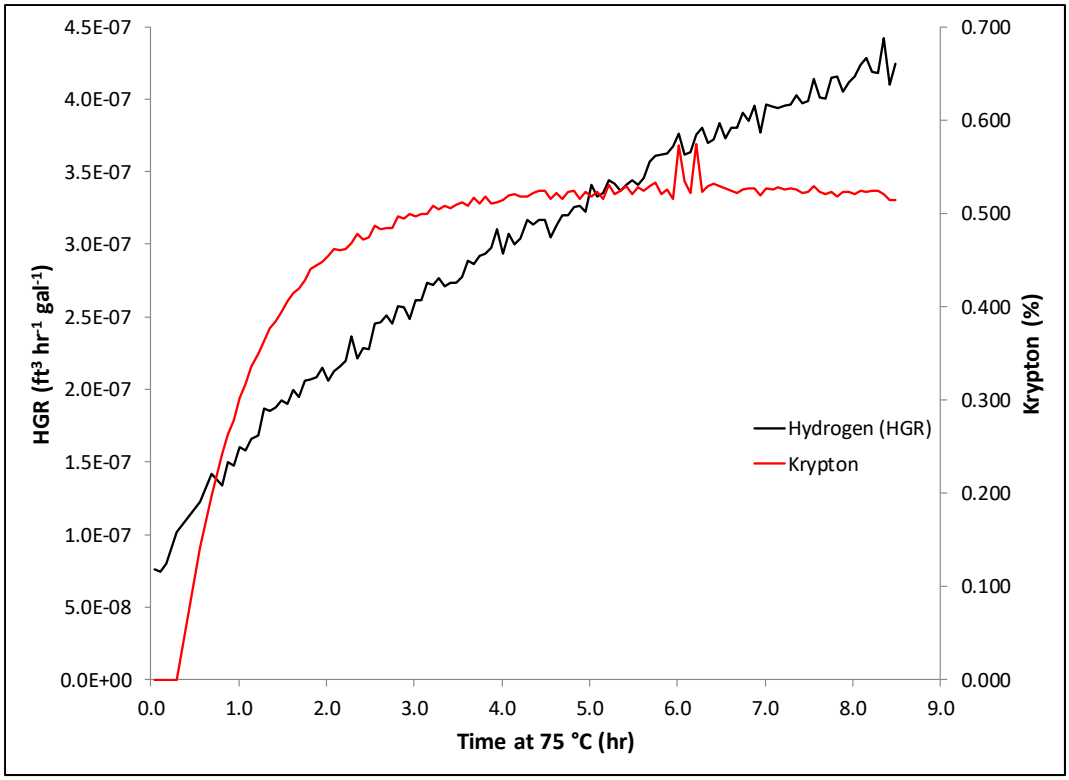


**Figure 3-8. Hydrogen Generation Rate as a Function of Time for Test HGR-ASH-5b. Red Line indicates krypton concentration as a function of time.**

The data from Figure 3-8 suggest that HGR from the salt solution simulant is significantly lower at 75 °C than at boiling (114 °C), with a maximum recorded generation rate for HGR-ASH-5b of $4.4\times10^{-7}$ $ft^3$ $hr^{-1}gal^{-1}$ (compared to the value of $2.5\times10^{-6}$ $ft^3$ $hr^{-1}$ $gal^{-1}$ observed in HGR-ASH-3). Note that the data shown in Figure 3-8 suggests a continuing, increasing trend, suggesting that the final, steady-state HGR at 75 °C is likely higher than values recorded. This final value is approximated by fitting the hydrogen concentration data recorded during HGR-ASH-5b to a first-principles model equation derived from the differential equations that govern the dynamics of vapor mixing in the headspace of the reaction vessel, such as shown in Equation 7.

$$y_{H_2}(t) = y_{H_2}^{MAX}\left(1 - e^{-t/\tau}\right) \qquad \text{Equation 7}$$

where $y_{H_2}(t)$ is the time-dependent concentration of hydrogen in the vessel headspace, $y_{H_2}^{MAX}$ is the maximum hydrogen concentration achieved at equilibrium, and $\tau$ is the characteristic timescale of the mixing phenomena (e.g., residence time). The results of this fit are shown in Figure 3-9.

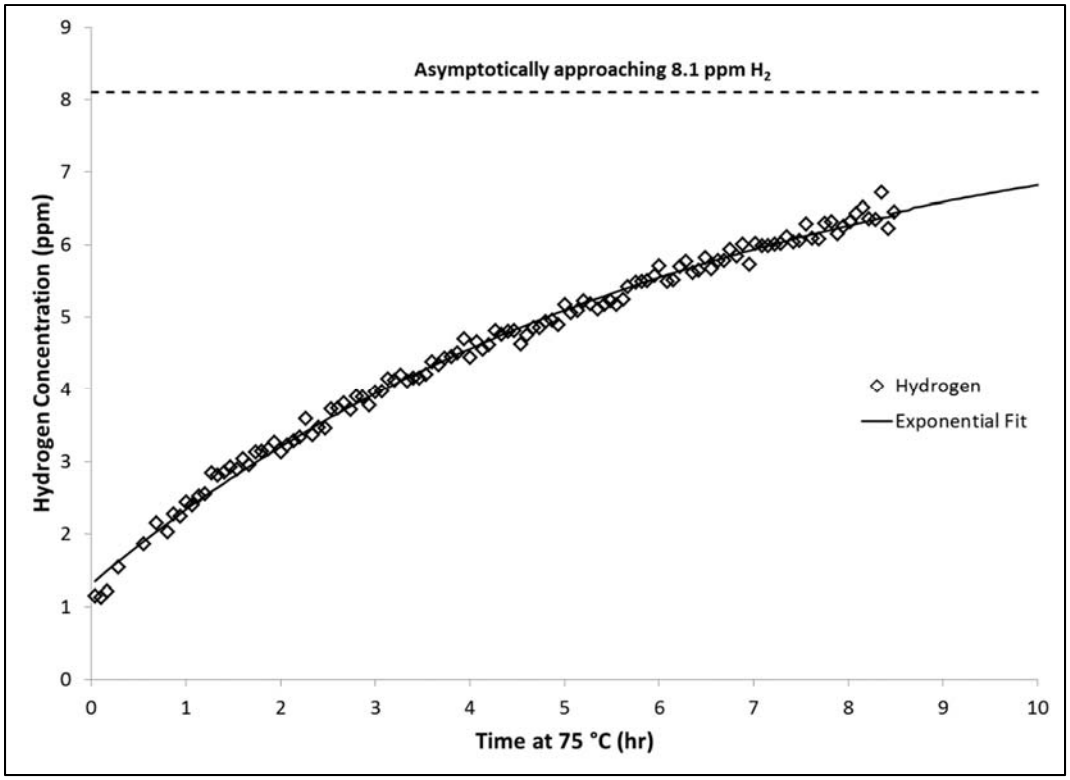


**Figure 3-9. Hydrogen Concentration as a Function of Time for Run HGR-ASH-5b.**

The fit shown in Figure 3-9 suggests that the steady state concentration of $H_2$ during HGR-ASH-5b is approximately 8.1 ppm, yielding an HGR of $5.4\times10^{-7}$ $ft^3$ $hr^{-1}$ $gal^{-1}$. This rate is significantly lower than that measured at 114 °C, suggesting an expected dependence of hydrogen generation on temperature. By using this estimated rate along with the average observed HGR at 114 °C ($3.8\times10^{-6}$ $ft^3$ $hr^{-1}$ $gal^{-1}$) and interpolating using an Arrhenius expression, the HGR at 100 °C can be estimated as $2.0\times10^{-6}$ $ft^3$ $hr^{-1}$ $gal^{-1}$. Note that this interpolation is empirically-derived and assumes that relative contributions to HGR from each H2 production mechanism involved remain constant. Additional testing at lower temperatures is recommended to more completely evaluate the temperature dependence of HGR observed in this testing if further understanding of temperature dependence is desired.

## 3.2 Results from High Boiling Point Simulant Test with Tank Farm Organics

### *3.2.1 HGR Results for HBP Simulant*

Figure 3-10 contains a summary of the results of the HGR measurements using the HBP simulant plotted on a log scale. The temperature is also included for reference. Additional data were collected after addition of 10,000 mg/L of glycolate, which will be included in a future report. Figure 3-10 and Figure 3-11 can be used to understand the sequence of testing and is useful in interpreting the results. Figure 3-11 contains data on the purge rate during the HBP simulant testing along with the process temperature and rod temperature. Purge rate was varied to attain hydrogen detection at low levels when HGR was low and avoid approaching the lower flammability limit for hydrogen when HGR was high. Purge rates up to 10 sccm are achieved using the purge gas (0.5% Kr, 20% $O_2$, 79.5% $N_2$). A purge rate of 370 sccm is achieved using dry air (i.e., compressed air treated to remove water and carbon dioxide). Intermediate purge rates (50 to 100 sccm) are achieved using mixtures of 10 sccm purge gas and the balance dry air. Note that the dry air contains small amounts of atmospheric hydrogen and helium (nominally 0.5 ppmv and 5.24 ppmv, respectively).[18]

Because the dry air purge is only used when the HGR is high, the impact of hydrogen in air on the hydrogen measurement is insignificant (i.e., <1% of the measurement value).

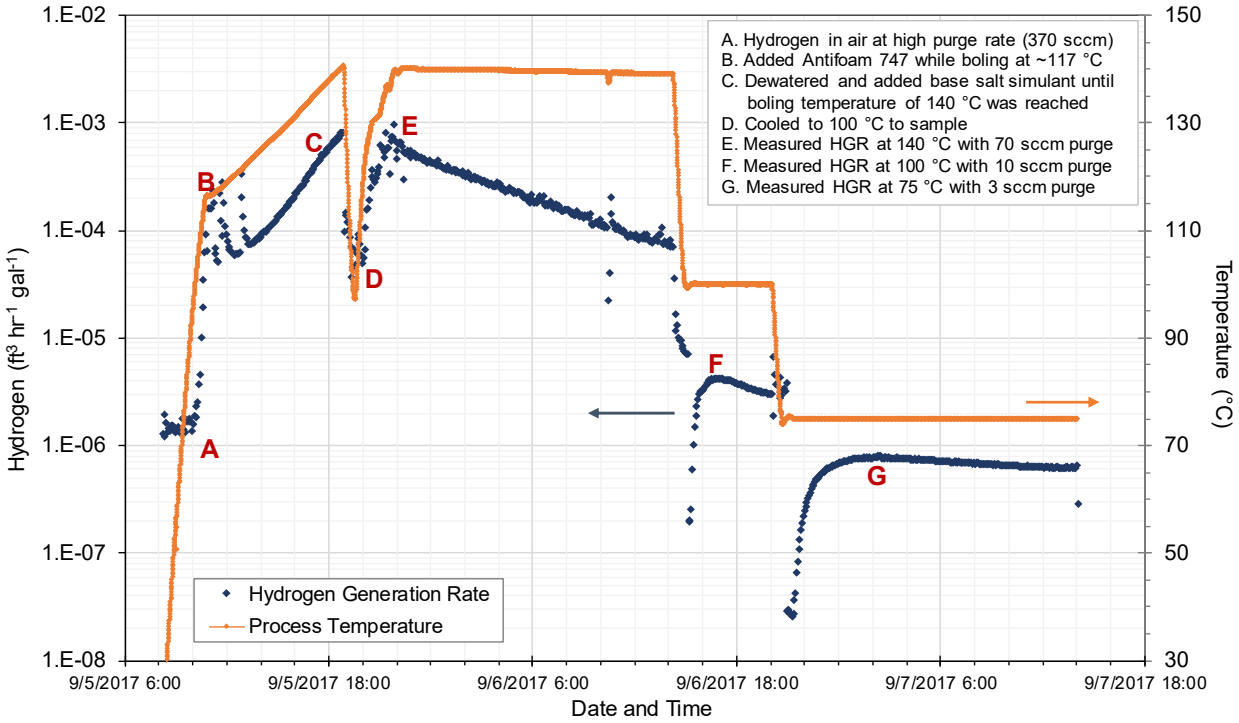


**Figure 3-10. Overall HGR Measurement Results for HBP Simulant**

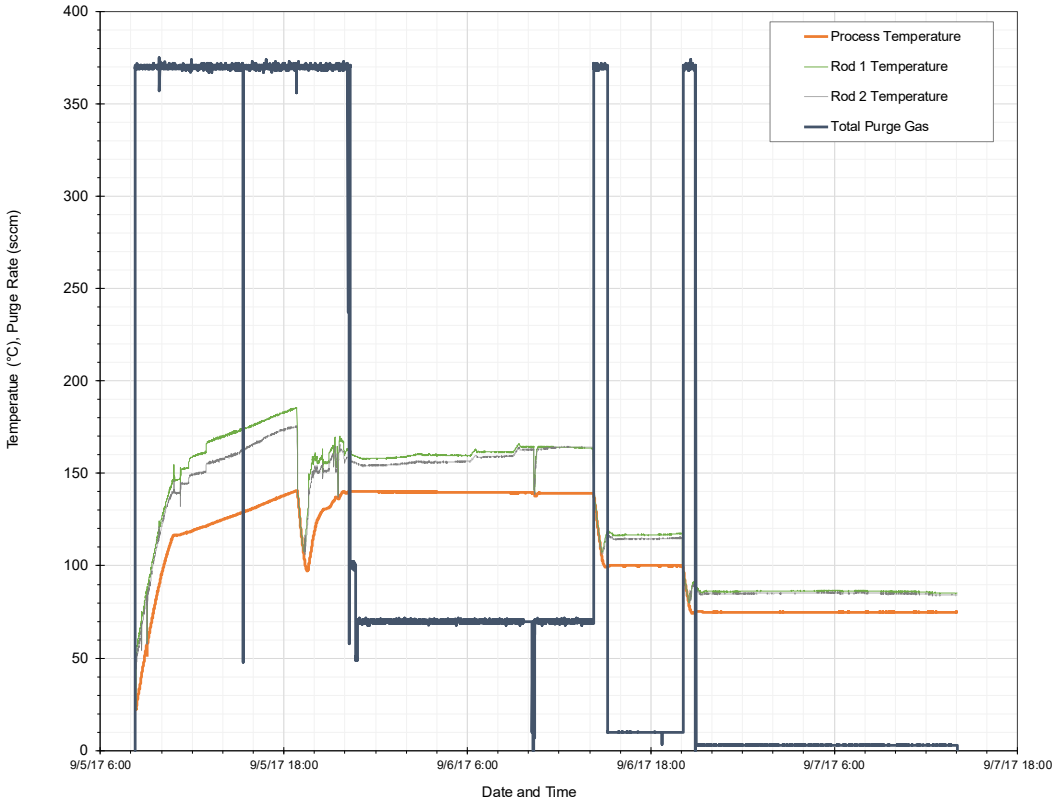


**Figure 3-11. Process Parameters During HBP Simulant HGR Measurements**

Figure 3-12 shows a greater detail of the HGR measurement increase during the dewatering and sampling period of the HBP simulant test. Testing started with the addition of 1685 grams (approximately 1.2 L) of the HBP simulant base salt solution to the vessel, followed by heating to boiling. This portion of testing corresponds to the period around Point A in Figure 3-10. The hydrogen measured at Point A does not constitute a real HGR measurement. Instead, the measured values at point A are due to the hydrogen in the dry air purge multiplied by the relatively large purge rate used during the dewatering phase of testing.

Point B in Figure 3-10 and Figure 3-12 corresponds to reaching the boiling point of the HBP simulant stock solution, which was approximately 117 °C. One quarter of the overall Antifoam 747 addition (3 mL) was made prior to reaching the boiling point of the HBP simulant base salt solution. The three subsequent 3 mL additions of Antifoam 747 were made while dewatering and feeding of additional HBP simulant base salt solution. The four small peaks in the HGR noted near Point B correspond to initially achieving boiling and the three subsequent Antifoam 747 additions. The HGR corresponding to the initial boiling and the subsequent three antifoam additions at boiling are $2.4\times10^{-4}$, $2.2\times10^{-4}$, $2.8\times10^{-4}$, and $3.4\times10^{-4}$ $ft^3\ hr^{-1}\ gal^{-1}$, respectively.

The period from Point B to Point C in Figure 3-10 and Figure 3-12 is the gradual dewatering and feeding additional HBP simulant base salt solution to attain a solution with an atmospheric pressure boiling point of 140 °C. An additional 1041 grams of HBP simulant base salt solution was added during this period. Subsequently, three isothermal HGR measurements were made at 140 °C, 100 °C, and 75 °C (i.e., Points E, F, and G, respectively).

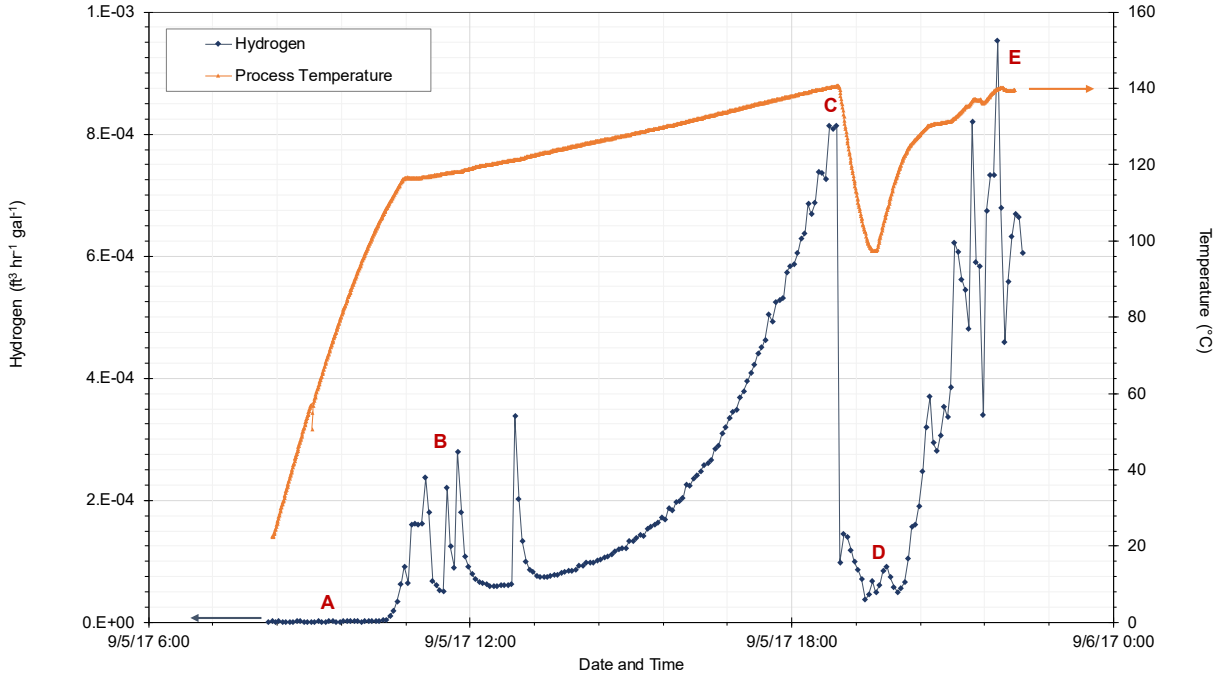


**Figure 3-12. HGR Measurement for the HBP Simulant during Initial Period of Testing**

As mentioned previously, peaks in HGR were noted when boiling at 117 °C was first achieved and at the subsequent additions of Antifoam 747. At the 370 sccm purge rate, little delay was noted between a processing event such as an antifoam addition and the observation of a change in the hydrogen measurement as expected given the higher purge rate of the vessel vapor space. This rapid response contrasts with the large delays noted at lower purge rates (3 to 10 sccm) used during portions of testing. Ultimately, the HGR at 140 °C was $8.1\times10^{-4}$ $ft^3$ $hr^{-1}$ $gal^{-1}$ in the freshly prepared HBP simulant. The solution was cooled to 100 °C so that the "Pre 140 °C" sample could be collected (Point D). At Point D, the HGR at 100 °C was approximately $5\times10^{-5}$ $ft^3$ $hr^{-1}$ $gal^{-1}$. The rates at Points C, D, and E, corresponding to HGR in the freshly prepared simulant, are not likely to be directly applicable to most of the tank farm conditions because the majority of the organics in the tank farm waste have already been processed through evaporators at some point. Thus, it may be justified for the tank farm to apply a lower persistent HGR rate rather than an initial peak HGR rate depending on their intended use.

It is expected that VOCs are released early in the processing. Isopar® L from the MCU solvent is likely released quickly at or just before when boiling is first attained (near Point B in Figure 3-10 and Figure 3-12). Hexamethyldisiloxane and trimethylsilanol from the decomposition of Antifoam 747 are likely released quickly at or just before the point when boiling is first attained and at the points when additional antifoam is added (Point B). Butanol from the decomposition of tributyl phosphate is likely released during simulant preparation (Point B to Point C) and may continue to be released at smaller amounts throughout the test. The release of these components would not be quantified by the only offgas instrument installed for this test, the GC with gas separation columns. An unidentified peak was seen in the GC chromatograms during HBP simulant testing at boiling and at 100 °C.

Figure 3-13, Figure 3-14, and Figure 3-15 contain the HGR measurement data for the HBP simulant tests at the isothermal conditions of 140 °C, 100 °C, and 75 °C, respectively. The error bars included on a portion of the HGR measurement points are the two sigma uncertainties from the uncertainty analysis described in Section 2.3.2. The data that display error bars are the data used as the initial and final HGR measurements.

Krypton data are also included on these graphs as an indication of the earliest that steady state measurements may have been detectable due to mixing delays. In general, krypton concentration is seen to increase, starting at 0 ppmv and ending at the mixture concentration with the relation expected of a continuous stirred tank reactor (CSTR). At the boiling condition, the krypton increases faster than would be expected for a CSTR of the same volume due to impacts of the extra water vapor present and the increased temperature.

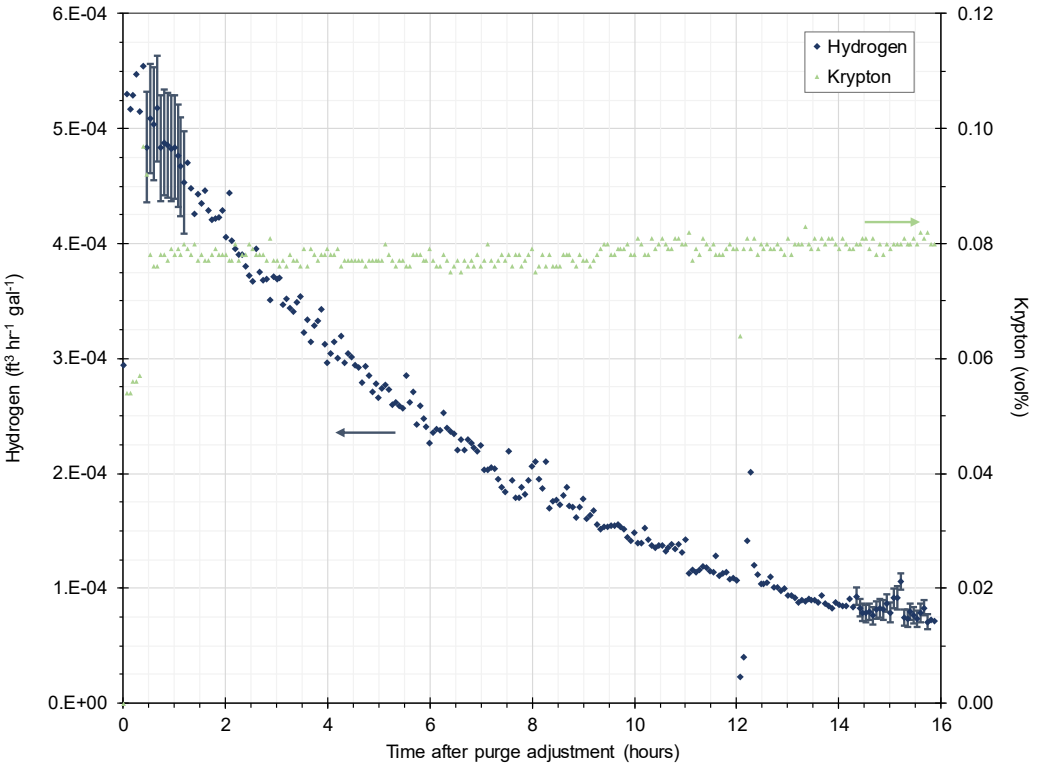


**Figure 3-13. HBP Simulant HGR Measurement at 140 °C**

Figure 3-13 displays the HGR measurement data for the HBP simulant at 140 °C with a purge rate of approximately 70 sccm. The inconsistency in HGR noted near 12 hours was due to a temporary disruption in the purge gas supply. The initial HGR averaged $4.9\times10^{-4}$ $ft^3$ $hr^{-1}$ $gal^{-1}$ and the final HGR averaged $8.1\times10^{-5}$ $ft^3$ $hr^{-1}$ $gal^{-1}$. The initial rate has a low bias because of the time delay in achieving the appropriate purge rate for accurate measurement after attaining the 140 °C boiling condition. The measurement condition was maintained for approximately 16 hours. The initial and final HGRs were measured for 48 and 88 minutes, respectively. Krypton measurements during this test indicate a relatively rapid approach to steady state. Because of the relatively large uncertainty in the flow rate of dry air, krypton was used to determine the precise purge rate. The two-sigma uncertainty associated with this data is 10%. Steady HGR values were not attained, and carrying out this measurement over a longer period of time would be expected to lead to a lower final HGR measurement. The decaying HGR with time at isothermal conditions and constant purge rates suggest either that the ongoing consumption of an organic reactant important in the production of hydrogen is appreciable on the time scale of the experiment, or that another factor is leading to poisoning of the reaction. For instance, Hu[11] and Ashby[10] suggest a dependence of thermolytic HGR on aluminum concentration, and the upcoming sections include data that show aluminum concentration decreased during testing likely due to the precipitation of sodium aluminosilicates. As will also be seen in upcoming sections, the portion of the TOC that corresponds to components other than formate and oxalate also decreased during HGR measurement at 140 °C.

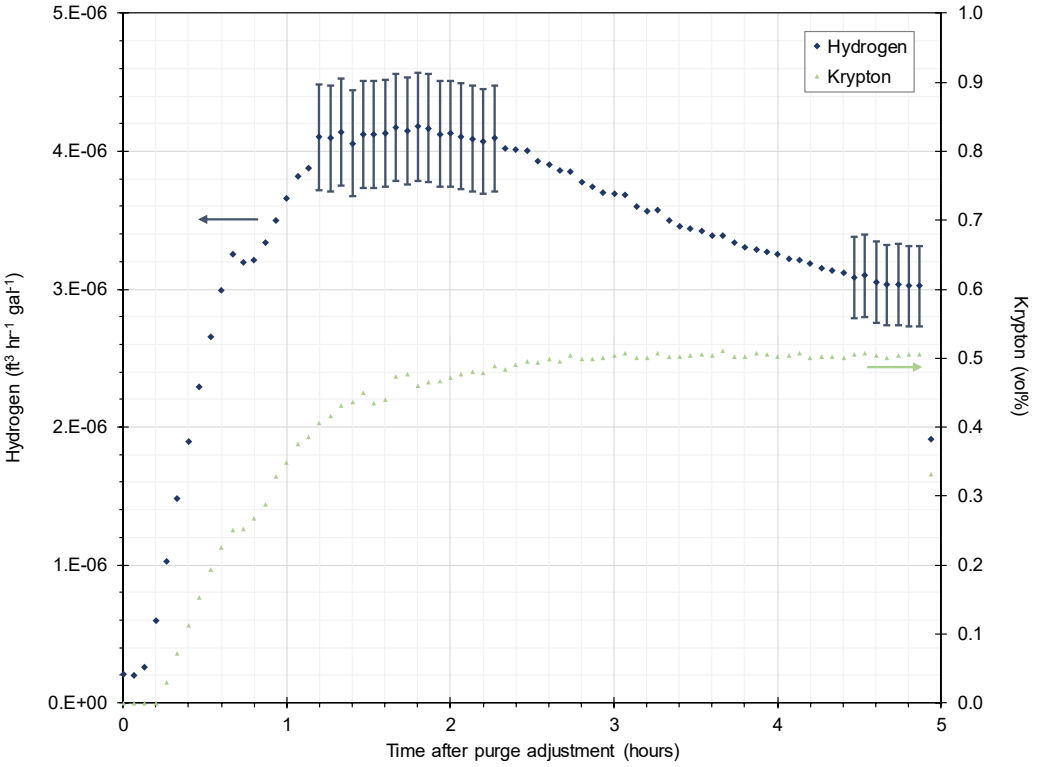


**Figure 3-14. HBP Simulant HGR Measurement at 100 °C**

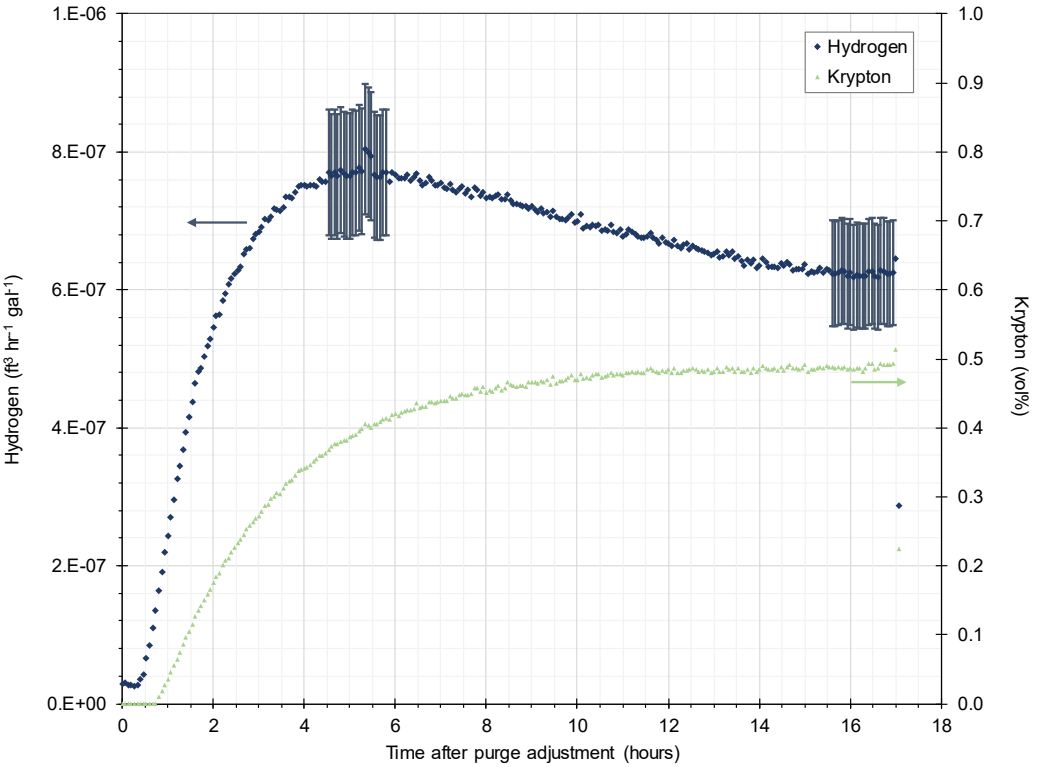


**Figure 3-15. HBP Simulant HGR Measurement at 75 °C**

Figure 3-14 displays the HGR measurement data for the HBP simulant at 100 °C with a purge rate of approximately 10 sccm. The initial HGR averaged $4.1\times10^{-6}$ $ft^3$ $hr^{-1}$ $gal^{-1}$ and the final HGR averaged $3.0\times10^{-6}$ $ft^3$ $hr^{-1}$ $gal^{-1}$. The two-sigma uncertainty associated with this data is 10%. Steady HGR values were not attained and these data are dependent on the process history of the previous 140 °C measurement. As with the 140 °C data, the offset of the HGRs determined for the initial and final periods suggest either that the ongoing consumption of a reactant important in the production or hydrogen (i.e., a specific organic or aluminum) is appreciable on the time scale of the experiment, or that another factor is leading to poisoning of the reaction. The measurement condition was maintained for approximately 5 hours. The initial and final HGRs were measured for 68 and 28 minutes, respectively.

Figure 3-15 displays the HGR measurement data for the HBP simulant at 75 °C with a purge rate of approximately 3 sccm. The initial HGR averaged $7.7\times10^{-7}$ $ft^3$ $hr^{-1}$ $gal^{-1}$ and the final HGR averaged $6.2\times10^{-7}$ $ft^3$ $hr^{-1}$ $gal^{-1}$. The two-sigma uncertainty associated with this data is 12%. A relatively steady HGR was attained for a final 75 °C measurement. These data are dependent on the process history of the previous measurements. As with the previous data, the offset of the HGRs determined for the initial and final periods suggest either that the ongoing consumption of a reactant important in the production of hydrogen (i.e., a specific organic or aluminum) is appreciable on the time scale of the experiment, or that another factor is leading to poisoning of the reaction. The measurement condition was maintained for approximately 17 hours. The initial and final HGRs were each measured for 80 minute periods.

A tabulated summary of the initial and final HGR measurements obtained during HBP simulant testing is contained in Table 3.4. The estimated uncertainties are two-sigma values based on the HGR measurement uncertainty analysis described in Section 2.3.2. An asterisk is placed by all uncertainties due to the impact of previous measurements would likely contribute to measurements well outside of the uncertainty if HGR measurements were repeated in a different sequence.

**Table 3.4. HGR Measurements for HBP Simulant**

| Temperature (°C) | Hydrogen Generation Rate ($ft^3$ $hr^{-1}$ $gal^{-1}$) | Estimated Uncertainty (95% confidence interval) |
|---|---|---|
| 140.1 (boiling) initial | $4.9\times10^{-4}$ | 10%* |
| 139.1 (boiling) final | $8.1\times10^{-5}$ | 10%* |
| 100.0 initial | $4.1\times10^{-6}$ | 10%* |
| 100.0 final | $3.0\times10^{-6}$ | 10%* |
| 75.0 initial | $7.7\times10^{-7}$ | 12%* |
| 75.0 final | $6.2\times10^{-7}$ | 12%* |

* Uncertainties do not reflect the consistent decrease in HGR with time, thus the inability to generate hydrogen at a steady rate at isothermal conditions. Reported uncertainties are thus only applicable to each condition considering the process history. The uncertainties for these results were calculated by inserting the inputs for Equations 5 and 4 (for 140 °C and other temperatures, respectively; see Section 2.3.2) into the software package, GUM workbench [23], to derive a formula for the overall uncertainty. This formula was then used to calculate uncertainty using the software package JMP™ Pro, Version 11.2.1[24].

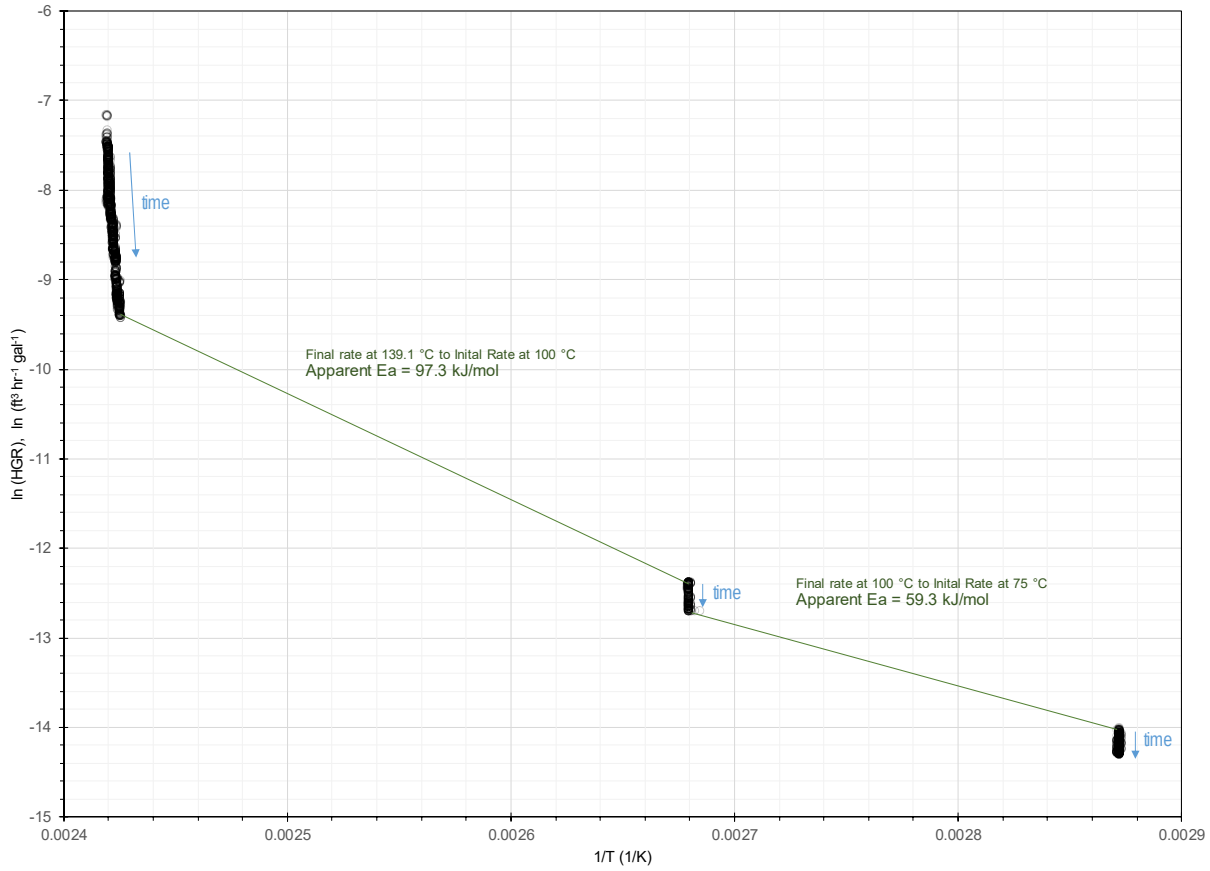


**Figure 3-16. Arrhenius Plot for HBP HGR Measurements**

Figure 3-16 is an Arrhenius plot for the HBP HGR measurements showing two apparent activation energies. Significant reduction of HGR was noted at each temperature, and the vertical lines of data correspond to the range of HGR measurement at each temperature. In general, the HGR trended lower with the progression time. Because the tests were performed in series using the same material and reaction rates were decreasing during measurements, it is not possible to formulate an activation energy that would represent the entire test. Figure 3-16 shows that the apparent activation energy based on the final measurements taken at 140 °C and the initial measurements taken at 100 °C is 97.3 kJ/mol. The apparent activation energy based on the final measurements taken at 100 °C and the initial measurements taken at 75 °C is 59.3 kJ/mol. In general, there are additional uncertainties because the precise mechanisms for hydrogen generation have not been identified. The various TOC components added in this testing would likely have their own individual reaction rate and temperature dependence. As seen in Section 3.1.4 and Appendix A, organic contaminants in the simulant components may also contribute to the overall HGR measurement.

In Table 3.5, inputs for TOC and aluminum concentration measured in samples were used to evaluate HGR by the methodology of Hu shown in Equation 1. A reactivity factor of 1 was used. Initial and final HGR measurements were used for each condition. By comparison to the HGR measured in this work, Equation 1 predictions were higher than the HBP simulant HGR measurements. By comparing the HGR measurement to the Equation 1 predictions, the apparent reactivity factor was 0.82 for the initial 140.1 °C condition and averaged 0.25 for the other five conditions. The decrease in reactivity in subsequent test conditions is greater

than the decrease in the Equation 1 predictions using the measured TOC and aluminum concentrations. Perhaps use of adjusted TOC (subtracting formate and oxalate) is a better parameter for this evaluation.

**Table 3.5. Comparison of HBP Simulant HGR Measurement to HGR Calculated by Equation 1**

| Temperature (°C) | HGR Measurement ($ft^3\ hr^{-1}\ gal^{-1}$) | TOC (wt%) | Al (wt%) | Hu (Eqn. 1) HGR ($ft^3\ hr^{-1}\ gal^{-1}$) |
|---|---|---|---|---|
| 140.1 (boiling) initial | $4.9\times10^{-4}$ | 0.119 | 1.55 | $5.9\times10^{-4}$ [a] |
| 139.1 (boiling) final | $8.1\times10^{-5}$ | 0.0958 | 0.657 | $3.2\times10^{-4}$ [a] |
| 100.0 initial | $4.1\times10^{-6}$ | 0.0958 | 0.657 | $2.0\times10^{-5}$ |
| 100.0 final | $3.0\times10^{-6}$ | 0.0875 | 0.624 | $1.8\times10^{-5}$ |
| 75.0 initial | $7.7\times10^{-7}$ | 0.0875 | 0.624 | $2.3\times10^{-6}$ |
| 75.0 final | $6.2\times10^{-7}$ | 0.0877 | 0.583 | $2.2\times10^{-6}$ |

[a] Calculation of the Hu HGR for the HBP test at ~140 °C is an extrapolation outside of the temperature range that the equation was developed for.

### *3.2.2 Nitrous Oxide Generation from HBP Simulant*

Nitrous oxide ($N_2O$) was observed during the first half of the test at the highest measurement temperature (140 °C), after which it was below the LOD of the GC of approximately 0.018 vol% $N_2O$. Figure 3-17 shows that $H_2$ was generated at approximately 1.8 times the concentration of $N_2O$ for the first several hours of the test. The $[H_2]/[N_2O]$ increased to almost 3 as the $N_2O$ concentration approached the LOD. The change in this concentration ratio may indicate a depletion of a reactant required for $N_2O$ generation or a change in the mechanism of $N_2O$ generation.

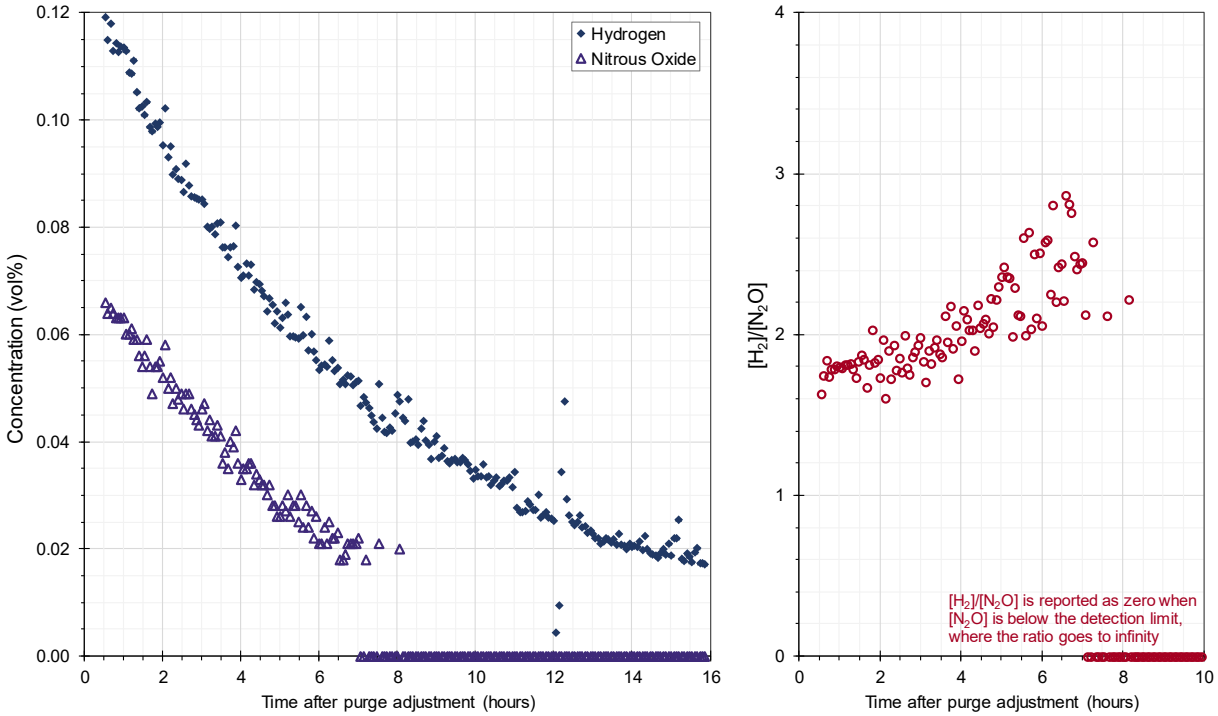


**Figure 3-17. Hydrogen and Nitrous Oxide Generated during HBP Test at 140 °C (left), and the Hydrogen to Nitrous Oxide Ratio for HBP Test at 140 °C (right)**

### *3.2.3 HBP Simulant Methane Results for HBP Simulant*

The time regimes A through G in Figure 3-18 correspond to the plot shown in Figure 3-10. There was a relatively constant methane concentration at 140 °C (regime E) concurrent with a decreasing hydrogen concentration. The nearly constant methane concentration trend matches the expectation for isothermal thermolysis production when the parent reactant (presumably organic) is present in excess. In contrast, the declining hydrogen concentration is more typical of a parent species present in limited quantities and rapidly reacting at the elevated temperature. (Although it is not possible to link the behavior with specific organics in the broad mixture and limited test data, pretest expectations were that the ion exchange resin would have higher relative stability and the antifoam would undergo rapid degradation.) In any case, the differing concentration trends may reflect different reaction schemes for hydrogen and methane. One caveat to mention in the HBP testing is that the highest temperature was tested first, followed by lower temperatures, thus some of the original organic could have been consumed and biased the remaining lower temperatures tested. However, this testing scheme should represent a bounding scenario of tank waste behavior after evaporation. Further thermolysis HGR testing involving the reverse of this temperature progression (i.e., from lower temperatures up to the boiling temperature) would be required to test tank waste behavior leading up to evaporation.

In contrast to the behavior during boiling (140 °C), at non-boiling conditions (100 °C for regime F, and 75 °C for regime G), the methane and hydrogen concentrations curves are highly correlated, and the methane concentration matches or slightly exceeds that of hydrogen after boiling. The shift in methane trend from constant at the higher temperature to varying at the lower temperature may suggest that the reaction occurring at boiling ceases, or is greatly diminished, at the lower temperature while a lower yield second reaction, obscured at the elevated temperature, continues at all three temperatures.

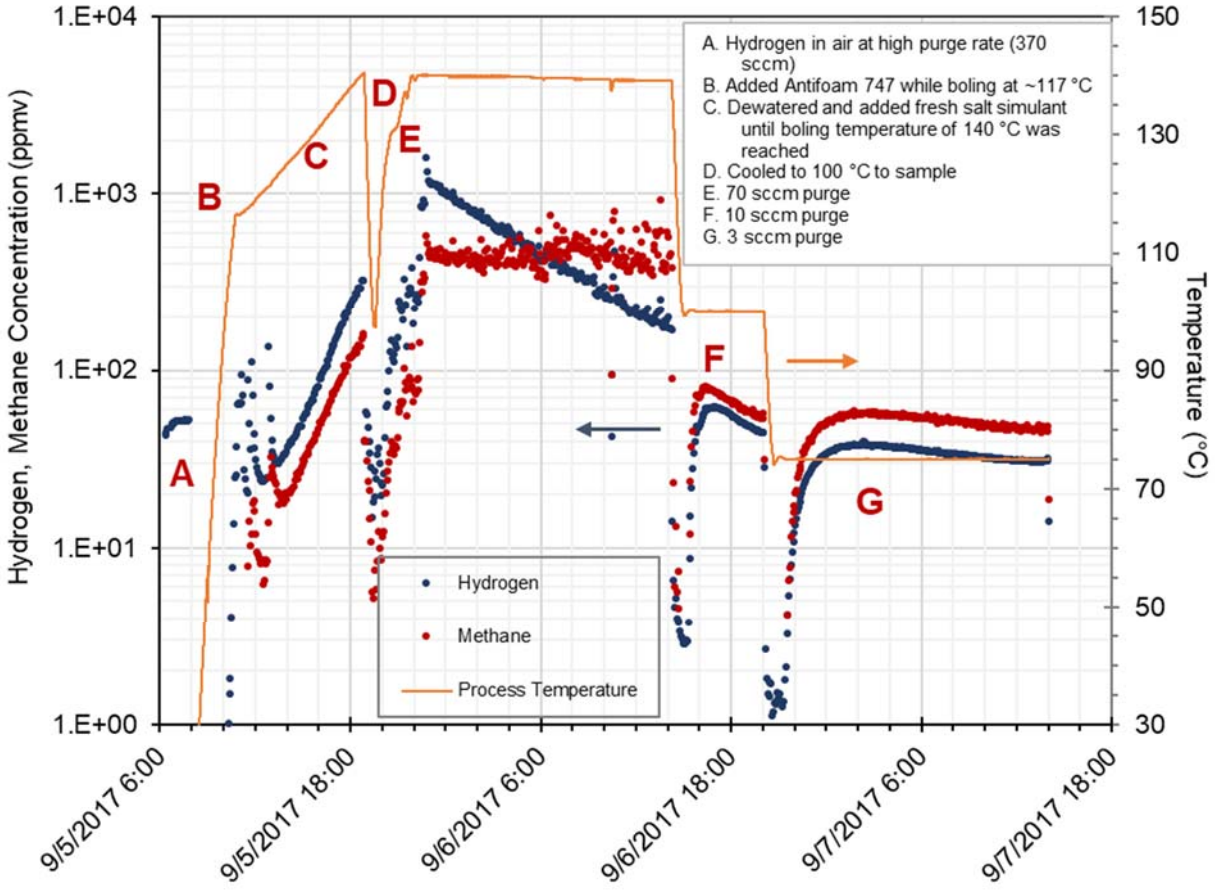


**Figure 3-18. Concentrations for Hydrogen and Methane for HBP Testing**

*3.2.4 Feed and Product Analysis*

Table 3.6 contains the results of the measurement of the base salt simulant used to create the HBP simulant prior to evaporation and concentration. The target recipe concentration (as first described in Section 2.1.3) is given for reference. OB is included in the table as an approximation of the aluminum (aluminate) concentration in the absence of ICP-AES analysis. Reasonable agreement is noted, but the hydroxide and aluminate (based on OB) were higher than the recipe target and the nitrate was lower than the recipe target. A TOC concentration of 258 mg carbon/L was measured, though no organic carbon was intentionally added in this simulant. No volatile or semivolatile organics were identified or measured above the detection limit.

**Table 3.6. Analysis of the Base Salt Solution Used to Create the HBP Simulant**

| Analyte | Units | AD Measurement | PSAL Measurement | Target |
|---|---|---|---|---|
| $OH^-$ | M | 5.71 | -- | 5.48 |
| $NO_2^-$ | M | 2.15 | 2.26 | 2.14 |
| $NO_3^-$ | M | 1.66 | 2.11 | 2.12 |
| $CO_3^{2-}$ | M | 0.0083 | -- | 0 |
| $CHO_2^-$ | M | < 0.002 | < 0.002 | 0 |
| $C_2O_4^{2-}$ | M | < 0.001 | < 0.001 | 0 |
| $PO_4^{3-}$ | M | < 0.001 | < 0.001 | 0 |
| $SO_4^{2-}$ | M | < 0.001 | < 0.001 | 0 |
| $F^-$ | M | < 0.005 | < 0.005 | 0 |
| $Cl^-$ | M | < 0.003 | < 0.003 | 0 |
| $Br^-$ | M | < 0.001 | -- | 0 |
| OB | M | 0.73 | -- | 0.52 |
| TC | mg C/L | 358 | -- | 0 |
| TOC | mg C/L | 258 | -- | 0 |
| SVOA | mg/L | < 1.0 | -- | 0 |
| VOA | mg/L | < 0.25 | -- | 0 |
| density | g/mL | -- | 1.4087 | -- |

Table 3.7 and Table 3.9 contain the analytical results of the samples taken during the HBP HGR measurement test and Table 3.8 is a summary of the carbon species identified in the samples. Table 3.9 also contains the PSAL ICP-AES analysis of the "Base Salt Solution" feed, which is the same solution that has analytical results reported in Table 3.6. The "Pre 140 °C" sample was collected after the organics have been added and additional Stock Solution was added continuously and boiled-down to a mixture that had an atmospheric boiling point of approximately 140 °C. This sample was effectively at the start of the 140 °C HGR measurement. The "Post 140 °C" sample was collected at the end of the 140 °C HGR measurement and just prior to the initiation of the 100 °C HGR measurement. Due to a salt blockage, the sampler needed to be replaced to take the "Post 140 °C" sample. The sampler that was removed after the "Post 140 °C" condition contained a portion of the resin beads that were added at the start of the test. The "Post 100 °C" sample was collected at the end of the 100 °C HGR measurement, prior to the initiation of the 75 °C HGR measurement. The "Post 75 °C" sample was collected at the end of the 75 °C HGR measurement. At ambient temperature, the pre- and post-measurement HBP simulant samples were saltcake mixtures with considerable solids. The physical characteristics of these samples made it difficult to determine the density.

An estimation of the density of the pre- and post-measurement HBP simulant samples is 1.66 g/mL at ambient temperature. This was determined through repeated measurement by volumetric flask of a heated sample while it was cooling. This method should be considered to have a greater uncertainty than the typical density measurement, possibly up to 10% 1σ uncertainty.

As seen in Table 3.7 and Table 3.9, many of the salt components remain constant during testing. Sodium, nitrite, nitrate, formate, and oxalate did not appear to significantly increase or decrease during testing beyond what can be attributed to analytical uncertainty. However, from Table 3.9 the soluble aluminum

(aluminate) dropped by more than 50% during the 140 °C HGR measurement and continued to drop at subsequent temperatures. This finding is consistent with the formation of sodium aluminosilicate noted during testing. This change in aluminum concentration is expected to contribute to a decrease in HGR during the measurement tests based on Equation 1. Silicon and potassium increased due to the dissolution of the borosilicate glassware.

The carbon balance of Table 3.8 shows that the portion of the soluble TOC that is not due to formate or oxalate is about 65% of the TOC in the pre-measurement sample and drops to roughly 40% of the TOC in post-measurement samples. Formate remained relatively constant at the amount added in the simulant while oxalate increased from the amount added in the post 140 °C sample. The added amounts listed in the table contain the full amount of carbon contained in formate, oxalate, antifoam, tributyl phosphate, and ion exchange resin. For the MCU solvent, only the non-volatile carbon is included in the carbon contribution because the Isopar L® would leave in the offgas prior to the pre 140 °C sample. The estimate of the added carbon is greater than the pre 140 °C measured TC, TOC, and adjusted TOC for several reasons. Portions of the carbon in tributyl phosphate and antifoam are expected to leave in the offgas before the pre 140 °C sample. Also, carbon in the ion exchange resin would be underrepresented in the sample because much of the resin beads were observed to be intact. If a portion of the organics were concentrated (e.g., at the liquid surface) rather than evenly dispersed in the aqueous phase, this would also bias TOC analysis low by comparison to what was added.

SVOA identified one component at above the detection limit of approximately 4 mg/L. 2,3-dimethyl-2-butanol was reported at levels corresponding to approximately 50 mg/L in the pre-measurement sample and two of the post-measurement samples. However, the library-matched identification of this component is tenuous as the MS spectra of the sample had fragments that were not contained in the library match. Some fragments indicate that the organic might be better identified as a compound with an aromatic ring, possibly one that is not in the MS instrument library.

**Table 3.7. Analysis of Samples Taken During HBP HGR Testing**

| analyte | method | units | 1σ unc. | Pre 140 °C | Post 140 °C | Post 100 °C | Post 75 °C |
|---|---|---|---|---|---|---|---|
| $Na^+$ | ICP-AES | M | 10% | 17.2 | 18.3 | 14.8 | 17.5 |
| $OH^-$ | IC | M | 10% | 9.50 | 10.9 | 9.51 | 10.1 |
| $NO_2^-$ | IC | M | 10% | 3.86 | 4.31 | 3.86 | 4.09 |
| $NO_3^-$ | IC | M | 10% | 3.19 | 3.45 | 3.06 | 3.20 |
| $Al(OH)_4^-$ | ICP-AES | M | 10% | 0.955 | 0.404 | 0.384 | 0.359 |
| $CO_3^{2-}$ | TIC/TOC | M | 10% | 2.45E-02 | 3.59E-02 | 2.89E-02 | 2.76E-02 |
| | | mg/L | | 1470 | 2150 | 1740 | 1660 |
| $CHO_2^-$ | IC | M | 10% | 5.87E-02 | 6.89E-02 | 6.20E-02 | 6.46E-02 |
| | | mg/L | | 2640 | 3100 | 2790 | 2910 |
| $C_2O_4^{2-}$ | IC | M | 10%[a] | < 5.8E-03 | 4.34E-03 | 3.94E-03 | 4.22E-03 |
| | | mg/L | | < 510 | 382 | 346 | 371 |
| TOC | TIC/TOC | mg C/L | 10% | 1980 | 1590 | 1450 | 1460 |

[a] The 1σ uncertainty for oxalate is likely greater than 10% because the measured values were below the instrument calibration curve

**Table 3.8. Summary of Inorganic and Organic Carbon in HBP Tests**

| carbon analyte | units | added[a] | Pre 140 °C | | Post 140 °C | | Post 100 °C | | Post 75 °C | |
|---|---|---|---|---|---|---|---|---|---|---|
| | | | result | 1σ | result | 1σ | result | 1σ | result | 1σ |
| Total Carbon (TIC+TOC) | mg C/L | 2490 | 2270 | 230 | 2020 | 200 | 1800 | 180 | 1790 | 180 |
| TIC (Carbonate Carbon) | mg C/L | 0 | 294 | 29 | 431 | 43 | 347 | 35 | 331 | 33 |
| TOC | mg C/L | 2490 | 1980 | 200 | 1590 | 160 | 1450 | 150 | 1460 | 150 |
| Formate Carbon | mg C/L | 800 | 705 | 70 | 828 | 83 | 744 | 74 | 776 | 78 |
| Oxalate Carbon | mg C/L | 24 | < 138 | -- | 104 | 10 | 95 | 9 | 101 | 10 |
| Adjusted TOC (TOC-Formate-Oxalate) | mg C/L | 1670 | 1280 | 210 | 660 | 180 | 610 | 160 | 580 | 170 |

[a] Does not include volatile MCU organics. Cabon from ion exchange resin and antifoam is approximate.

**Table 3.9. PSAL ICP-AES Analysis of Samples Taken During HBP HGR Testing**

| analyte | units | Base Salt Soluton | Pre 140 °C | Post 140 °C | Post 100 °C | Post 75 °C |
|---|---|---|---|---|---|---|
| Ag | mg/L | < 1.0E+00 | < 4.2E+01 | < 5.0E+01 | < 4.7E+01 | < 4.3E+01 |
| Al | mg/L | 1.61E+04 | 2.58E+04 | 1.09E+04 | 1.04E+04 | 9.69E+03 |
| Ba | mg/L | < 1.0E-01 | < 4.2E+00 | < 5.0E+00 | < 4.7E+00 | < 4.3E+00 |
| Ca | mg/L | 9.01E-01 | 5.57E+00 | 1.09E+01 | 9.48E+00 | 1.04E+01 |
| Cr | mg/L | 6.65E-01 | < 4.2E+00 | < 5.0E+00 | < 4.7E+00 | < 4.3E+00 |
| Cu | mg/L | < 1.0E+00 | < 4.2E+01 | < 5.0E+01 | < 4.7E+01 | < 4.3E+01 |
| Fe | mg/L | 5.93E+00 | 1.10E+01 | 9.63E+00 | 7.89E+00 | 9.51E+00 |
| Hg | mg/L | < 1.0E+00 | < 4.2E+01 | < 5.0E+01 | < 4.7E+01 | < 4.3E+01 |
| K | mg/L | 1.59E+01 | 5.45E+01 | 1.82E+02 | 1.73E+02 | 2.02E+02 |
| Li | mg/L | < 1.0E+00 | < 4.2E+01 | < 5.0E+01 | < 4.7E+01 | < 4.3E+01 |
| Mg | mg/L | < 1.0E-01 | < 4.2E+00 | < 5.0E+00 | < 4.7E+00 | < 4.3E+00 |
| Mn | mg/L | < 1.0E-01 | < 4.2E+00 | < 5.0E+00 | < 4.7E+00 | < 4.3E+00 |
| Na | mg/L | 2.68E+05 | 3.96E+05 | 4.21E+05 | 3.41E+05 | 4.02E+05 |
| Ni | mg/L | < 1.0E-01 | < 4.2E+00 | < 5.0E+00 | < 4.7E+00 | < 4.3E+00 |
| P | mg/L | < 2.0E+00 | < 8.5E+01 | < 1.0E+02 | < 9.4E+01 | < 8.5E+01 |
| Pd | mg/L | < 1.0E+00 | < 4.2E+01 | < 5.0E+01 | < 4.7E+01 | < 4.3E+01 |
| Rh | mg/L | < 1.0E+00 | < 4.2E+01 | < 5.0E+01 | < 4.7E+01 | < 4.3E+01 |
| Ru | mg/L | < 1.0E+00 | < 4.2E+01 | < 5.0E+01 | < 4.7E+01 | < 4.3E+01 |
| S | mg/L | 6.39E+00 | < 4.2E+01 | < 5.0E+01 | < 4.7E+01 | < 4.3E+01 |
| Si | mg/L | 9.69E+00 | 1.80E+03 | 1.08E+03 | 1.28E+03 | 6.32E+02 |
| Sn | mg/L | < 1.0E+00 | < 4.2E+01 | < 5.0E+01 | < 4.7E+01 | < 4.3E+01 |
| Ti | mg/L | < 3.0E+00 | < 1.3E+02 | < 1.5E+02 | < 1.4E+02 | < 1.3E+02 |
| Zn | mg/L | < 1.0E+00 | < 4.2E+01 | < 5.0E+01 | < 4.7E+01 | < 4.3E+01 |
| Zr | mg/L | < 1.0E+00 | < 4.2E+01 | < 5.0E+01 | < 4.7E+01 | < 4.3E+01 |

### *3.2.5 Precipitated Solids Analysis*

After completion of the HBP simulant test (including tests with glycolate that are not included in this report), the mixer and heating rods were removed from the pot while the material was cooling. Figure 3-19 contains two photographs taken early in the cooling period. The image on the left shows the yellow to brown colored liquid above white solids at the bottom of the vessel. The presence of the white solids at the bottom of the vessel was noted during simulant boil down and the first set of testing at 140 °C and these solids persisted throughout the test. The image on the right shows a small amount of persistent foam on the surface of the liquid. The image also shows some of the solids that accumulated above the final liquid level.

After the bulk of the cooled simulant was removed from the kettle, the kettle and internals were rinsed several times with water followed by scraping of the residual deposited solids from the surfaces. Figure 3-20 shows an example of the white solids deposited on the agitator that were not removed with water rinsing and subsequent scraping. Similar white solids were noted on the heating rods and on portions of the glass

kettle. Figure 3-21 shows two types of solids that were removed from the kettle that were not very soluble in water. The image on the left shows a portion of a gray colored clump of solids that was unique in appearance from the other solids at the bottom of the kettle. The image on the right shows flakes of the more typical water insoluble solids removed from the kettle.


**Figure 3-19. Appearance of HBP Simulant Material after Testing**

**Figure 3-20. Solids Deposited on Mixer Impeller (and Heating Rods) after HBP Simulant Testing**

**Figure 3-21. Solids Removed from Bottom of Kettle upon Completion of HBP Simulant Testing**

The deposits associated with the sampling tube removed after the 140 °C HGR measurement were rinsed with water and analyzed by SEM with XEDS. Figure 3-22 shows an SEM image for the solid deposits. The XEDS indicated that this material was likely sodium aluminosilicate phases consistent with SRS HLW evaporators. There were also possible nitrate and carbonate salt crystals associated with this deposited material (although these compounds are commonly seen from the dried liquid from solutions of these compositions).

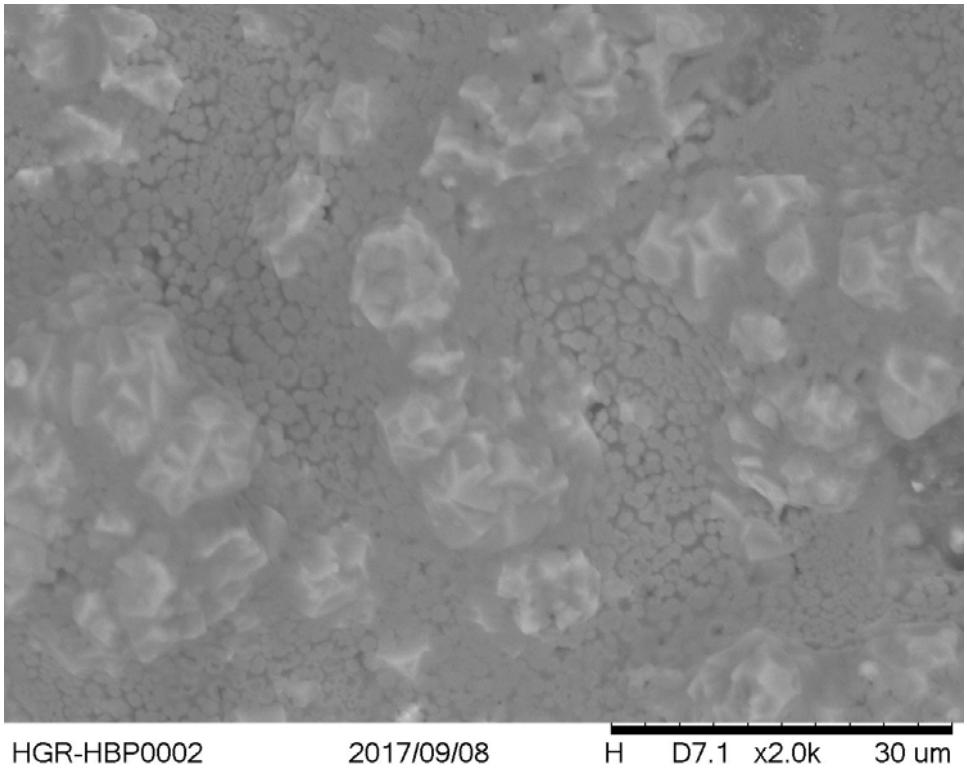


**Figure 3-22. SEM Image of Solid Material Deposited during 140 °C HGR Measurement**

Figure 3-23 contains XRD results for the solids removed from the mixer (and rinsed with deionized water) after the full set of tests with the HBP simulant (including tests with sodium glycolate not included in this report). This white material is shown in Figure 3-20. The results for solids removed from the heating rods and washed from the kettle wall were identical to this result for the mixer solids and thus are not included here separately. The results show either a cancrinite or sodalite phase of sodium aluminosilicate ($Na_8Al_6Si_6O_{24}\cdot(H_2O)_{3,4}\cdot(CO_3)$). The analogous nitrate or hydroxy versions of sodalite and cancrinite are consistent with what is expected in SRS evaporator systems.[29-30] The source of the silicon is likely from the dissolution of the glass kettle material by the concentrated hydroxide solution during this high temperature testing. The Antifoam 747 also contains silicon that could potentially contribute to sodium aluminosilicate formation. Because of the use of the glass kettle, this testing has a much greater silicon concentration than would be typical in the SRS Tank Farm evaporators. Thus, aluminosilicate formation in this testing is not quantitatively representative of the evaporators.

Figure 3-24 contains XRD results for the clump of gray solids removed from the pot after the testing and rinsed with deionized water prior to analysis. This corresponds to the material in left image of Figure 3-21. In addition to the sodalite or cancrinite phase noted in other locations ($Na_8Al_6Si_6O_{24}\cdot(H_2O)_{3,4}\cdot(CO_3)$), this material contained lesser amounts (in decreasing order) of solid sodium oxalate ($Na_2C_2O_4$), the sodium carbonate phase trona ($Na_3H(CO_3)_2\cdot(H_2O)$), and sodium nitrate ($NaNO_3$). There also may be some amorphous material that was not identified by the XRD method.

From Figure 3-25, bright areas of the SEM backscatter image of the gray solids correspond to mercury, as identified by the XEDS. Some localized areas include rod shapes in the SEM image, which is typical of sodium oxalate.

Additional SEM, XEDS, and XRD results for the simulant solids are in Appendix B.

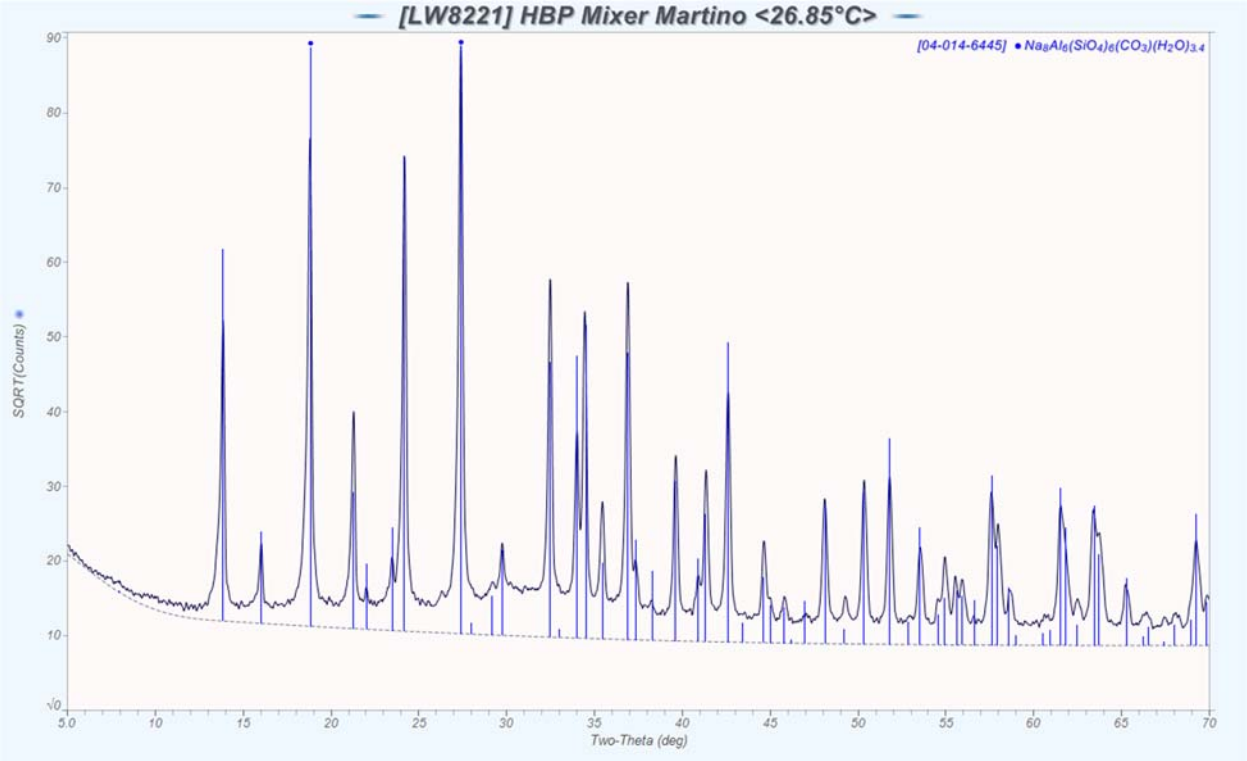


**Figure 3-23. Representative XRD of Solids Deposited on Mixer, Heating Rods, and Walls of Kettle**

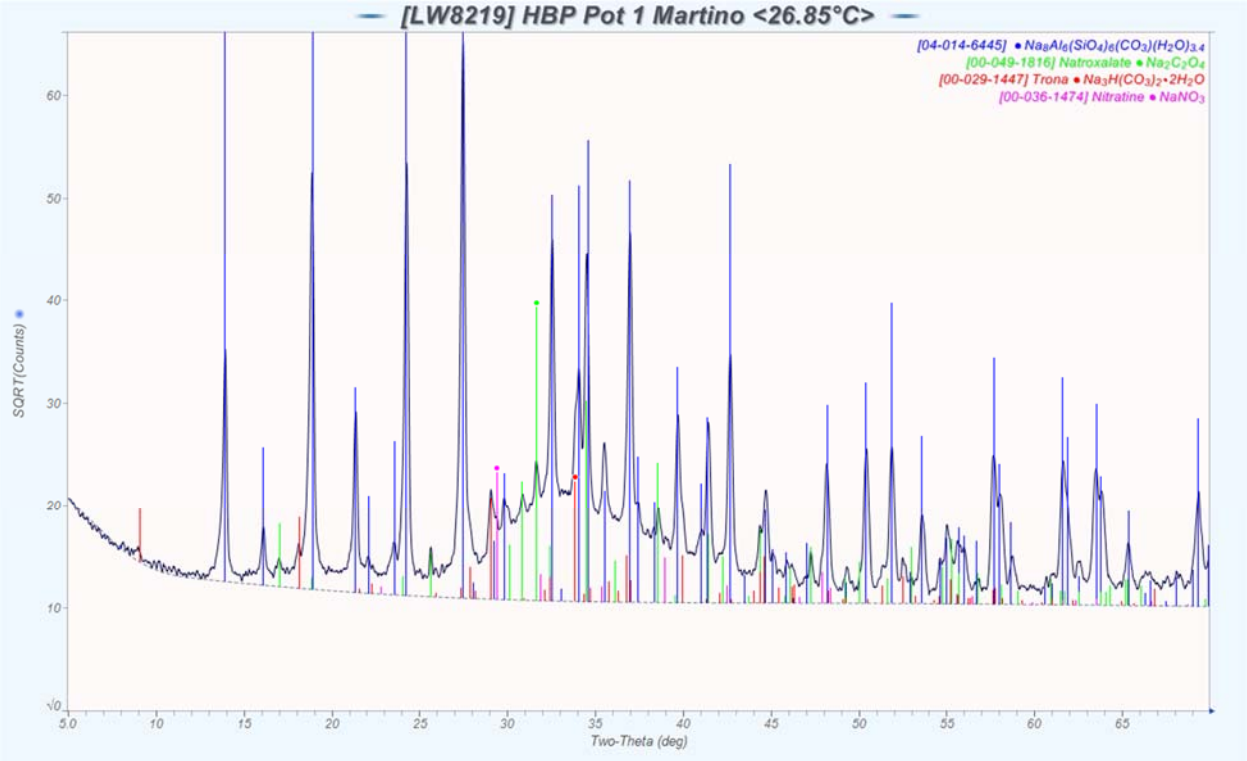


**Figure 3-24. XRD of a Gray Solid Mass Precipitated in the HGR Kettle**

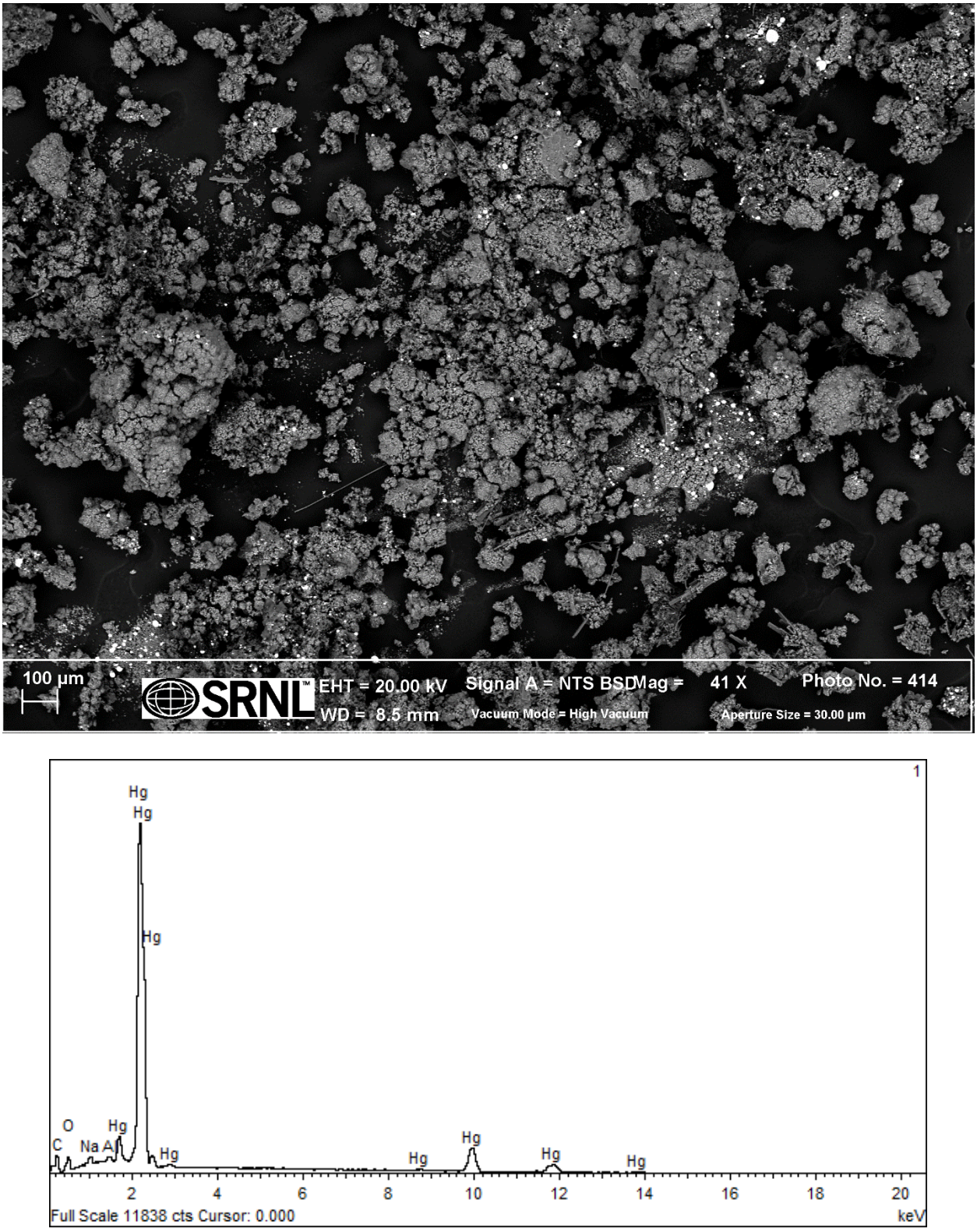


**Figure 3-25. SEM Backscatter Image (top) and XEDS (bottom) of the Gray Solid Mass Precipitated in the HGR Kettle**

## 3.3 Tank 38 Sample Characterization

### *3.3.1 Sample HTF-38-17-60*

Tank 38 waste sample HTF-38-17-60 was taken using a three liter sampler and delivered to SRNL on July 10, 2017. This supernate sample was slightly hazy due to the sample containing a small quantity of insoluble solids. Figure 3-26 shows three photographs of the sample. Insoluble solids had settled to the bottom of the sample bottle (see photograph b). After the solids were resuspended, a portion of the sample was poured into a 125 mL polymethylpentene beaker (see photograph c). The markings on the back of the beaker are only slightly visible through the HTF-38-17-60 material. This is appearance is consistent with tank supernate samples with considerably less than 1 wt% of insoluble solids.

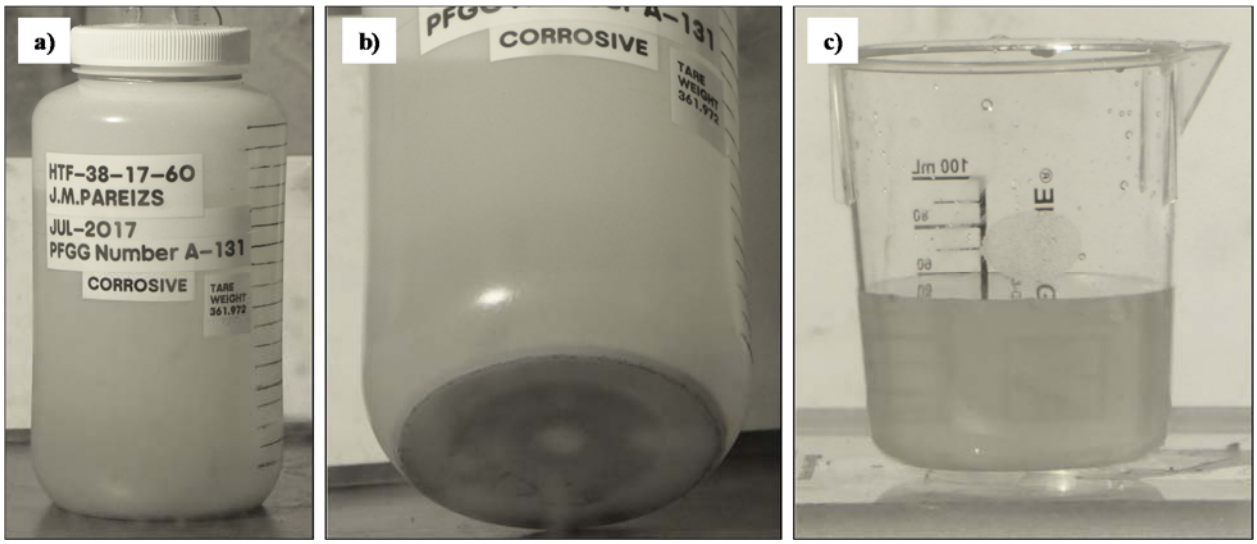


**Figure 3-26. Photographs of sample HTF-38-17 60 in SRNL Shielded Cells, Cell 3: a) sample in 4 L poly bottle, b) solids settled at bottom of bottle, c) 60 mL portion of sample in a clear beaker**

Tank 38 sample HTF-38-17-60 contained 4143.92 g of material. An initial analytical subsample of approximately 157 grams was prepared from the original sample. A portion of the analytical subsample was filtered to produce approximately 40 g of filtrate. Subsequently, the remainder of Tank 38 sample HTF-38-17-60 was split into two approximately 1.1 L portions for testing (1466.44 g and 1465.79 g) and a remaining portion of 1127.71 g. The 1466.44 g portion was used as feed for the test described in Section 3.4 of this report. The other two portions were retained for potential future testing.

### *3.3.2 Initial Analysis of HTF-38-17-60*

The density of the Tank 38 sample HTF-38-17-60 material, including insoluble solids, was 1.327 g/mL (Relative Standard Deviation (RSD) = 0.67%, number of replicates ($n$) = 8). Density was measured at 25 to 27 °C. SVOA was used to determine whether there were any identifiable organic components. The result of SVOA was that all individual SVOA analytes were less than 1 mg/L in sample HTF-38-17-60.

Table 3.10 contains results for sodium, anions, TB/OH/OB, and TIC/TOC. Table 3.11 contains results for other analyses, primarily ICP-AES, ICP-MS, AA, and CVAA. The ICP-AES results for sodium (as $Na^+$) and aluminum (as $Al(OH_4)^-$) are also included in Table 3.10 so that an they can be included in the cation/anion balance. Other ICP-ES, ICP-MS, and AA analytes are ignored in the cation/anion balance due to their expected minimal impact on the balance.

As seen in Table 3.10, the 7.79 M of sodium balanced with the anions (i.e., 8.14 N) within analytical uncertainty, indicating a 0.35 N imbalance toward anions. The major anions were 2.85 M hydroxide, 2.37 M nitrite, 1.27 M nitrite, 0.67 M carbonate, and 0.094 M aluminate. The formate and oxalate were 1570 mg/L and 441 mg/L, respectively. The overall TOC was measured on an undiluted portion of sample as 676 mg carbon/L. Each of these measurements have a 1σ analytical uncertainty of 10%. The unidentified species that contribute to TOC not due to carbon from formate and oxalate thus sum to 136 mg carbon/L with a 1σ uncertainty of 80 mg carbon/L.

Surface and sub-surface samples from Tank 38 were previously analyzed most recently for samples HTF-38-17-52 and HTF-38-17-53 collected in June 2017.[31] The density, sodium, hydroxide, and many of the major components were very similar in HTF-38-17-52, HTF-38-17-53, and HTF-38-17-60. The formate is slightly (~10%) lower in the current sample HTF-38-17-60 when compared to the previous surface sample HTF-38-17-52. Oxalate in the current sample is only 60% of the concentration in the previous sample.

Table 3.11 shows agreement within analytical uncertainty for the acid diluted sample and the water diluted filtrate. One high value for water diluted filtrate silicon analysis is not included in the overall average because it is an outlier when compared with the other five measurements. The lower detection limit value of the two preparations is reported as the overall best detection limit.

**Table 3.10. Ionic Composition of Tank 38 Sample HTF-38-17-60**

| analyte | method | units | 1σ unc. | water diluted filtrate | |
|---|---|---|---|---|---|
| | | | | average | RSD |
| $Na^+$ | ICP-ES | M | 10% | 7.79E+00 | 0.4% |
| $OH^-$ | TB/OH/OB | M | 10% | 2.85E+00 | 3.5% |
| $NO_2^-$ | IC | M | 10% | 2.37E+00 | 0.8% |
| $NO_3^-$ | IC | M | 10% | 1.27E+00 | 0.6% |
| $Al(OH)_4^-$ | ICP-ES | M | 10% | 9.42E-02 | 0.8% |
| $CO_3^{2-}$ | TIC/TOC | M | 10% | 6.72E-01 | 0.4% |
| | | mg/L | | 4.03E+04 | |
| $CHO_2^-$ | IC | M | 10% | 3.49E-02 | 0.6% |
| | | mg/L | | 1.57E+03 | |
| $C_2O_4^{2-}$ | IC | M | 10% | 5.01E-03 | 0.8% |
| | | mg/L | | 4.41E+02 | |
| $PO_4^{3-}$ | IC | M | 10% | 3.89E-03 | 6.5% |
| $SO_4^{2-}$ | IC | M | 10% | 6.08E-02 | 2.2% |
| $F^-$ | IC | M | 10% | 2.97E-02 | 0.3% |
| $Cl^-$ | IC | M | 10% | 6.90E-03 | 0.3% |
| $Br^-$ | IC | M | -- | < 1.27E-03 | -- |
| $Na^+$/anions | calculation | N/N | -- | 0.96 | -- |

**Table 3.11. Other Analysis of Tank 38 Sample HTF-38-17-60**

| analyte | method | units | 1σ unc. | acid diluted sample | | water diluted filtrate | | overall | | |
|---|---|---|---|---|---|---|---|---|---|---|
| | | | | average | RSD | average | RSD | best | RSD | *n* |
| Ag | ICP-AES | mg/L | -- | < 7.7E+00 | -- | < 1.6E+01 | -- | < 7.7E+00 | -- | -- |
| Al | ICP-AES | mg/L | 10% | 2.59E+03 | 1.0% | 2.54E+03 | 0.8% | 2.57E+03 | 1.3% | 6 |
| As | AA | mg/L | 20% | 1.76E+00 | -- | -- | -- | 1.76E+00 | -- | -- |
| B | ICP-AES | mg/L | 10% | 1.81E+02 | 1.4% | 1.83E+02 | 0.6% | 1.82E+02 | 1.1% | 6 |
| Ba | ICP-AES | mg/L | -- | < 5.9E-01 | -- | < 1.2E+00 | -- | < 5.9E-01 | -- | -- |
| Be | ICP-AES | mg/L | -- | < 2.4E-01 | -- | < 4.9E-01 | -- | < 2.4E-01 | -- | -- |
| Ca | ICP-AES | mg/L | -- | < 6.3E+00 | -- | < 1.3E+01 | -- | < 6.3E+00 | -- | -- |
| Cd | ICP-AES | mg/L | -- | < 7.6E+00 | -- | < 1.5E+01 | -- | < 7.6E+00 | -- | -- |
| Ce | ICP-AES | mg/L | -- | < 2.0E+01 | -- | < 4.1E+01 | -- | < 2.0E+01 | -- | -- |
| Co | ICP-AES | mg/L | -- | < 8.2E+00 | -- | < 1.7E+01 | -- | < 8.2E+00 | -- | -- |
| Cr | ICP-AES | mg/L | 10% | 1.05E+02 | 0.7% | 1.03E+02 | 0.2% | 1.04E+02 | 0.8% | 6 |
| Cs-137 | gamma | dpm/mL | 5% | 3.27E+08 | -- | 3.32E+08 | 1.5% | 3.30E+08 | 1.4% | 4 |
| Cu | ICP-AES | mg/L | -- | < 2.8E+01 | -- | < 5.5E+01 | -- | < 2.8E+01 | -- | -- |
| Fe | ICP-AES | mg/L | -- | < 1.0E+01 | -- | < 2.1E+01 | -- | < 1.0E+01 | -- | -- |
| Gd | ICP-AES | mg/L | -- | < 5.8E+00 | -- | < 1.2E+01 | -- | < 5.8E+00 | -- | -- |
| Hg | CVAA | mg/L | 20% | 3.03E+02 | 2.6% | 3.19E+02 | 3.4% | 3.11E+02 | 3.8% | 6 |
| K | ICP-AES | mg/L | 10% | 4.42E+02 | 4.2% | 4.36E+02 | 5.8% | 4.39E+02 | 4.6% | 6 |
| La | ICP-AES | mg/L | -- | < 4.6E+00 | -- | < 9.1E+00 | -- | < 4.6E+00 | -- | -- |
| Li | ICP-AES | mg/L | 10% | 9.75E+01 | 1.2% | 9.13E+01 | 1.4% | 9.44E+01 | 3.8% | 6 |
| Mg | ICP-AES | mg/L | -- | < 1.1E+00 | -- | < 2.2E+00 | -- | < 1.1E+00 | -- | -- |
| Mn | ICP-AES | mg/L | -- | < 1.1E+00 | -- | < 2.1E+00 | -- | < 1.1E+00 | -- | -- |
| Mo | ICP-AES | mg/L | -- | < 2.4E+01 | -- | < 4.7E+01 | -- | < 2.4E+01 | -- | -- |
| Na | ICP-AES | mg/L | 10% | 1.80E+05 | 0.6% | 1.79E+05 | 0.4% | 1.79E+05 | 0.4% | 6 |
| Ni | ICP-AES | mg/L | -- | < 1.3E+01 | -- | < 2.6E+01 | -- | < 1.3E+01 | -- | -- |
| P | ICP-AES | mg/L | -- | < 2.3E+02 | -- | < 2.1E+02 | -- | < 2.3E+02 | -- | -- |
| Pb | ICP-AES | mg/L | -- | < 1.1E+02 | -- | < 2.1E+02 | -- | < 1.1E+02 | -- | -- |
| Rh | ICP-MS | mg/L | 10% | 4.88E-01 | 1.6% | 5.10E-01 | 0.9% | 4.99E-01 | 2.7% | 6 |
| Ru | ICP-MS | mg/L | 10% | 4.31E+00 | 1.4% | 4.47E+00 | 1.8% | 4.39E+00 | 2.2% | 6 |
| S | ICP-AES | mg/L | -- | < 6.6E+03 | -- | < 1.3E+04 | -- | < 6.6E+03 | -- | -- |
| Sb | ICP-AES | mg/L | -- | < 1.1E+02 | -- | < 2.21E+02 | -- | < 1.1E+02 | -- | -- |
| Se | AA | mg/L | -- | < 5.7E-01 | -- | -- | -- | < 5.7E-01 | -- | -- |
| Si | ICP-AES | mg/L | 11% | 1.58E+02 | 1.8% | 1.54E+02 | 4.1% | 1.56E+02 | 2.8% | 5[a] |
| Sn | ICP-AES | mg/L | -- | < 6.6E+01 | -- | < 1.3E+02 | -- | < 6.6E+01 | -- | -- |
| Sr | ICP-AES | mg/L | -- | < 2.1E-01 | -- | < 4.3E-01 | -- | < 2.1E-01 | -- | -- |
| Tc-99 | ICP-MS | mg/L | 10% | 1.94E+00 | 0.8% | 1.84E+00 | 1.3% | 1.89E+00 | 3.1% | 6 |
| Th | ICP-AES | mg/L | -- | < 6.0E+00 | -- | < 1.2E+01 | -- | < 6.0E+00 | -- | -- |
| Ti | ICP-AES | mg/L | -- | < 2.3E+01 | -- | < 4.7E+01 | -- | < 2.3E+01 | -- | -- |
| U-235 | ICP-MS | mg/L | 10% | 2.54E-01 | 1.9% | 2.58E-01 | 1.6% | 2.56E-01 | 1.8% | 6 |
| U-236 | ICP-MS | mg/L | 10% | 1.55E-02 | 2.9% | 1.61E-02 | 1.7% | 1.58E-02 | 3.0% | 6 |
| U-238 | ICP-MS | mg/L | 10% | 4.07E+01 | 0.8% | 4.12E+01 | 1.5% | 4.09E+01 | 1.3% | 6 |
| Total U | ICP-MS | mg/L | 10% | 4.09E+01 | 0.8% | 4.15E+01 | 1.5% | 4.12E+01 | 1.5% | 6 |
| V | ICP-AES | mg/L | -- | < 3.1E+00 | -- | < 6.2E+00 | -- | < 3.1E+00 | -- | -- |
| Zn | ICP-AES | mg/L | 12% | 1.29E+01 | 2.6% | 1.26E+01 | 5.7% | 1.27E+01 | 4.2% | 6 |
| Zr | ICP-AES | mg/L | -- | < 3.6E+00 | -- | < 7.2E+00 | -- | < 3.6E+00 | -- | -- |

[a] one high silicon outlier value is not included.

Table 3.12 contains results of a water dilution performed on the sample material without filtration. The purpose of this analysis was to measure oxalate and other salts that might have been partially insoluble in the sample at the shielded cell temperature. By comparison with Table 3.10, the results for oxalate and most other salts agree within analytical uncertainty for preparations with and without filtration.

**Table 3.12. Sample Dilution with Water for Insoluble Oxalate**

| analyte | method | units | 1σ unc. | water diluted sample average | water diluted sample RSD |
|---|---|---|---|---|---|
| $NO_2^-$ | IC | M | 10% | 2.36E+00 | 1.3% |
| $NO_3^-$ | IC | M | 10% | 1.30E+00 | 1.1% |
| $CO_3^{2-}$ | TIC/TOC | M | 10% | 6.68E-01 | 0.4% |
| $CHO_2^-$ | IC | M | 10% | 3.55E-02 | 0.4% |
| $C_2O_4^{2-}$ | IC | M | 10% | 5.03E-03 | 6.7% |
| $PO_4^{3-}$ | IC | M | 10% | 4.46E-03 | 1.0% |
| $SO_4^{2-}$ | IC | M | 10% | 5.85E-02 | 1.8% |
| $F^-$ | IC | M | -- | < 1.51E-02 | -- |
| $Cl^-$ | IC | M | -- | < 8.10E-03 | -- |
| $Br^-$ | IC | M | -- | < 3.60E-03 | -- |

The estimated 1-sigma uncertainty for individual analytical methods are as follows: 10% for ICP-AES, ICP-MS, IC, TIC/TOC, and TB/OH/OB; 20% for CVAA and AA; and 5% for gamma. The RSD is a representation of repeatability and includes the uncertainty introduced by the dilution preparation and a portion of the analytical method uncertainty.

### *3.3.3 Post HGR Measurement Analysis of HTF-38-17-60*

Table 3.13 contains the post HGR measurement sample analysis results and a comparison to the pre HGR measurement sample analysis results. ICP-AES results are only included for analytes measured above the limit of quantification. The pre HGR sample results were initially reported in Table 3.10 and Table 3.11. The column “post/pre” is an indication of the fractional increase of a component measured after the test when compared with the value measured before the test. Post/pre values between approximately 0.8 and 1.2 would not indicate a statistically significant difference in the pre and post HGR measurement samples.

Dissolution of the borosilicate glass kettle of the HGR apparatus is evident by the increase in silicon and boron concentrations. There was also a marked decrease in aluminum concentration in the sample taken after the test. The decrease in aluminum concentration is consistent with the formation of sodium aluminosilicate, which is favored at high temperatures in the presence of sufficient silicon. White solids were observed in the bottom of the kettle at the end of HGR testing. XRD analysis confirmed that the solids were sodium aluminosilicates (see Figure 3-27). The other identified sodium salts are likely from dried Tank 38 material; the solids were not washed prior to submission for analyses.

Formate concentration appeared unchanged during the test. Oxalate and nitrate are slightly lower in the post HGR measurement sample analysis, which may be due to analytical uncertainty or may indicate the precipitation or decomposition of oxalate and the precipitation of nitrate. The increases in sulfate and phosphate in the post HGR measurement sample may be due to analytical uncertainty or may indicate an actual increase in the soluble sulfate and phosphate concentration. The disagreement between pre and post HGR measurement of fluoride is outside of the analytical uncertainty and the cause has not been identified. All other concentrations in the pre and post HGR measurement sample analysis results match within the analytical uncertainty.

**Table 3.13. Pre- and Post-HGR-Measurement Sample Analysis Results Comparison**

| analyte | method | units | 1σ unc. | pre HGR measurement | | post HGR measurement | | post/pre |
|---|---|---|---|---|---|---|---|---|
| | | | | average | RSD | average | RSD | |
| $Na^+$ | ICP-AES | M | 10% | 7.79E+00 | 0.4% | 7.71E+00 | 1.8% | 0.99 |
| $OH^-$ | TB/OH/OB | M | 10% | 2.85E+00 | 3.5% | 2.73E+00 | -- | 0.96 |
| $NO_2^-$ | IC | M | 10% | 2.37E+00 | 0.8% | 2.30E+00 | 0.5% | 0.97 |
| $NO_3^-$ | IC | M | 10% | 1.27E+00 | 0.6% | 1.06E+00 | 0.8% | 0.84 |
| $Al(OH)_4^-$ | ICP-AES | M | 10% | 9.42E-02 | 0.8% | 3.66E-03 | 5.4% | 0.039 |
| $CO_3^{2-}$ | TIC/TOC | M | 10% | 6.72E-01 | 0.4% | 6.53E-01 | 0.4% | 0.97 |
| | | mg/L | | 4.03E+04 | | 3.92E+04 | | |
| $CHO_2^-$ | IC | M | 10% | 3.49E-02 | 0.6% | 3.59E-02 | 0.9% | 1.03 |
| | | mg/L | | 1.57E+03 | | 1.62E+03 | | |
| $C_2O_4^{2-}$ | IC | M | 10% | 5.01E-03 | 0.8% | 4.30E-03 | 1.2% | 0.86 |
| | | mg/L | | 4.41E+02 | | 3.79E+02 | | |
| $PO_4^{3-}$ | IC | M | 10% | 3.89E-03 | 6.5% | 4.58E-03 | 0.9% | 1.2 |
| $SO_4^{2-}$ | IC | M | 10% | 6.08E-02 | 2.2% | 7.14E-02 | 0.8% | 1.2 |
| $F^-$ | IC | M | 10% | 2.97E-02 | 0.3% | 1.19E-02 | 0.7% | 0.40 |
| $Cl^-$ | IC | M | 10% | 6.90E-03 | 0.3% | 7.53E-03 | 0.1% | 1.09 |
| $Br^-$ | IC | M | -- | < 1.27E-03 | -- | < 8.19E-03 | -- | -- |
| $Na^+$/anions | calculation | N/N | N/N | 0.96 | -- | 1.01 | -- | -- |
| TOC | TIC/TOC | mg C/L | 10% | 6.76E+02 | -- | 6.88E+02 | -- | 1.02 |
| Al | ICP-AES | mg/L | 10% | 2.57E+03 | 1.3% | 9.88E+01 | 5.4% | 0.039 |
| B | ICP-AES | mg/L | 10% | 1.82E+02 | 1.1% | 5.59E+02 | 1.9% | 3.1 |
| Cr | ICP-AES | mg/L | 10% | 1.04E+02 | 0.8% | 1.03E+02 | 2.1% | 0.99 |
| K | ICP-AES | mg/L | 10% | 4.39E+02 | 4.6% | 5.31E+02 | 0.7% | 1.2 |
| Li | ICP-AES | mg/L | 10% | 9.44E+01 | 3.8% | 1.03E+02 | 0.9% | 1.09 |
| Na | ICP-AES | mg/L | 10% | 1.79E+05 | 0.4% | 1.77E+05 | 1.8% | 0.99 |
| P | ICP-AES | mg/L | 10% | < 2.28E+02 | -- | 1.98E+02 | 0.4% | -- |
| Si | ICP-AES | mg/L | 11% | 1.56E+02 | 2.8% | 1.03E+03 | 0.005% | 6.6 |
| Zn | ICP-AES | mg/L | 12% | 1.27E+01 | 4.2% | 1.34E+01 | 0.7% | 1.05 |

The 7.71 M of sodium balanced with the anions (i.e., 7.62 N) within analytical uncertainty in the post-HGR-measurement, indicating a 0.09 N imbalance toward sodium. The major anions were 2.73 M hydroxide, 2.30 M nitrite, 1.06 M nitrite, an 0.65 M carbonate. The overall TOC was measured on an undiluted portion of sample as 688 mg carbon/L. As seen in Table 3.14, the adjusted TOC corresponding to the unidentified species that contribute to TOC not due to carbon from formate and oxalate sum to 154 mg carbon/L (with a 1σ uncertainty of 82 mg carbon/L). Despite minor inconsistencies, Table 3.14 shows reasonable agreement between the pre- and post-HGR-measurement materials with respect to organic carbon content. In both the pre- and post- measurement samples, the portion of the soluble TOC that is not due to formate or oxalate is about 20% of the TOC.

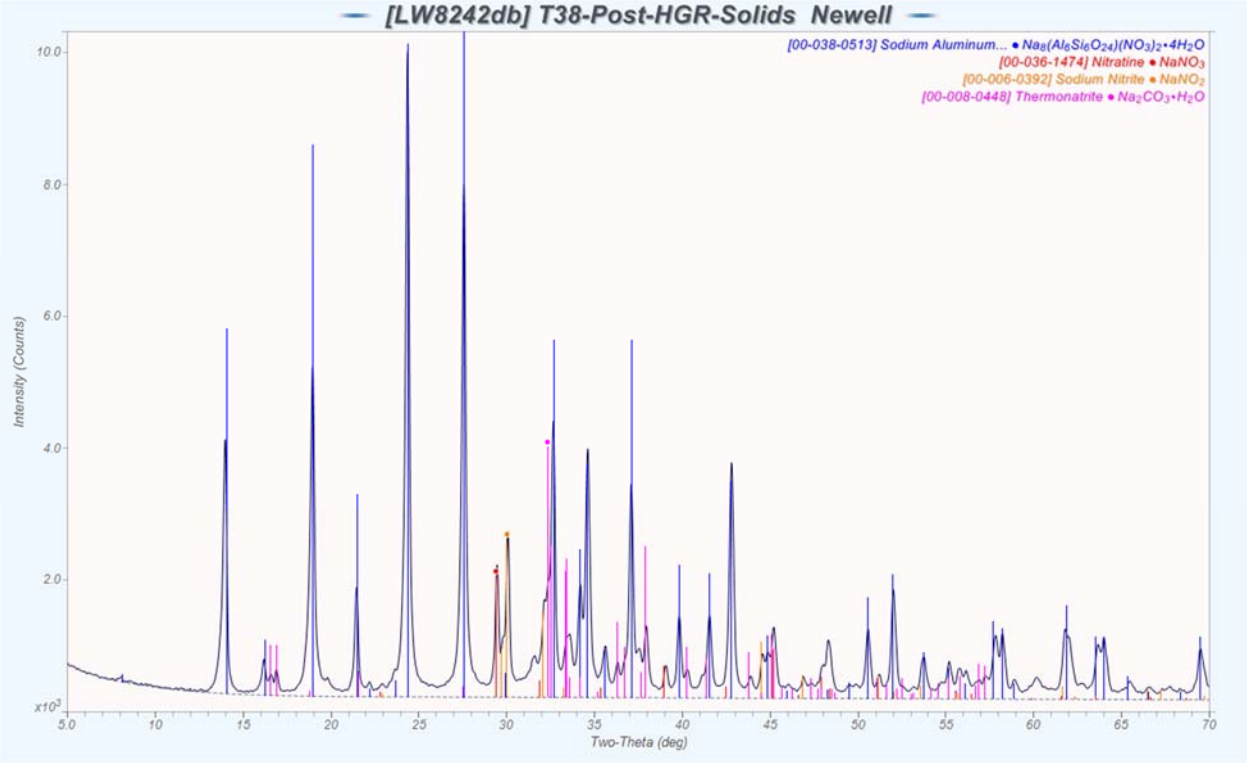


**Figure 3-27. XRD of White Solids Precipitated in the Tank 38 HGR Kettle**

**Table 3.14. Summary of Inorganic and Organic Carbon for Tank 38 Pre- and Post-HGR Measurement Samples**

| carbon analyte | units | pre HGR | | post HGR | |
|---|---|---|---|---|---|
| | | result | 1σ | result | 1σ |
| Total Carbon (TIC+TOC) | mg C/L | 8750 | 870 | 8540 | 850 |
| TIC (Carbonate Carbon) | mg C/L | 8070 | 810 | 7850 | 780 |
| TOC | mg C/L | 676 | 68 | 688 | 69 |
| Formate Carbon | mg C/L | 419 | 42 | 431 | 43 |
| Oxalate Carbon | mg C/L | 120 | 12 | 103 | 10 |
| Adjusted TOC (TOC-Formate-Oxalate) | mg C/L | 136 | 80 | 154 | 82 |

3.4 Results from Tank 38 Actual Waste Test

Hydrogen generation rates from Tank 38 sample material were determined from measured hydrogen concentrations using Equation 3. The Tank 38 sample was mixed and purged for multiple hours at Shielded Cells ambient temperature (27 °C). The sample was then heated to boiling (110.5 °C), cooled to 90 °C, cooled to 80 °C, and finally heated to 100 °C. The material was held at each temperature until a constant or declining hydrogen generation rate was observed. Results are presented graphically in Figure 3-28.

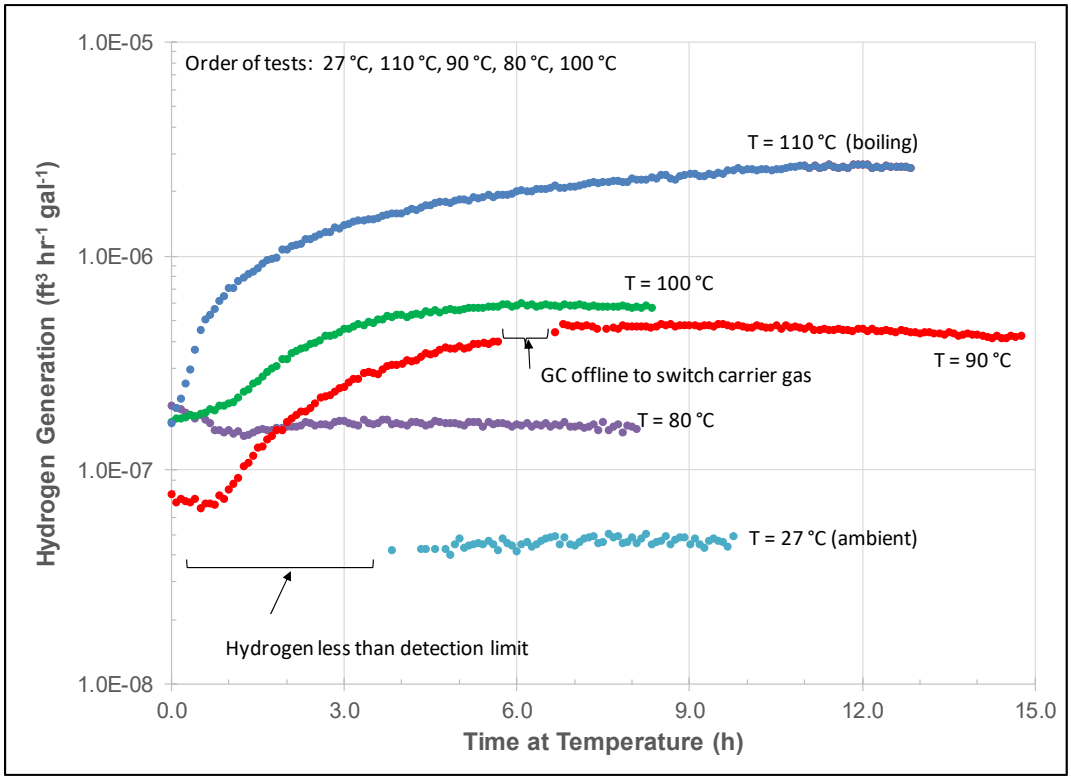


**Figure 3-28. Tank 38 Hydrogen Generation Rates as a Function of Time at Temperature**

The hydrogen generation rates for each temperature are given in Table 3.15. Because the hydrogen generation rates in some tests began to decrease over time, a rolling average of 10 generation rates were calculated. For example, in the 90 °C test, hydrogen generation rate decreased to $4.2\times10^{-7}$ ft$^3$ hr$^{-1}$ gal$^{-1}$ after peaking at $4.7\times10^{-7}$ ft$^3$ hr$^{-1}$ gal$^{-1}$, a decrease of 11%. The maximum rolling average generation rate for each temperature was chosen as the generation rate.

**Table 3.15. HGR Measurements for Tank 38**

| Temperature (°C) | Hydrogen Generation Rate (ft$^3$ hr$^{-1}$ gal$^{-1}$) | Estimated Uncertainty (95% confidence interval)* |
|---|---|---|
| 27 | $4.8\times10^{-8}$ † | NA |
| 80 | $1.7\times10^{-7}$ | 10% |
| 90 | $4.7\times10^{-7}$ | 10% |
| 100 | $5.9\times10^{-7}$ | 10% |
| 110.5 (boiling) | $2.6\times10^{-6}$ | 10% |

* The uncertainties for these results were calculated by inserting the inputs for Equation 2 (see Section 2.3.2) into the software package, GUM workbench [23], to derive a formula for the overall uncertainty. This formula was then used to calculate uncertainty using the software package JMP™ Pro, Version 11.2.1[24].

† This value is less than the limit of quantification but above the limit of detection; hydrogen is indeed present, but this number should not be used.

The hydrogen generation rates were fit to an Arrhenius model (exponential decay) to estimate an activation energy. This approach assumes no appreciable change in Al concentration, first order kinetics, and neglects any other factors (e.g., such as competing reactions to form aluminosilicates).

$$Rate = Ae^{-\frac{Ea}{RT}}$$ Equation 8

The results and Excel's exponential fit of the data are presented graphically in Figure 3-29, with $x = 1/T$, $A = 1.92 \times 10^{-7}$, and $Ea/R = 1.14 \times 10^{4}$ $K^{-1}$. *Ea*, the activation energy, can be calculated by multiplying by R = 8.314 $J \cdot K^{-1} \cdot mol^{-1}$ yielding an activation energy of 94.8 kJ/mol which compares favorably with the 89.6 ±1.96 kJ/mol proposed by Hu[11] for the Hanford waste (see Equation 1).

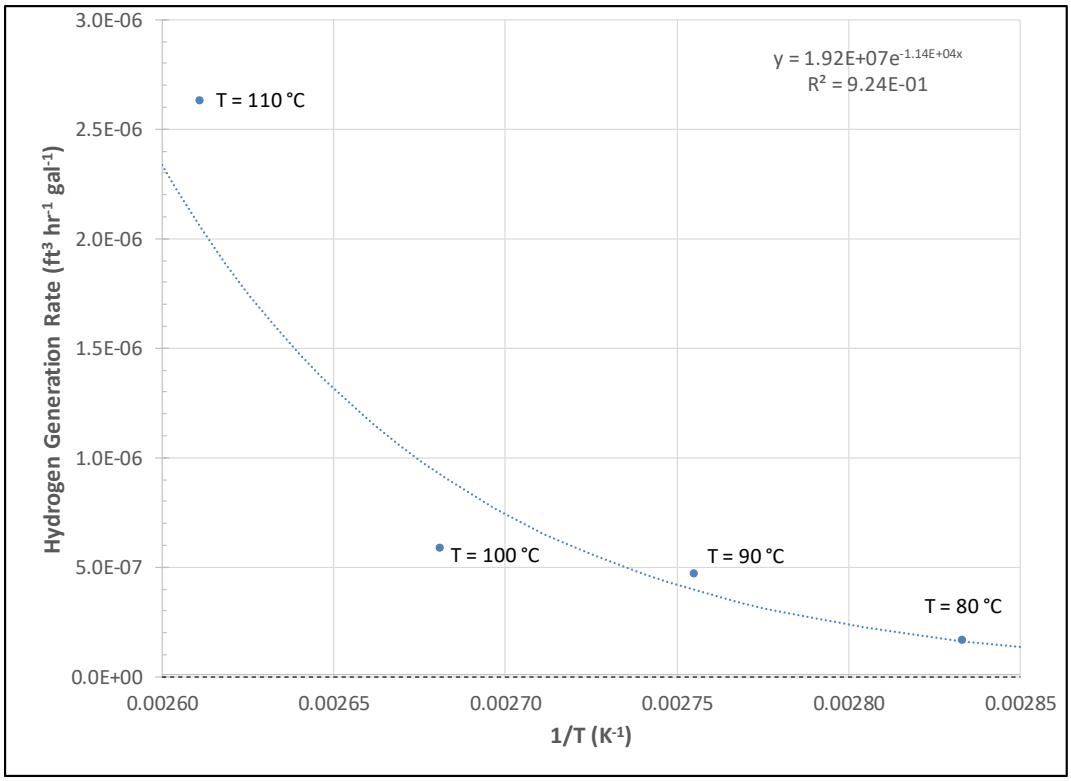


**Figure 3-29. Curve Fit of Hydrogen Generation Rate vs 1/T to Calculate Activation Energy**

The HGR measurements appear to be somewhat dependent on the order in which the measurements were performed. The data in Figure 3-29 show that the first two experimental measurements taken (110 °C and 90 °C) are above the curve fit and the latter two experimental measurements (80 °C and 100 °C) are near or below the curve fit. This trend is possibly due to the fact that subsequent measurements at different temperatures used the material from the previous experiment rather than fresh material, leading to possible consumption of reagents necessary for hydrogen production. Inspection of the data in Table 3.13 reveals that the only compounds exhibiting significant changes in concentration between the beginning and ending of testing are soluble silicon (560% increase), soluble boron (210% increase) and soluble aluminum (96% decrease). Note that these changes are likely due to dissolution of the glass vessel and subsequent formation of aluminosilicate solids (for further discussion on evidence of glass dissolution in these tests, see Appendix A). Note also that the trendline given in Figure 3-29 yields an $R^2$ value of 0.924, suggesting reasonable agreement with Arrhenius behavior despite the large changes in Al, Si, and B. This agreement indicates that aluminum, boron, and silicon likely have little effect on the hydrogen generation mechanism captured

in this testing at the concentrations examined. Note that this does not mean that aluminum, boron, and silicon are exempt from participation in hydrogen generation mechanisms not captured in this testing (including thermolysis of other organic molecules). It is unclear if the apparent decrease in reaction rate as a function of experiment order is due to the lesser consumption of analytes other than aluminum, silicon, or boron. It is also unclear if this apparent decrease is a secondary effect from glass.

During heating to boiling, nitrous oxide was detected and quantified by the GC. The generation rate is presented in Figure 3-30. Within 2.5 hours of boiling, nitrous oxide was no longer detected. The estimated detection limit of nitrous oxide is 0.005% or $10^{-6}$ $ft^3$ $hr^{-1}$ $gal^{-1}$ in this experiment. Unlike the HBP simulant, the release rate of nitrous oxide during the Tank 38 test did not appear to be related to the thermolytic HGR. Based on the measurement delays in the test system at the low 3 sccm gas purge rate, the nitrous oxide profile is consistent with a short-term release at or just before boiling and the subsequent dilution by the purge gas. One possibility is that the nitrous oxide was formed from the radiolysis of nitrate and nitrite[17] prior to the test and released from the solution as its solubility decreased as the temperature increased. Another possibility is that the nitrous oxide was formed by a thermolysis reaction in which a reactant was quickly depleted.

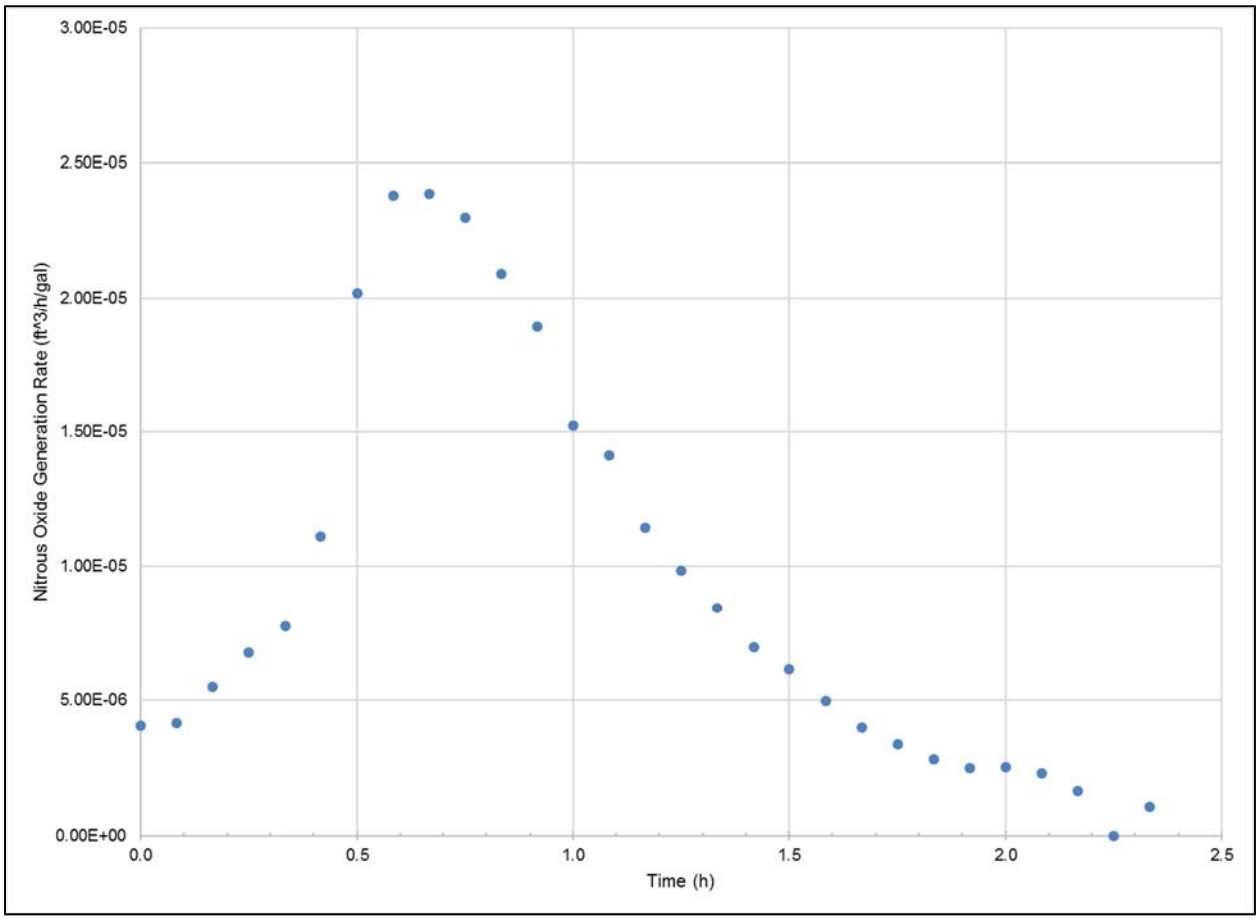


**Figure 3-30. Nitrous Oxide Generation during Boiling of Tank 38**

*3.4.1 Tank 38 Methane*

Figure 3-31 shows hydrogen and methane concentration results for the Tank 38 testing. Methane concentration was determined by multiplying the response factor calculated in Section 2.3.4 by the methane area from the GC software. As discussed in Section 2.3.4, methane was not detected in a 2 ppmv standard. However, the GC did detect peaks that yielded some results less than 2 ppmv. This further illustrates that these results are semi-quantitative. Ultimately, a rigorous statistically determined limit of quantification should be determined for methane analogous to the determination done for hydrogen.

The plot shows that methane is strongly correlated with hydrogen - peaking when hydrogen peaked, with highest concentrations observed during the higher temperatures of 110 °C and 100 °C with higher hydrogen concentrations. The Tank 38 data shows that the postulated methane concentrations are approximately one third of the hydrogen value (i.e., methane at 40 ppmv and hydrogen at 120 ppmv at 110 °C, and methane at 10 ppmv and hydrogen at 30 ppmv at 100 °C).

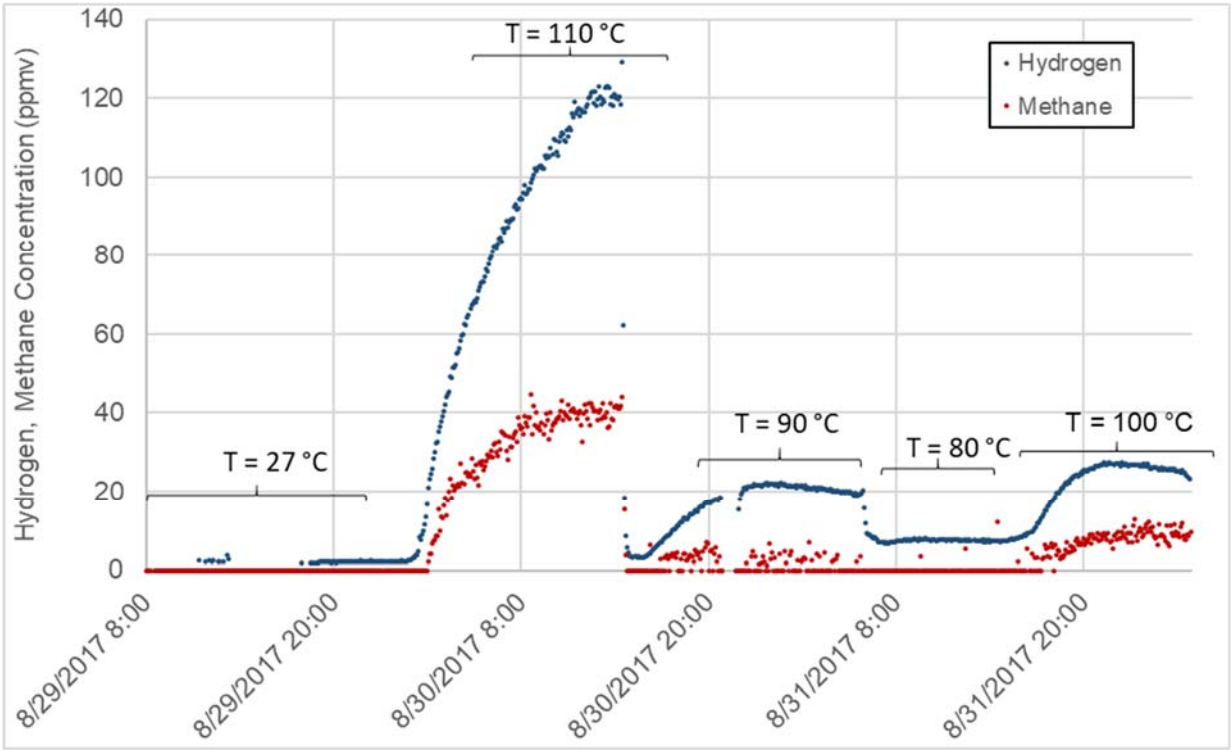


**Figure 3-31. Concentrations for Hydrogen and Methane for Tank 38 Testing**

3.5 Comparisons Between Simulant Tests, Tank 38 Tests, and Hu Equation Predictions

Table 3.16 summarizes the measured hydrogen generation rates given throughout this report, the TOC and Al concentration, and the generation rate calculated using the Hu correlation (e.g., Equation 1). For Tank 38, the initial TOC and Al concentrations were used to calculate the generation rates by the Hu correlation, since Al concentrations at each specific temperature is not known. Calculated generation rates using the final TOC and Al concentrations would yield generation rates of approximately one fourth of the values in the table.

In all cases, a reactivity factor, $r_f$, of one was used in the Hu equation. As stated in Section 1.0, the constants in the Hu equation (activation energy and pre-exponential factor) were regressed from hydrogen generation measurements specific to Hanford actual waste samples, and the reactivity factor was used to improve the fit of the data, with recommended values varying between 0.15 and one.

A reactivity factor for the SRNL tests was calculated by dividing the measured HGR by the calculated Hu HGR (see last column). In the three HBP tests, the calculated reactivity factor was consistent, ~0.3. For the two SY1-SIM-91B-NG tests, the reactivity factors were significantly different. Note that the generation rate for the 75 °C test was an extrapolation.

**Table 3.16. Comparison of HGR Measurement to HGR Calculated by the Hu Equation 1**

| Test | HGR Measurement ($ft^3$ $hr^{-1}$ $gal^{-1}$) | TOC (wt%) | Al (wt%) | Hu (Eqn. 1) HGR ($ft^3$ $hr^{-1}$ $gal^{-1}$) | Measured HGR/ Hu HGR (calc. reactivity factor) |
|---|---|---|---|---|---|
| SY1-SIM-91B-NG (T = 75 °C) | $5.4\times10^{-7}$ | 0.0135 | 3.27 | $5.9\times10^{-7}$ | 0.92 |
| SY1-SIM-91B-NG Persistent HGR (T = 114 °C boiling) | $3.8\times10^{-6}$ | 0.0135 | 3.27 | $1.3\times10^{-5}$ | 0.29 |
| HBP (T = 75 °C) final | $6.2\times10^{-7}$ | 0.0877 | 0.583 | $2.2\times10^{-6}$ | 0.28 |
| HBP (T = 100 °C) final | $3.0\times10^{-6}$ | 0.0875 | 0.624 | $1.8\times10^{-5}$ | 0.17 |
| HBP (T = 139.1 °C boiling) final | $8.1\times10^{-5}$ | 0.0958 | 0.657 | $3.2\times10^{-4}$ [a] | 0.26 |
| Tank 38 (T = 80 °C) | $1.7\times10^{-7}$ | 0.0509 | 0.194 | $1.0\times10^{-6}$ | 0.16 |
| Tank 38 (T = 90 °C) | $4.7\times10^{-7}$ | 0.0509 | 0.194 | $2.4\times10^{-6}$ | 0.20 |
| Tank 38 (T = 100 °C) | $5.9\times10^{-7}$ | 0.0509 | 0.194 | $5.4\times10^{-6}$ | 0.11 |
| Tank 38 (T = 110.5 °C boiling) | $2.6\times10^{-6}$ | 0.0509 | 0.194 | $1.2\times10^{-5}$ | 0.22 |

[a] Calculation of the Hu HGR for the HBP test at 139.1 °C is an extrapolation outside of the temperature range that the equation was developed for.

For Tank 38, the reactivity factor decreased as testing progressed (order of tests: 110 °C, 90 °C, 80 °C, and finally 100 °C). The decrease in this calculated result is likely caused by using the initial Al concentration in the Hu equation; based on initial and final analysis of Tank 38, Al concentration was changing. For example, the final Tank 38 test (100 °C), using the final Al concentration, the Hu HGR is calculated to be $1.4\times10^{-6}$ $ft^3$ $hr^{-1}$ $gal^{-1}$, yielding a reactivity factor of 0.42 (compared to a reactivity factor of 0.11 calculated when using the initial aluminum concentration).

Tank 38 generation rates cannot be directly compared to simulant generation rates because the organic species present (other than formate and oxalate) are not necessarily the same.

Based on information on previous HGR testing, the reactivity factors for formate and oxalate are likely very near zero.[10] The calculations of Hu HGR via Equation 1 in Table 3.16 use measured TOC, which includes the contribution of both oxalate and formate. An adjusted TOC, which is TOC minus the zero reactivity factor components formate and oxalate, has been calculated for the HBP and Tank 38 tests (see Table 3.8 and Table 3.14, respectively). Roughly 60% of the TOC in the HBP post-measurement samples and 80% of the TOC in the Tank 38 pre- and post-measurement are formate and oxalate. If the adjusted TOC is used

in the Hu HGR calculation, the calculated reactivity factors move closer to one. Note that the adjusted TOC has a much larger relative uncertainty than the original measurements have because the adjusted TOC calculation is a difference.

In addition to differences in apparent reactivity, simulant and radioactive-waste experiments exhibited somewhat different GC behavior. GC monitoring of Tank 38 experiments recorded the appearance of two unknown peaks. These peaks appear in process gas, air samples, and calibration gas. It has been concluded and discussed previously that these peaks are artifacts for the particular GC.[26] See Figure 3-32 for an example. A calibration gas sample is overlaid on a Tank 38 process gas sample, showing the unknown peaks at just over 25 s and 30 s in both samples.

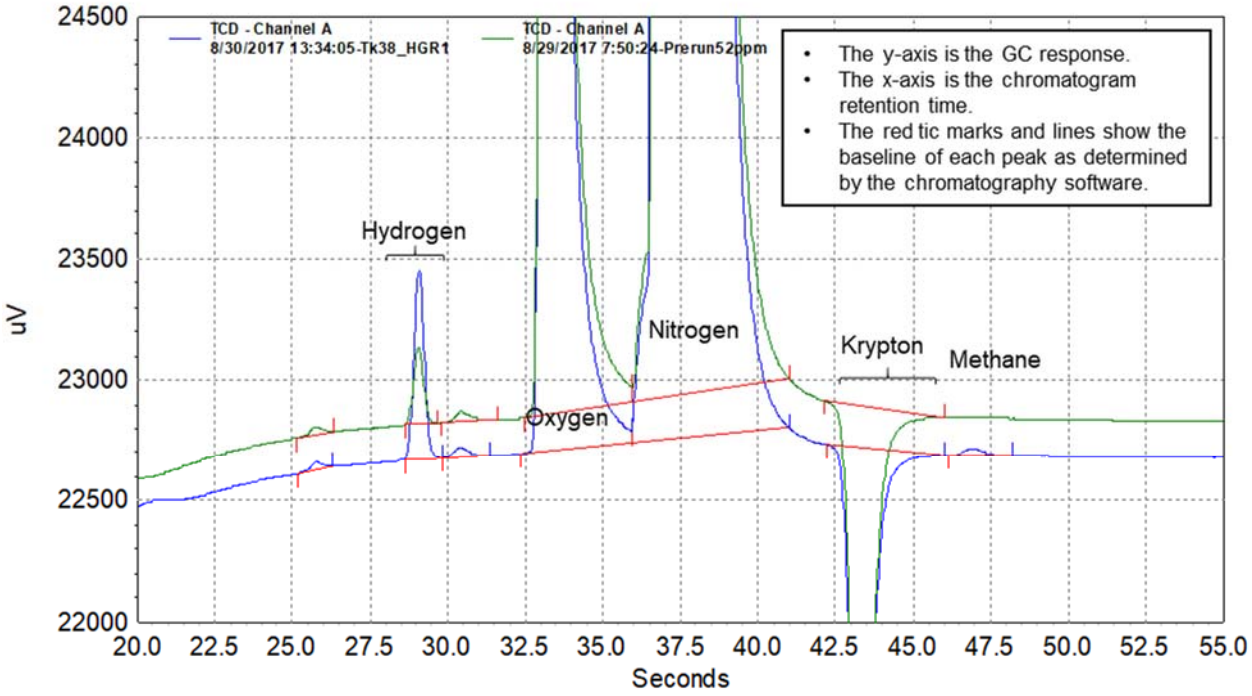


**Figure 3-32. A 52 ppm Hydrogen, 0.5% Krypton, 20% Oxygen, Balance Nitrogen, Chromatogram Overlaid on a Tank 38 HGR Measurement Chromatogram[26]**

## 4.0 Conclusions

The following conclusions have been drawn from the results presented in this report:

The HGR measurement apparatus has been successfully employed to replicate hydrogen production rate experiments reported by Ashby and predicted by Crawford. Simulant without deliberately added organic carbon was found to contain approximately 200 mg/L of organic carbon from tramp organics in the reagents used to prepare the solution. The tests using such simulant generated hydrogen at rates consistent with, but somewhat lower than, those predicted by the Hu equation at equivalent carbon and aluminum loadings. Prior to identifying the organic contaminants, potential sources of hydrogen in simulants without deliberately added organic carbon were examined. Testing determined that this hydrogen is not due to caustic reaction of organic materials of construction within the reaction vessel, electrolysis due to current leak, anode/cathode reactions, corrosion, or the method of heating employed in the experiment. Tests conducted at boiling (114 °C) exhibited an average HGR of $3.8\times10^{-6}$ $ft^3$ $hr^{-1}$ $gal^{-1}$. Extrapolation of test data

taken at 75 °C provides an estimated HGR of $5.4\times10^{-7}$ $ft^3$ $hr^{-1}$ $gal^{-1}$. Arrhenius interpolation of these points yields an estimated HGR of $2.0\times10^{-6}$ $ft^3$ $hr^{-1}$ $gal^{-1}$ at 100 °C.

HGR was measured in a HBP simulant with major known SRS Tank Farm organic compounds. Testing used fresh organics and did not simulate the long-term exposure of these organics already experienced in the waste. Hence, testing is expected to provide high bias to the hydrogen generation rates. The final HGR measurements at 75, 100, and 140 °C were $6.2\times10^{-7}$, $3.0\times10^{-6}$, and $8.1\times10^{-5}$ $ft^3$ $hr^{-1}$ $gal^{-1}$, respectively. Decreases in the HGR were noted at isothermal conditions with steady gas tracer concentration, which clouds development of a temperature dependent correlation for generation rate. While the simulant contains high concentrations of major SRS organics tested at high temperatures found in the 3H Evaporator, this limited data set may not fully bound values under all possible operating conditions.

HGR was measured for an actual-waste Tank 38 sample. The HGR measurements at 80, 90, 100, and 110 °C were $1.7\times10^{-7}$, $4.7\times10^{-7}$, $5.9\times10^{-7}$, and $2.6\times10^{-6}$ $ft^3$ $hr^{-1}$ $gal^{-1}$, respectively. The Limit of Detection and Limit of Quantification for the HGR measurements were $2.6\times10^{-8}$ $ft^3$ $hr^{-1}$ $gal^{-1}$ and $5.1\times10^{-8}$ $ft^3$ $hr^{-1}$ $gal^{-1}$, respectively.

During the HBP and Tank 38 testing, a peak was identified at a retention time greater than the retention time of the inert tracer of krypton. This peak has been identified as methane, and the data have been reexamined to obtain methane concentrations. For the HBP testing, methane concentration was constant at the highest temperature studied (140 °C) and higher than hydrogen. At the lower temperatures (100 and 75 °C), methane and hydrogen tracked closely, with methane concentration generally lower than hydrogen. For Tank 38, methane concentration was approximately 1/3 of the hydrogen concentration during testing (100 and 110 °C). At lower temperatures for Tank 38 testing (90, 80, and 27 °C), methane fell below the quantification range.

## 5.0 Recommendations

Proceed with the planned HGR measurements using a sealed system, which is described in Section 4.4 of the TTQAP and requested by Task 6 of the TTR. The sealed system is designed to measure the low HGR expected for a Tank 50 actual waste sample. The sealed system vessels are constructed of stainless steel in contrast to the glass vessel used in the flow system testing reported here.

As discussed in the TTR and TTQAP, the program should consider HGR measurements for actual-waste samples of tanks representing other portions of the SRS Tank Farm system. A single test with Tank 38 material may not provide adequate information for the entirety of the liquid waste system. Special consideration should be given to tanks that have a history of high organic content. The program should also assess the need for thermolytic HGR for Tank Farm operations such as aluminum dissolution and oxalic acid cleaning. A test with a sample from the 3H Evaporator system may be appropriate due to the hydrogen measured in the HBP test.

If the rates from the HBP and Tank 38 testing prove restrictive when applied to DSA development, additional simulant test to decipher the contributions from individual organic sources in tank waste may be warranted. In such testing, a control test should be performed to establish a baseline HGR without the addition of organics. Use of irradiated organic bearing solutions may be more appropriate to represent the current waste conditions. Additional instrumentation may be warranted on simulant testing if identification and quantification of VOC species is to be tested.

Additional simulant testing should be performed to evaluate the effect of anion concentrations on organic thermolytic HGR, particularly in concentrations ranges relevant to SRS waste.

Additional measurements should be made with the flow system to examine potential contribution of glass dissolution and aluminosilicate precipitation toward hydrogen generation. Comparison should be made between testing of identical solutions in the glass and stainless steel vessels, preferably at sub-boiling temperature.

Future testing should include quantification of methane, including establishment of limits of quantification.

## 6.0 References

[1] W. A. Condon, "Potentially inadequate recognition of the effect of organics on hydrogen generation rates in CSTF.", PI-2017-0003, February 28, 2017.

[2] A. V. Staub, "Potentially inadequate recognition of the effect of organics on hydrogen generation rates in Saltstone", PI-2017-0002, February 28, 2017.

[3] K. M. Brotherton, "Potentially inadequate recognition of the effect of organics on hydrogen gas generation rates in DWPF process vessels", PI-2017-0004, February 28, 2017.

[4] J. E. Occhipinti, "Research and Development for Tank Farm, DWPF, and Saltstone HGR PISAs", X-TTR-G-00003, Revision 0, June 7, 2017.

[5] C. J. Martino; J. D. Newell; J. M. Pareizs; M. R. Duignan; M. L. Restivo, "Task Technical and Quality Assurance Plan for Testing to Support Hydrogen Generation Rate in the Savannah River Site Tank Farm, Defense Waste Processing Facilities, and Saltstone", SRNL-RP-2017-00305, Revision 1, September 20, 2017.

[6] C. J. Martino; J. D. Newell; W. H. Woodham, "Run Plan for Thermolysis Tests with Ashby Simulant for Equipment Checkout", SRNL-L3300-2017-00022, Revision 0, August 1, 2017.

[7] C. J. Martino; J. D. Newell; J. M. Pareizs, "Run Plan for Tank 38 Actual-Waste Thernolysis Tests", SRNL-L3300-2017-00024, Revision 1, August 28, 2017.

[8] W. H. Woodham; C. J. Martino; J. D. Newell, "Run Plan for Thermolysis Tests with High Boiling Point Simulant and Common Tank Farm Organics", SRNL-L3300-2017-00023, Revision 0, August 29, 2017.

[9] C. Delegard, "Laboratory Studies of Complexed Waste Slurry Volume Growth in Tank 241-SY-101", RHO-LD-124, 1980.

[10] E. C. Ashby; A. Annis; E. K. Barefield; D. Boatright; F. Doctorovich; C. L. Liotta; H. M. Neumann; A. Konda; Y. C.F.; K. Zhang; N. G. McDuffie, "Synthetic Waste Chemical Mechanism Studies", WHC-EP-0823, Revision 0, October 1994.

[11] T. A. Hu, "Empirical Rate Equation Model and Rate Calculations of Hydrogen Generation for Hanford Tank Waste", HNF-3851, Revision 1, September 2004.

[12] A. T. Clare, "Inclusion of Organic Contribution to Radiolytic and Thermolytic Hydrogen Generation at DWPF", X-ESR-S-00320, Revision 2, 2017.

[13] A. B. Chandler, "Safety Analysis Input: Thermolytic Hydrogen Generation Rate", SF-I-GE-0063, 2017.

[14] D. D. Walker, "Organic Compounds in Savannah River Site High-Level Waste", WSRC-TR-2002-00391, Revision 0, September 30, 2002.

[15] C. L. Crawford; W. D. King, "Impacts of Glycolate and Formate Radiolysis and Thermolysis on Hydrogen Generation Rate Calculations for the Savannah River Site Tank Farm", SRNL-STI-2017-00303, Revision 0, August 2017.

[16] B. Speight, "09/19/13 DIRT Meeting Minutes", SRR-LWE-2013-00174, 2013.

[17] C. H. Keilers, Jr; S. N. Altman; C. L. Crawford; S. D. Fink; D. Henley; J. Mills; B. J. Wiersma, "Flammable Gas Generation Mechanisms for High Level Liquid Waste Facilities", X-ESR-G-00062, Revision 1, October 25, 2017.

[18] "U.S. Standard Atmosphere, 1976", NOAA-S/T 76-1562, October 1976.

[19] M. E. Stone; D. J. Adamson; D. J. Pak; J. M. Pareizs, "Hydrogen Generation Rate Measurement Apparatus: Final Design Package", SRNL-RP-2014-00866, Revision 0, September 2014.

[20] M. E. Stone; J. D. Newell; T. E. Smith; J. M. Pareizs, "WTP Waste Feed Qualification: Hydrogen Generation Rate Measurement Apparatus Testing Report", SRNL-STI-2016-00247, Revision 0, June 2016.

[21] J. D. Newell; J. M. Pareizs; C. J. Martino; S. H. Reboul; C. J. Coleman; T. B. Edwards; F. C. Johnson, "Actual Waste Demonstration of the Nitric-Glycolic Flowsheet for Sludge Batch 9 Qualification", SRNL-STI-2016-00327, Revision 1, March 9, 2017.

[22] J. M. Pareizs; J. D. Newell; C. J. Martino; C. L. Crawford; F. C. Johnson, "Sludge Washing and Demonstration of the DWPF Nitric/Formic Flowsheet in the SRNL Shielded Cells for Sludge Batch 9 Qualification", SRNL-STI-2016-00355, Revision 0, October 2016.

[23] Metrodata GmbH, "GUM Workbench: User Manual for Version 1.3, 2.3, and 2.4", 2009.

[24] "SAS Institute Inc., JMP™ Pro, Ver. 11.2.1", Cary, NC, 2014.

[25] J. K. Taylor, *Quality Assurance of Chemical Measurements*. Lewis Publishers, Inc.: Chelsea, MI, 1987.

[26] C. L. Crawford; S. D. Fink; C. A. Nash; J. M. Pareizs, "Evaluation of the Current State of Knowledge for Thermolysis of Organics within SRS Waste Forming Volatile Organic Compounds (VOCs)", SRNL-STI-2018-00163, Rev. 0, October 2018.

[27] "Technical Reviews", Manual E7, Procedure 2.60, Revision 17, August 25, 2016.

[28] "Savannah River National Laboratory Technical Report Design Check Guidelines", WSRC-IM-2002-00011, Revision 2, August 2004.

[29] C. M. Jantzen; J. E. Laurinat; K. G. Brown, "Thermodynamic Modeling of the SRS Evaporators: Part I. The 2H and 2F Systems (U)", WSRC-TR-2000-00293, Revision 1, April 4, 2002.

[30] J. Addai-Mensah; J. Li; M. Zbik; S. W. Rosencrance, "The Chemistry, Crystallization, Physicochemical Properties and Behavior of Sodium Aluminosilicate Solid Phases: Final Report", WSRC-MS-2002-00907, Revisioin 0, November 20, 2002.

[31] M. S. Hay; C. J. Coleman; D. P. DiPrete, "Analysis of Tank 38H (HTF-38-17-52, -53) and Tank 43H (HTF-43-17-54, -55) Samples for Support of the Enrichment Control and Corrosion Control Programs", SRNL-STI-2017-00472, Revision 0, August 2017.

## Appendix A. Thermolysis Testing to Determine Components Producing Hydrogen

The hydrogen generated by the SYI-SIM-91B-NG simulant without added glycolate exceeded pre-test expectations. SRNL conducted a series of tests to determine whether any single component or components (i.e., sodium hydroxide, sodium carbonate, sodium nitrite, sodium nitrate, and sodium aluminate) of the SYI-SIM-91B simulant are responsible for hydrogen generation.[1] A test with aluminum nitrate was also conducted, as the impurity level of aluminum nitrate is believed to be significantly lower than that of sodium aluminate.

These experiments used a nominal 1.2 L borosilicate glass kettle as a reaction vessel that was joined to a nominal 0.6 L borosilicate glass top. (A full description of the equipment is included in the body of the report.) Purge gas of 0.5% Kr, 20% $O_2$, and 79.5% $N_2$ was supplied through a port at the top of the vessel. The purge gas swept the vessel headspace and carried generated products through a condenser for downstream GC analysis. Heat was supplied to the vessel contents via Inconel heating rods. Prior to testing, the glass vessel and INCOLOY 800 heating rods were soaked in acid and scrubbed to remove residue from previous tests. A new stainless steel agitator and shaft was installed. All components were rinsed with deionized water before use. Three 8.79 M solutions (sodium hydroxide, sodium nitrite, and sodium nitrate) were prepared. Since the solubility of sodium carbonate, aluminum nitrate, and sodium aluminate in water is significantly less than 8.79 M, these components were added as solid reagents, additional water was added to return the volume to 1 L.

Testing started with sodium hydroxide and the remaining components were added separately in five subsequent tests. The composition of the solution at the start of the sixth test approximated the composition of the SYI-SIM-91B-NG simulant (2.00 M sodium hydroxide, 0.42M sodium carbonate, 2.24 sodium nitrite, 2.59 M sodium nitrate, and 1.54 M sodium aluminate) with exception made for deviations due to aluminum nitrate addition (aluminum nitrate requires addition of excess sodium hydroxide and generates an excess of nitrate due to the 1:3 Al:$NO_3^-$ ratio). The solution volume was kept at approximately 1 L. The tests were performed at the boiling point (atmospheric pressure) of the solution with a purge rate of 3 mL/min. The agitator speed ranged from 200 to 400 rpm. After the completion of the sixth test, a total of 1,604.1 g of simulant (containing approximately 171 g insoluble solids) were removed from the vessel. Table A-1 lists the test conditions.

**Table A-1. Tests HGR DC-1 Through HGR DC-6.**

| Test # | Required Component Added | Pre-Test Mass Added (g) | Water Addition | Post-Test Mass Removed (g) |
|---|---|---|---|---|
| HGR DC-1 | 8.79 M NaOH | 1293.6 | - | 224.6 |
| HGR DC-2 | $Na_2CO_3$ | 161.5 | Adjust Volume to 1 L | 639.9 at 80 °C |
| HGR DC-3 | 8.79 M $NaNO_2$ | 675.4 | - | 482.3 |
| HGR DC-4 | 8.79 M $NaNO_3$ | 521.6 at 83 °C | - | 232.7 |
| HGR DC-5 | $Al(NO_3)_3 \cdot 9(H_2O)$<br>8.79 M NaOH | 143.6<br>169.4 | Adjust Volume to 1 L | 0 |
| HGR DC-6 | $Na_2O \cdot Al_2O_3 \cdot 3H_2O$ | 125.89 | Rinse Water | 1,604.1 |

Since there was concern that organic impurities in the reagents might be responsible for higher hydrogen generation rate than expected, the total organic carbon (TOC) concentrations of each reagent was analyzed. Reagents of interest were diluted to target concentrations corresponding to the composition of SY1-SIM-91B-NG with DI water (hydroxide solution was used to dissolve $NaAlO_2$) prior to analysis, then the amount

of TOC in the resulting solution measured. The results are summarized in Table A-2 on a µg carbon per g reagent basis. According to these results, sodium aluminate contributes significantly more TOC to the simulant than the other additives with a concentration of 2311 µg/g. Note that sodium aluminate is a lower grade compound (i.e., it is technical grade, not ACS reagent grade) compared to the other chemicals utilized in this study and possibly contains humic acid as an impurity.[2]

**Table A-2. Total Organic Carbon Concentration of Reagents Used in Testing.**

| Required Component Added | TOC Impurity (µg/g reagent) |
|---|---|
| 50% NaOH Solution | 154 |
| $Na_2CO_3$ | 1,137 |
| $NaNO_2$ | 6.8 |
| $NaNO_3$ | 0.8 |
| $Na_2O \cdot Al_2O_3 \cdot 3H_2O$ | 2,311 |
| DI Water | 0.2 |

After the completion of the first set of six tests, the glass vessel, glass thermowell, the agitator, and the heating rods were thoroughly rinsed with deionized water. The initial test (HGR-DC-1) was repeated with the rinsed apparatus components (reported as HGR DC-7) following the same experimental parameters. Following this test, the stainless-steel agitator was removed and a fresh solution of 8.79 M NaOH was charged to the reaction vessel for the HGR DC-8 test. The results of HGR-DC-7 and 8 are summarized in Table A-3.

.

**Table A-3. Tests HGR DC-7 and HGR DC-8.**

| Test # | Pre-Run Mass Added (g) | Post-Run Mass Removed (g) |
|---|---|---|
| HGR DC-7 | 1294.5 | 1274.4 |
| HGR DC-8[a] | 1293.6 | 1279.3 |

[a]Stainless-steel agitator was removed for this test.

The maximum hydrogen generation rates for all tests described above are summarized in Table A-4 and Figure A-1. The largest hydrogen generation rate was observed in test HGR DC-1 (containing only 8.79 M sodium hydroxide). The hydrogen generation rate peaked at $2.2\times10^{-4}$ $ft^3$ $hr^{-1}$ $gal^{-1}$. Hydrogen generation declined in subsequent tests, dropping two orders of magnitude to $8.4\times10^{-6}$ $ft^3$ $hr^{-1}$ $gal^{-1}$ in HGR DC-2. After the addition of sodium aluminate (HGR DC-6), an increase in hydrogen generation was observed relative to DC-5 ($1.1\times10^{-5}$ vs $1.7\times10^{-6}$ $ft^3$ $hr^{-1}$ $gal^{-1}$). This result is similar to what was observed during the previous SYI-SIM-91B-NG simulant testing, suggesting that sodium aluminate and its relatively high quantities of TOC may be responsible for hydrogen generation. Note that the increase in HGR observed in DC-6 relative to the HGR observed in DC-5 is not expected to be due to the addition of aluminum, as aluminum was present in DC-5.

**Table A-4. Maximum Hydrogen Generation Rates.**

| Test # | Boiling Temperature (°C) | Maximum HGR ($ft^3\ hr^{-1}\ gal^{-1}$) |
|---|---|---|
| HGR DC-1 | 114.3 | $2.2\times10^{-4}$ |
| HGR DC-2 | 113.3 | $8.4\times10^{-6}$ |
| HGR DC-3 | 113.3 | $6.4\times10^{-6}$ |
| HGR DC-4 | 113.1 | $3.1\times10^{-6}$ |
| HGR DC-5 | 111.3 | $1.7\times10^{-6}$ |
| HGR DC-6 | 113.1 | $1.1\times10^{-5}$ |
| Cleaned glassware, agitator, and heating rods with deionized water | | |
| HGR DC-7 | 114.5 | $1.8\times10^{-5}$ |
| HGR DC-8 | 114.4 | $8.9\times10^{-6}$ |

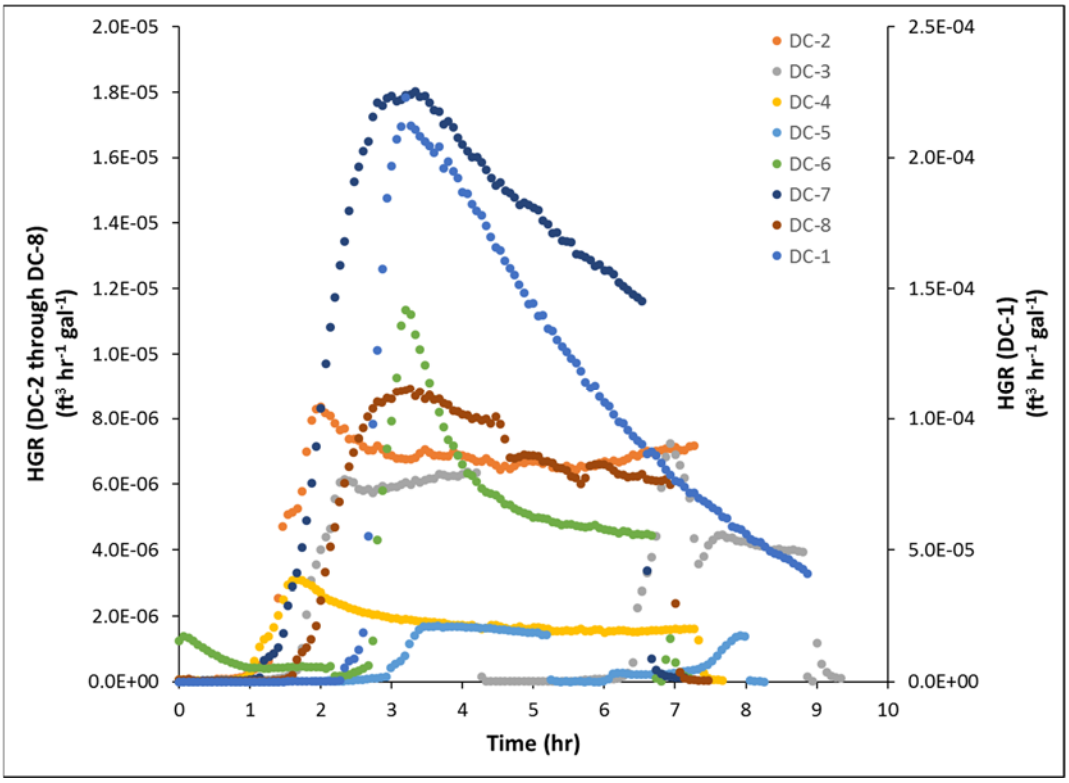


**Figure A-1. Hydrogen Generation Rates for DC-1 Through DC-8.**

In the later sodium hydroxide-only tests (i.e., HGR DC-7 and HGR DC-8), the hydrogen generation rates reached maximums of $1.8\times10^{-5}$ and $8.9\times10^{-6}$ $ft^3\ hr^{-1}\ gal^{-1}$, respectively; 1-2 orders of magnitude lower than the chemically-identical test HGR DC-1. It is possible that the reduced hydrogen rate from HGR DC-1 to HGR DC-7 and HGR DC-8 is due to the use of new or cleaned equipment (vessel, agitator, etc.) in the first experiments vs. the use of equipment that had only been rinsed in the latter two experiments. If this hypothesis is true, it may suggest the presence of a corrosive mechanism of hydrogen production due to the caustic corrosion of stainless-steel (agitator shaft), INCOLOY 800 (heating rods), or borosilicate glass

(reaction vessel and thermowell). Note that the sodium hydroxide solutions lack nitrite and nitrate which act as inhibitors for the formation of hydrogen generated from the corrosion of steel in the SRS Tank Farm.

To investigate the influence of corrosion in this testing, liquid samples were pulled at the completion of each test. Filtrate was analyzed for anions and metals by ion chromatography, titration, and ICP-ES. Borosilicate glass has a composition of 79.7-80.6% $SiO_2$, 10.3-13.0% $B_2O_3$, 4.0-5.2% $Na_2O$, 2.3-3.1% $Al_2O_3$, and residual traces of CaO, MgO, and other miscellaneous oxides by weight.[3,4] The compositions of 316L stainless steel and INCOLOY 800 are summarized in Table A-5.[5,6] This data is included to allow identification of metals in samples and determine whether corrosion of glassware, agitator, or heating rods might lead to the increase in concentration in samples.

**Table A-5. 316L Stainless-Steel & INCOLOY 800 Compositions[4,5]**

| Elemental Composition | 316L Stainless Steel (wt.%) | INCOLOY 800 (wt.%) |
|---|---|---|
| Chromium | 16.00 – 18.00 | 19.00 – 23.00 |
| Nickel | 10.00 – 14.00 | 30.00 – 35.00 |
| Molybdenum | 2.00 – 3.00 | - |
| Manganese | < 2.00 | < 1.50 |
| Copper | - | < 0.75 |
| Aluminum | - | 0.15 – 0.60 |
| Aluminum & Titanium | - | 0.3 – 1.20 |
| Silicon | < 0.75 | - |
| Phosphorus | < 0.05 | - |
| Sulfur | < 0.03 | - |
| Carbon | < 0.08 | < 0.10 |
| Nitrogen | 0.10 | - |
| Iron | Balance (~65) | Balance (~42) |

Table A-6 summarizes the results of the titration and ICP-ES analyses for samples pulled during testing. No sample was pulled following the completion of DC-5. Note that the silicon concentration increased from 43.65 mg/L before the beginning of testing (DC-1 Pre-Run) to 4150 mg/L after completion of the first NaOH-only test (DC-1 Post-Run). A similar trend is seen in aluminum concentration, increasing from <1 mg/L before HGR DC-1 to 106 mg/L after HGR DC-1. The DC-1 Post Test ratio of Si to Al is approximately 39:1 on a mass basis. This ratio is consistent with the Si:Al ratio in borosilicate glass (31:1 on a mass basis). Similar Si:Al ratios are observed for DC-7 Post Test and DC-8 Post Test samples (35:1 and 42:1). These observations indicate that glass corrosion occurs during the testing with NaOH. The fact that the three tests exhibit comparable concentrations of dissolved silicon in the product filtrate (4150, 3260, and 3380 mg/L, respectively) suggests that glass corrosion occurs in each of these tests to a comparable extent despite the fact that hydrogen generation varies by 2 orders of magnitude. This variation in HGR with relatively consistent glass corrosion suggests that the corrosion of glass does not correlate with HGR.

**Table A-6. Feed and Product Analytical Results from Titrations and ICP-ES.**

| Sample ID[b] | Total Base (mol/L) | Al (mg/L) | Fe (mg/L) | Si (mg/L) | Cr (mg/L) |
|---|---|---|---|---|---|
| DC-1 Pre-Test | 8.85 | < 1.00 | < 1.00 | 43.65 | < 1.00 |
| DC-1 Post-Test | 8.80 | 106 | 16.4 | 4,150 | 3.20 |
| DC-2 Post-Test | 8.64 | 191 | 15.0 | 6,680 | 2.90 |
| DC-3 Post-Test | 4.41 | 109 | 8.14 | 3,850 | 1.43 |
| DC-4 Post-Test | 2.89 | 7.41 | 1.33 | 4,055 | < 1.00 |
| DC-6 Post-Test | 3.97 | 37,900 | 11.3 | 32.5 | 2.81 |
| Cleaned glassware, agitator, and heating rods with deionized water | | | | | |
| DC-7 Post-Test | NA[a] | 93.9 | 3.69 | 3,260 | < 1.00 |
| DC-8 Post-Test | NA[a] | 81.2 | 2.51 | 3,380 | < 1.00 |

[a]NA = Not Analyzed.
[b]Titanium concentration was reported below detection limit of 1 mg/L in every sample except DC-2 Post-Test (1.46 mg/L).

An increase in the soluble iron and chromium concentrations were also observed during testing. This trend suggests corrosion of the stainless-steel agitator employed during testing. The low titanium concentrations and absence of aluminum in excess of what is expected from glass dissolution (discussed above) suggests that corrosion of the INCOLOY 800 heating rods is minimal. Note that the increase of Al after HGR DC-6 is due to the addition of aluminum as aluminum nitrate and sodium aluminate, not corrosion of the heating rods. Comparison of the concentrations of dissolved iron in DC-1 Post-Test and DC-7 Post-Test samples suggest that approximately 80% less iron was dissolved during HGR DC-7 than during HGR DC-1. This closely matches the 90% decrease in HGR observed between HGR DC-1 and HGR DC-7 ($2.2\times10^{-4}$ vs. $1.8\times10^{-5}$ $ft^3$ $hr^{-1}$ $gal^{-1}$), suggesting that corrosion of the stainless-steel agitator shaft may play a significant role in HGR measured during NaOH-only testing. The reduction of HGR from $1.8\times10^{-5}$ $ft^3$ $hr^{-1}$ $gal^{-1}$ to $8.9\times10^{-6}$ $ft^3$ $hr^{-1}$ $gal^{-1}$ in HGR DC-8 (performed without steel agitator) suggests that a less-dominant hydrogen production mechanism exists that is eclipsed by the larger HGR observed during HGR DC-1.

Results from titration and IC analyses for total base, nitrite, and nitrate concentrations following selected tests are given in Figure A-2, Figure A-3, and Figure A-4 respectively. Additionally, predicted concentrations based on dilution and sampling effects are given for each species and test.

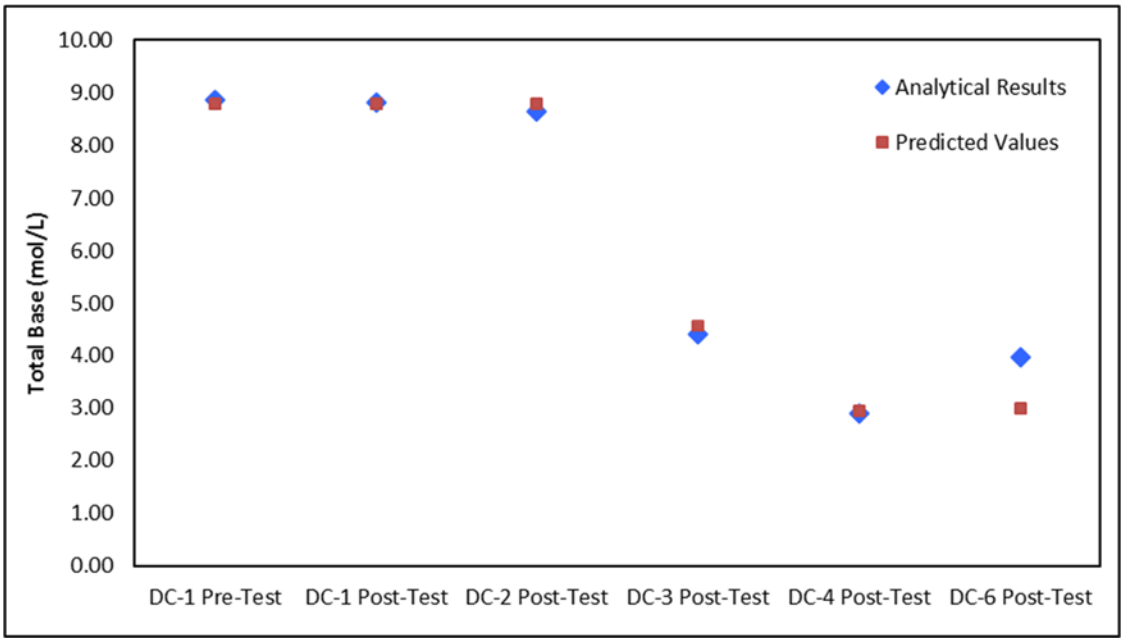


**Figure A-2. Predicted and Measured Concentrations of Total Base for Tests.**

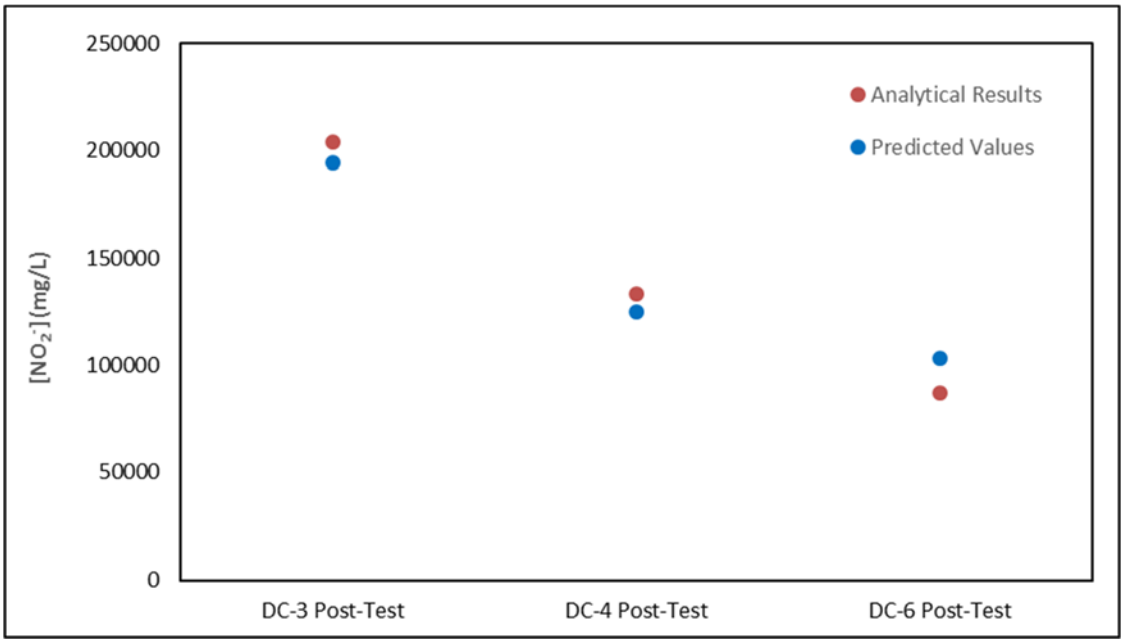


**Figure A-3. Predicted and Measured Concentrations of Nitrite for Selected Tests.**

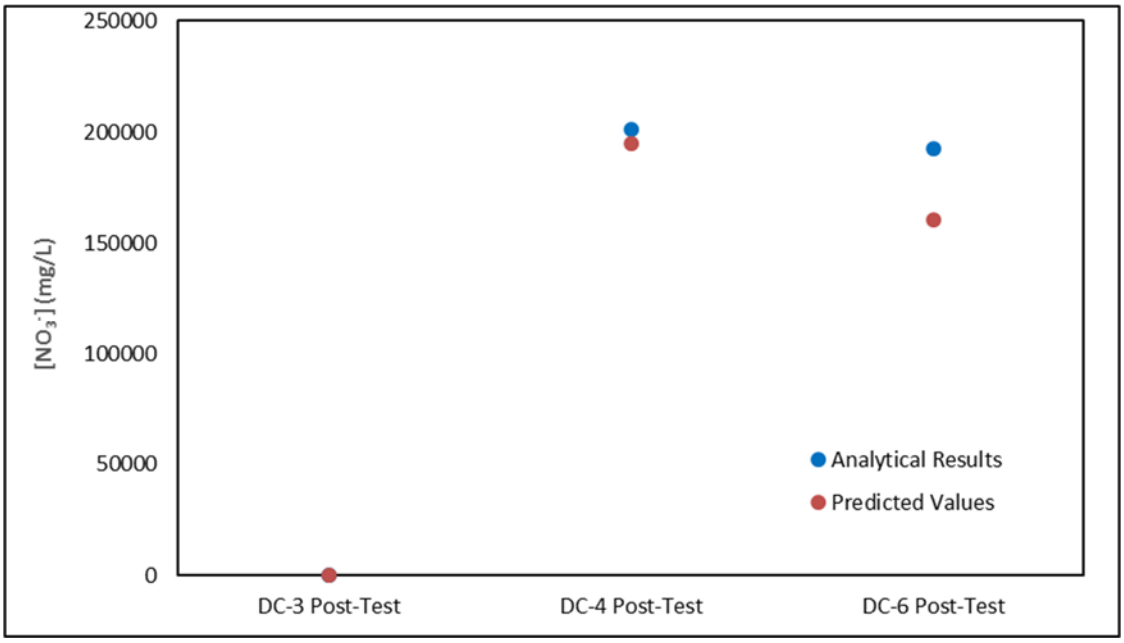


**Figure A-4. Predicted and Measured Concentrations of Nitrate for Selected Tests4, & DC-6.**

The similarity between predicted and measured concentrations of total base, nitrite, and nitrate shown in Figure A-2 through Figure A-4 suggest that changes in anion concentrations throughout this testing are negligible, implying slow or non-existent consumption.

In conclusion, eight follow-on experiments were conducted to evaluate the formation of hydrogen in testing with SY1-SIM-91B-NG simulant. The following conclusions have been drawn from this follow-on testing.

- The increase of silicon observed in solution after the HGR DC-1 test suggests that corrosion of glassware occurs in the presence of sodium hydroxide. The large variation in observed HGR and small variation in glass corrosion suggests that glass corrosion is not the dominant source of hydrogen production in this testing.
- The relative absence of titanium and aluminum in excess of that expected from glass dissolution suggests that the corrosion of the INCOLOY 800 heating rods is negligible throughout this testing.
- The presence of iron and chromium in post-test solutions suggests that measurable corrosion of the stainless-steel agitator does occur in the presence of NaOH. The HGR and iron dissolution measurements in this subset of experiments suggest that appreciable hydrogen generation due to corrosion occurred in the absence of corrosion inhibitors.
- Total organic carbon measurements confirmed the presence of organic impurities in each of the stock chemicals used to prepare the SY1-SIM-91B-NG simulant. The greatest source of TOC impurity is sodium aluminate (due to a combination of relatively high contamination of stock material and target simulant concentration). The lowest source of TOC impurity is the DI water employed in simulant preparation.
- Results from DC-6 suggest that the addition of sodium aluminate in SY1-SIM-91B-NG testing is a dominating source of hydrogen production. The decrease in HGR observed despite addition of aluminum when transitioning between DC-4 and DC-5 suggests that the increase in HGR observed in DC-6 is due to an impurity rather than the additional aluminum present.

**Appendix A References**

1. D.P. Lambert, A.M. Howe "Run Plan for Thermolysis with Ashby Simulant to Determine Components Producing Hydrogen," Savannah River National Laboratory, SRNL-L3300-2017-00038
2. Susic, Armstrong LG (1990) High-performance liquid chromatographic determination of humic acid in sodium aluminate solution. Journal of Chromatography. 502: 443-446.
3. Properties of PYREX®, PYREXPLUS® and LOW Actinic PYREX Code 7740 Glasses. (n.d.). Retrieved October 23, 2017, from http://www.quartz.com/pxprop.pdf
4. M.B. Volf, "Technical Glasses", 1961, London and Prague
5. 316 and 316L Stainless Steel Sheet, Coil & Bar - AMS 5524, 5507, UNS S31600, S31603. (n.d.). Retrieved October 23, 2017, from https://www.upmet.com/products/stainless-steel/316316l
6. INCOLOY® 800H / 800HT®. (n.d.). Retrieved October 23, 2017, from http://megamex.com/incoloy_800H_800HT.html

**Appendix B. Analysis of Solids Produced in Simulant Tests**

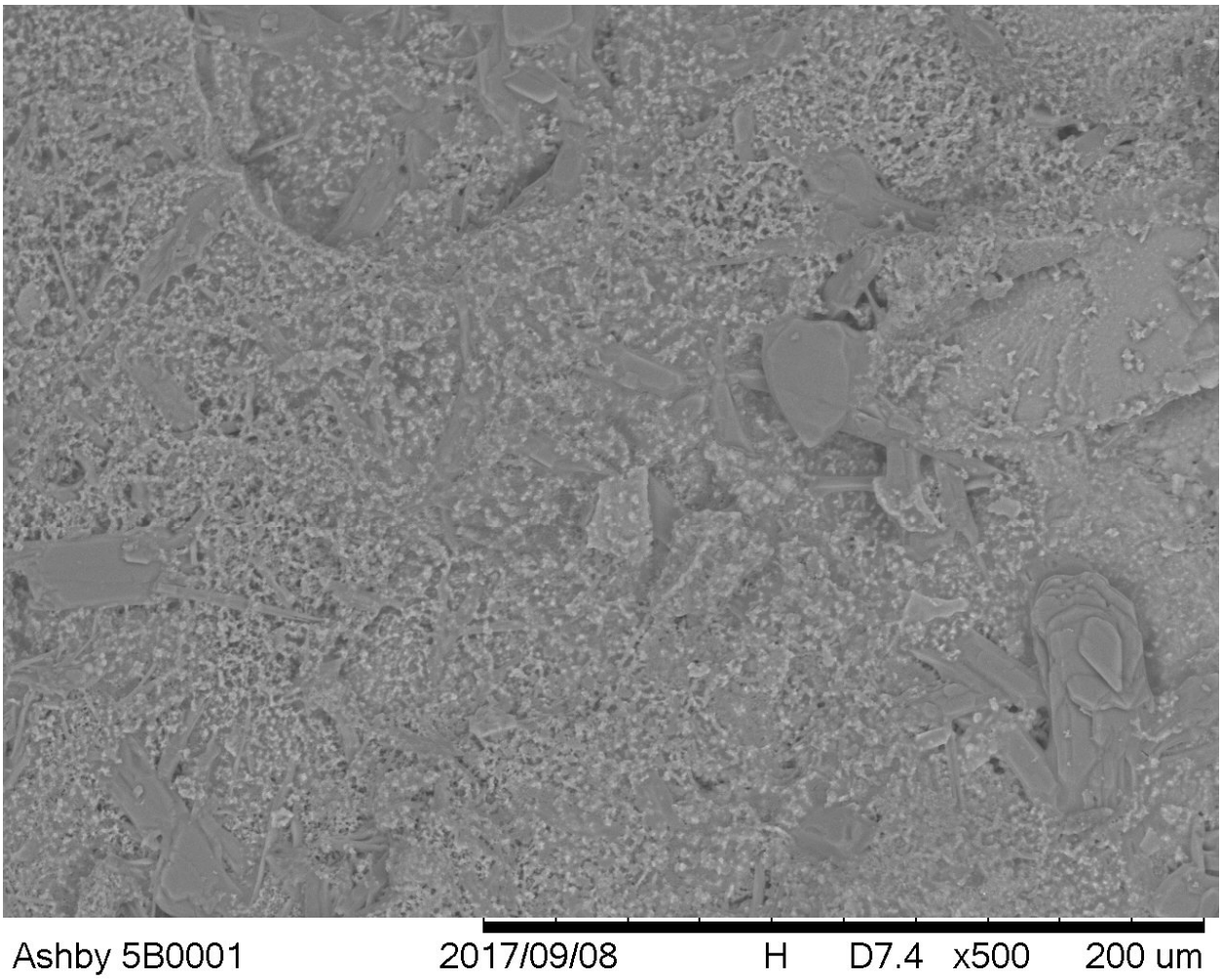


**Figure B-1. SEM of Solids from HGR-ASH-5 and 5B**

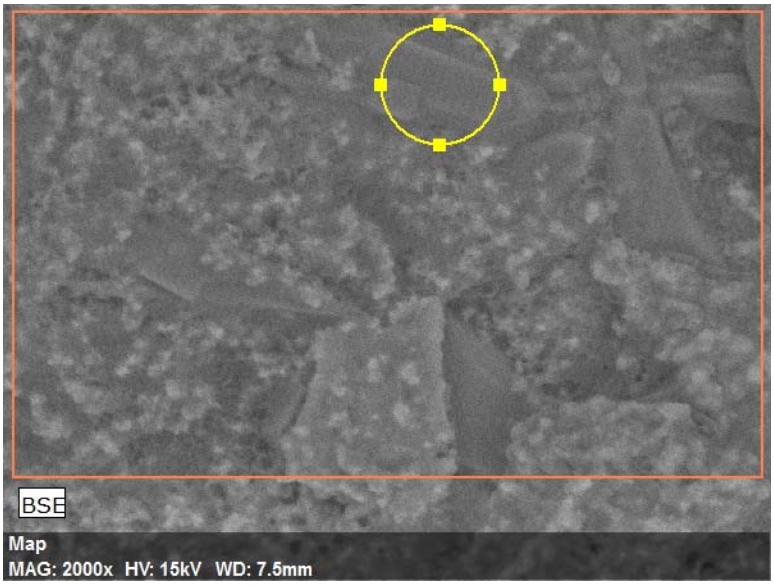


| Element | AN | series | Net | [wt.%] | [norm. wt.%] | [norm. at.%] | Error in % |
|---|---|---|---|---|---|---|---|
| Oxygen | 8 | K-series | 9734 | 59.2969 | 53.43397 | 58.94581 | 7.156705 |
| Sodium | 11 | K-series | 10675 | 39.60166 | 35.68608 | 27.39702 | 2.471061 |
| Carbon | 6 | K-series | 429 | 8.933468 | 8.050179 | 11.82948 | 1.780481 |
| Aluminum | 13 | K-series | 668 | 2.131103 | 1.920392 | 1.25621 | 0.123493 |
| Silicon | 14 | K-series | 367 | 1.009161 | 0.909381 | 0.571482 | 0.066832 |
| | | | Sum: | 110.9723 | 100 | 100 | |

**Figure B-2. XEDS of an Area of the HGR-ASH-5 and 5B Solids**

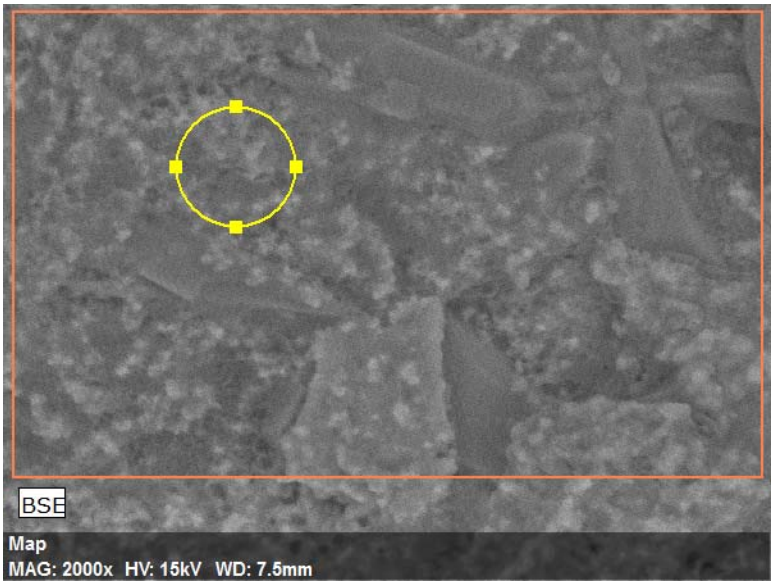


| Element | AN | series | Net | [wt.%] | [norm.wt.%] | [norm.at.%] | Error in % |
|---|---|---|---|---|---|---|---|
| Oxygen | 8 | K-series | 4298 | 33.38238 | 52.77526 | 59.74133 | 4.381668 |
| Sodium | 11 | K-series | 4530 | 18.60453 | 29.41249 | 23.17103 | 1.174139 |
| Nitrogen | 7 | K-series | 389 | 5.295182 | 8.371322 | 10.82446 | 1.091798 |
| Aluminum | 13 | K-series | 1280 | 4.197684 | 6.636253 | 4.454556 | 0.219005 |
| Silicon | 14 | K-series | 591 | 1.774063 | 2.804672 | 1.808623 | 0.098539 |
| | | | Sum: | 63.25383 | 100 | 100 | |

**Figure B-3. XEDS of an Area of the HGR-ASH-5 and 5B Solids**

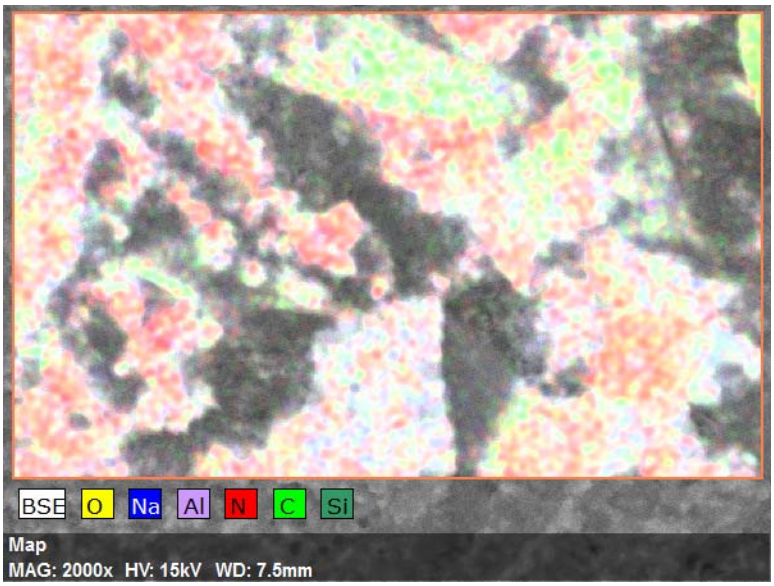


**Figure B-4. XEDS Composite SEM Image for the HGR-ASH-5 and 5B Solids**

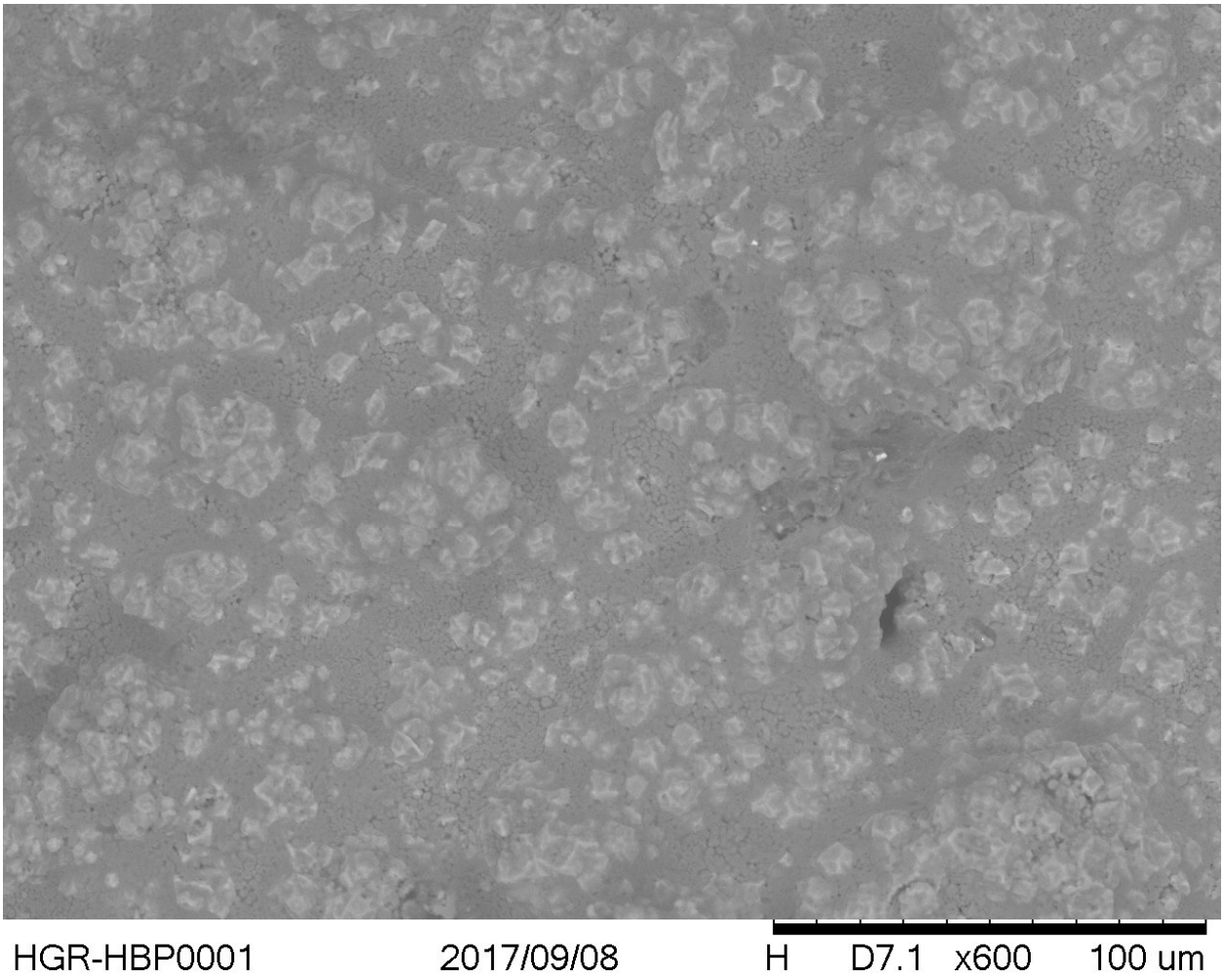


**Figure B-5. SEM of Solids from HBP Simulant Test Sampler**

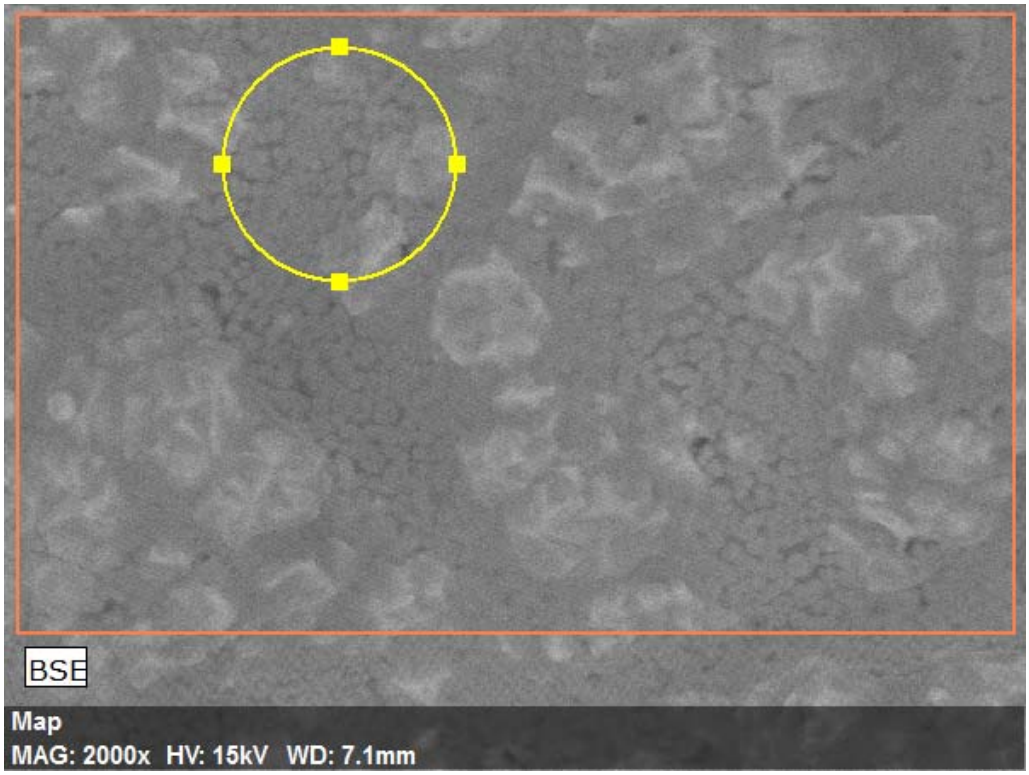


| Element | AN | series | Net | [wt.%] | [norm. wt.%] | [norm. at.%] | Error in % |
|---|---|---|---|---|---|---|---|
| Oxygen | 8 | K-series | 9543 | 82.20149 | 51.23381 | 56.17846 | 9.928127 |
| Sodium | 11 | K-series | 9991 | 41.11452 | 25.62549 | 19.55485 | 2.564505 |
| Nitrogen | 7 | K-series | 643 | 11.2846 | 7.033363 | 8.809355 | 2.043714 |
| Carbon | 6 | K-series | 416 | 10.06253 | 6.271685 | 9.160558 | 2.017788 |
| Aluminum | 13 | K-series | 3032 | 9.602981 | 5.98526 | 3.891644 | 0.468822 |
| Silicon | 14 | K-series | 2125 | 6.177719 | 3.850393 | 2.405137 | 0.281081 |
| | | | Sum: | 160.4438 | 100 | 100 | |

**Figure B-6. XEDS of an Area of Solids from HBP Simulant Test Sampler**

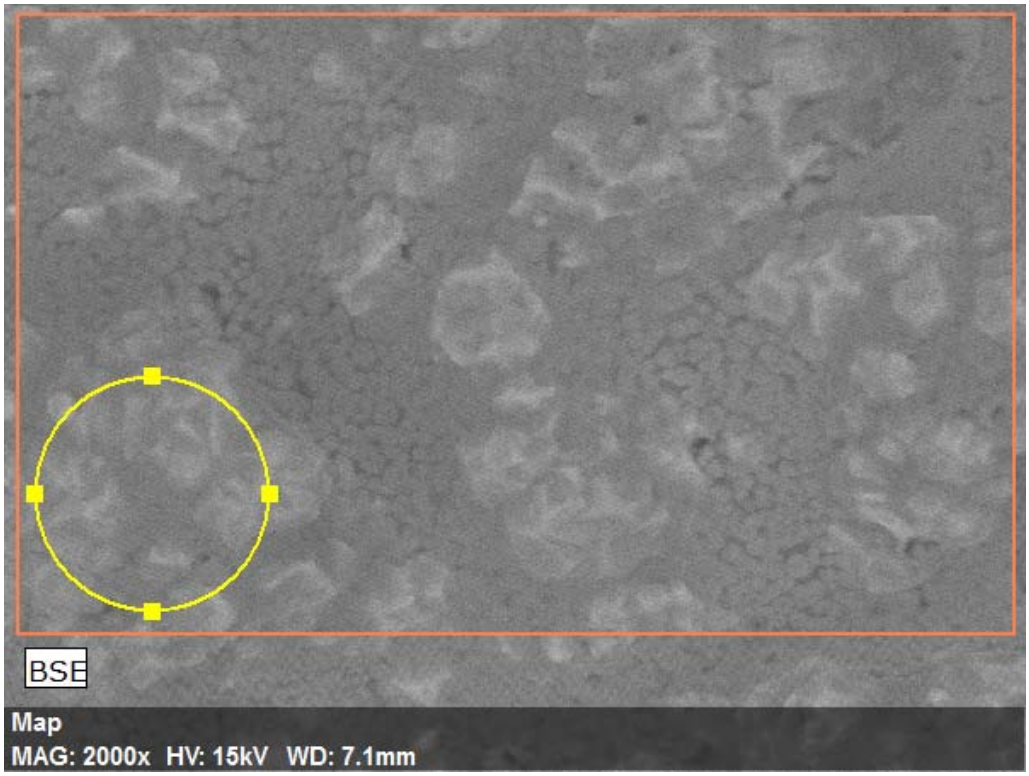


| Element | AN | series | Net | [wt.%] | [norm. wt.%] | [norm. at.%] | Error in % |
|---|---|---|---|---|---|---|---|
| Oxygen | 8 | K-series | 7324 | 45.30824 | 49.76673 | 60.69456 | 5.614638 |
| Sodium | 11 | K-series | 6681 | 23.67492 | 26.00461 | 22.07141 | 1.48732 |
| Aluminum | 13 | K-series | 4542 | 12.84351 | 14.10736 | 10.20219 | 0.61859 |
| Silicon | 14 | K-series | 3248 | 9.214558 | 10.1213 | 7.031835 | 0.406966 |
| | | | Sum: | 91.04122 | 100 | 100 | |

**Figure B-7. XEDS of an Area of Solids from HBP Simulant Test Sampler**

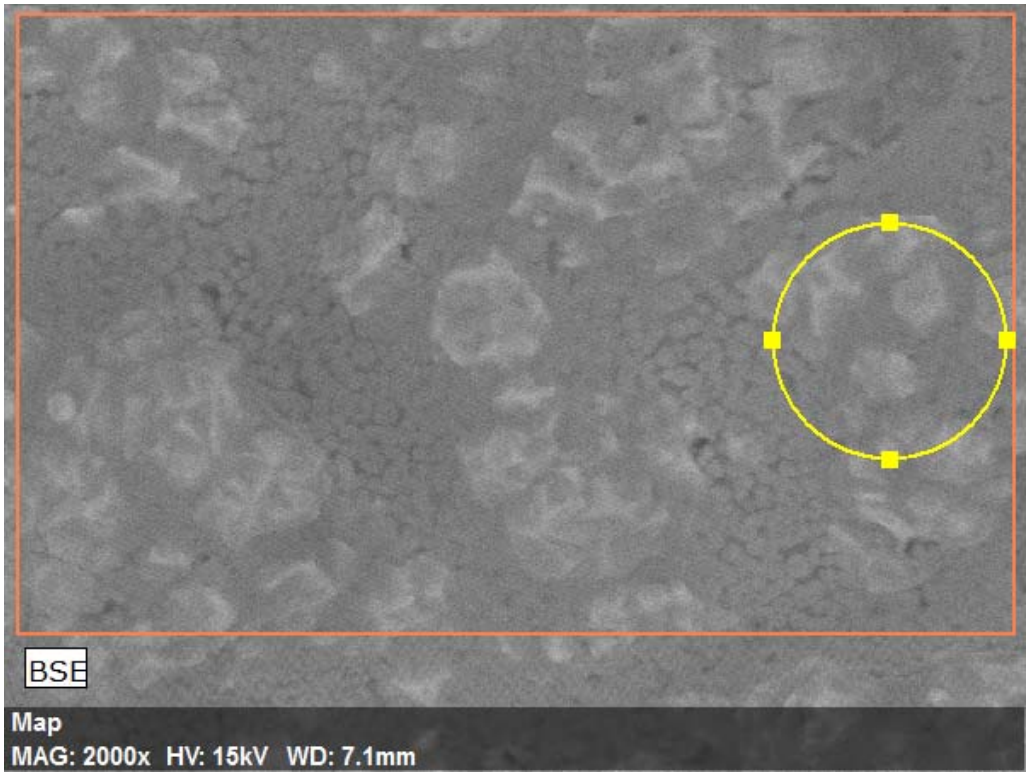


| Element | AN | series | Net | [wt.%] | [norm. wt.%] | [norm. at.%] | Error in % |
|---|---|---|---|---|---|---|---|
| Oxygen | 8 | K-series | 9540 | 68.84123 | 52.6494 | 60.45716 | 8.318766 |
| Sodium | 11 | K-series | 8500 | 31.86017 | 24.36649 | 19.47226 | 1.992896 |
| Aluminum | 13 | K-series | 4286 | 12.20809 | 9.336684 | 6.357465 | 0.589223 |
| Nitrogen | 7 | K-series | 688 | 9.516842 | 7.27843 | 9.546846 | 1.702223 |
| Silicon | 14 | K-series | 3069 | 8.327721 | 6.368996 | 4.166265 | 0.370204 |
| | | | Sum: | 130.7541 | 100 | 100 | |

**Figure B-8. XEDS of an Area of Solids from HBP Simulant Test Sampler**

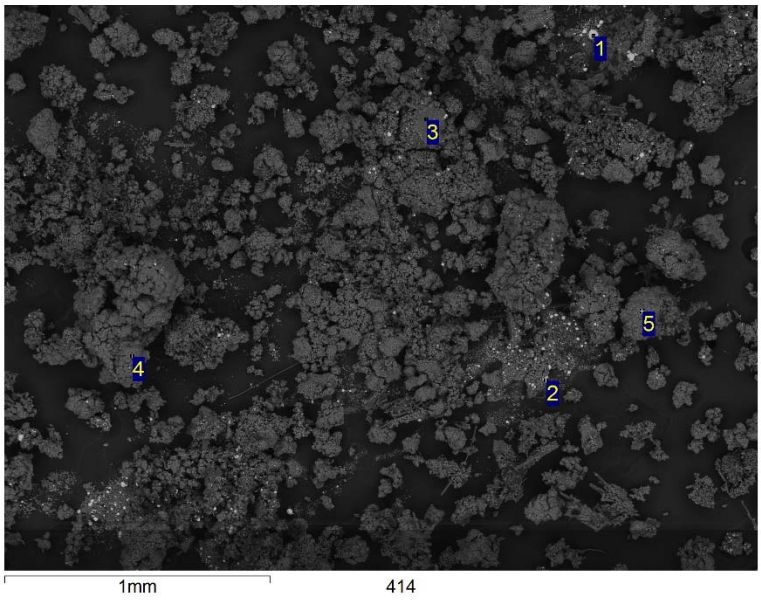
1
3
4
2
5
1mm
414

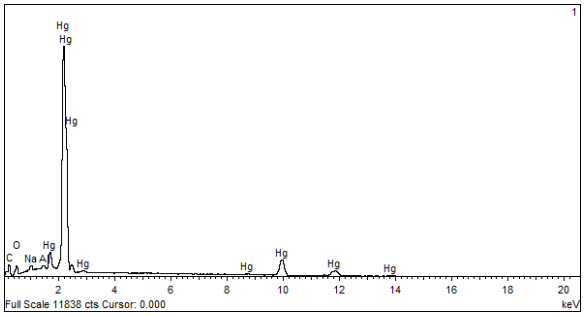
1
Hg
Hg
Hg
O
C
Na
Al
Hg
Hg
Hg
Hg
Hg
Hg
2 4 6 8 10 12 14 16 18 20
Full Scale 11838 cts Cursor: 0.000
keV

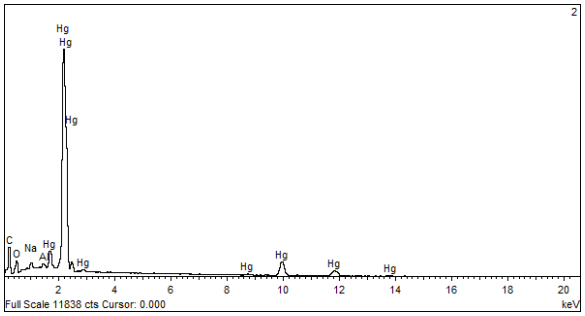
2
Hg
Hg
Hg
C
O
Na
Al
Hg
Hg
Hg
Hg
Hg
Hg
2 4 6 8 10 12 14 16 18 20
Full Scale 11838 cts Cursor: 0.000
keV

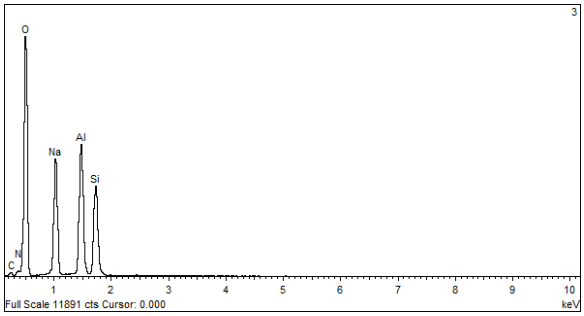
3
O
Na
Al
Si
N
C
1 2 3 4 5 6 7 8 9 10
Full Scale 11891 cts Cursor: 0.000
keV

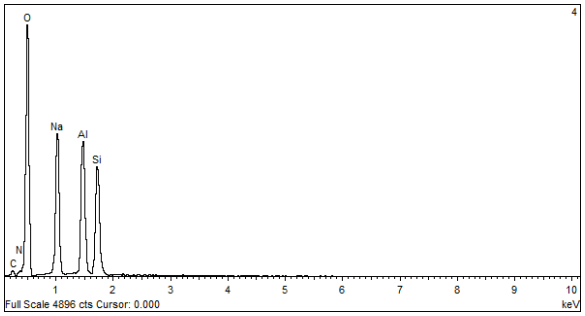
4
O
Na
Al
Si
N
C
1 2 3 4 5 6 7 8 9 10
Full Scale 4896 cts Cursor: 0.000
keV

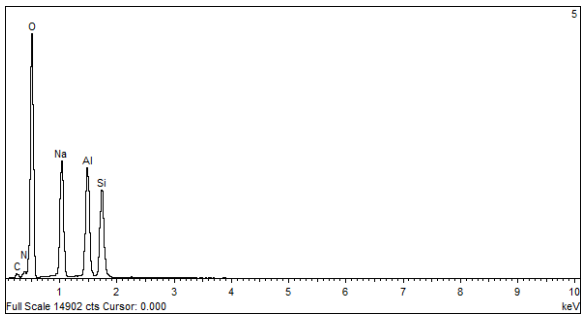
5
O
Na
Al
Si
N
C
1 2 3 4 5 6 7 8 9 10
Full Scale 14902 cts Cursor: 0.000
keV

**Figure B-9. SEM and XEDS of Gray Solids from HGR Simulant Test**

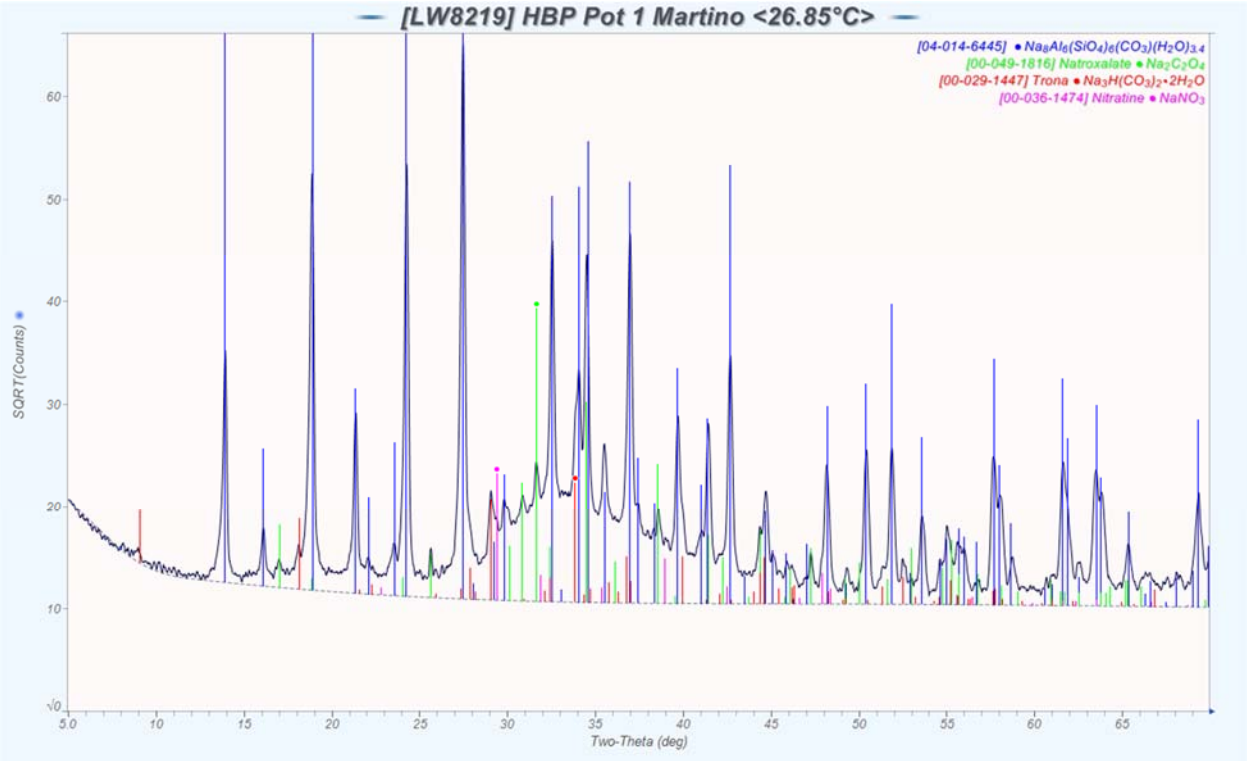


**Figure B-10. XRD of Gray Solids from HGR Simulant Test**

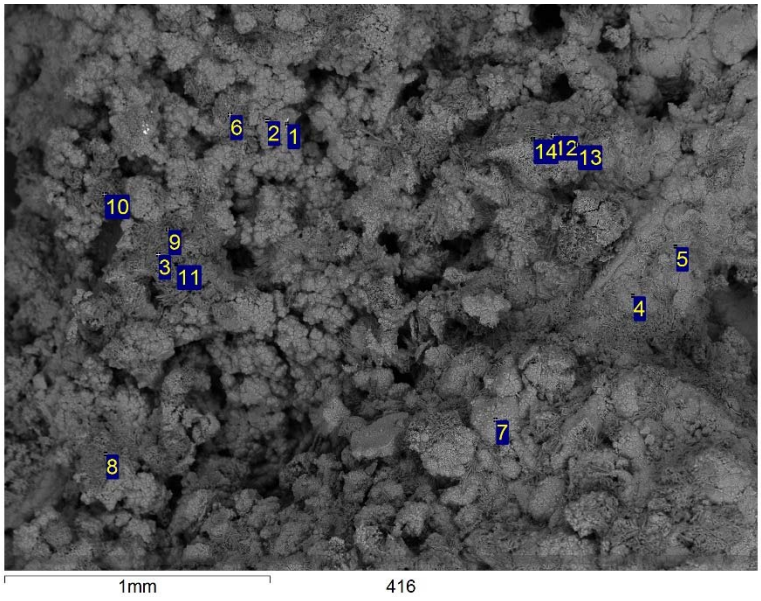
6
2
1
14
12
13
10
9
3
11
5
4
7
8
1mm
416

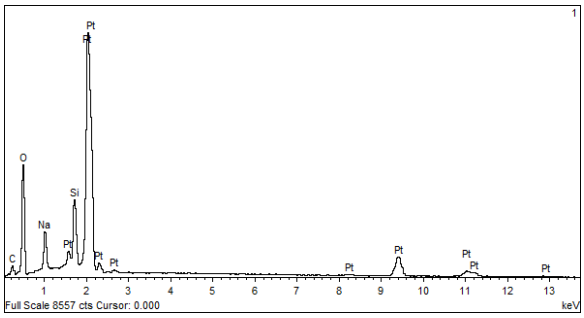
1
O
Na
Si
Pt
C
Full Scale 8557 cts Cursor: 0.000
keV

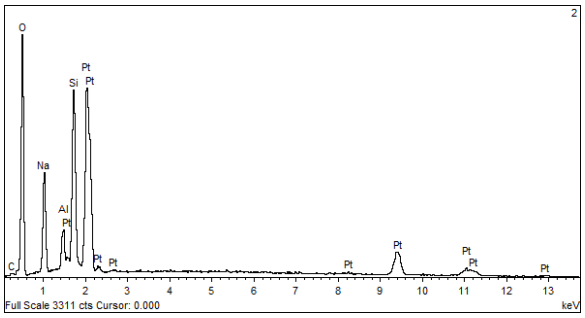
2
O
Na
Si
Al
Pt
C
Full Scale 3311 cts Cursor: 0.000
keV

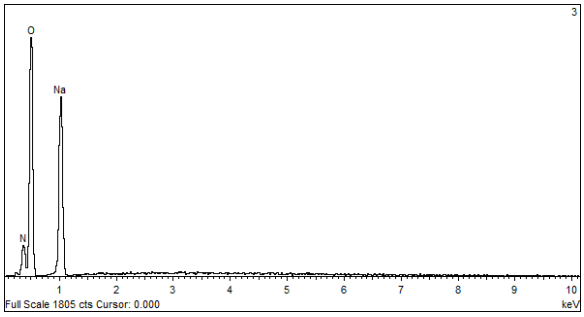
3
O
Na
Ni
Full Scale 1805 cts Cursor: 0.000
keV

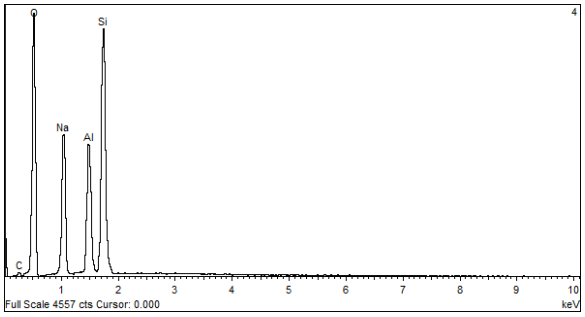
4
O
Si
Na
Al
C
Full Scale 4557 cts Cursor: 0.000
keV

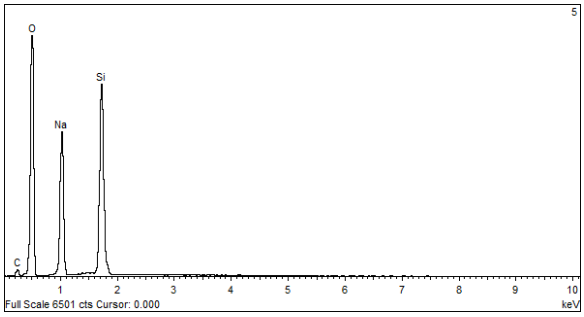
5
O
Na
Si
C
Full Scale 6501 cts Cursor: 0.000
keV

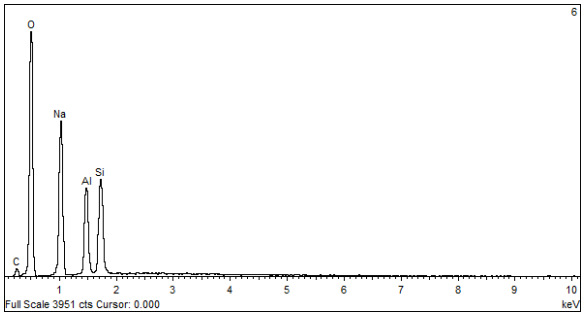
6
O
Na
Al
Si
C
Full Scale 3951 cts Cursor: 0.000
keV

**Figure B-11. SEM and XEDS of White Solids from the Kettle of HGR Simulant Test**

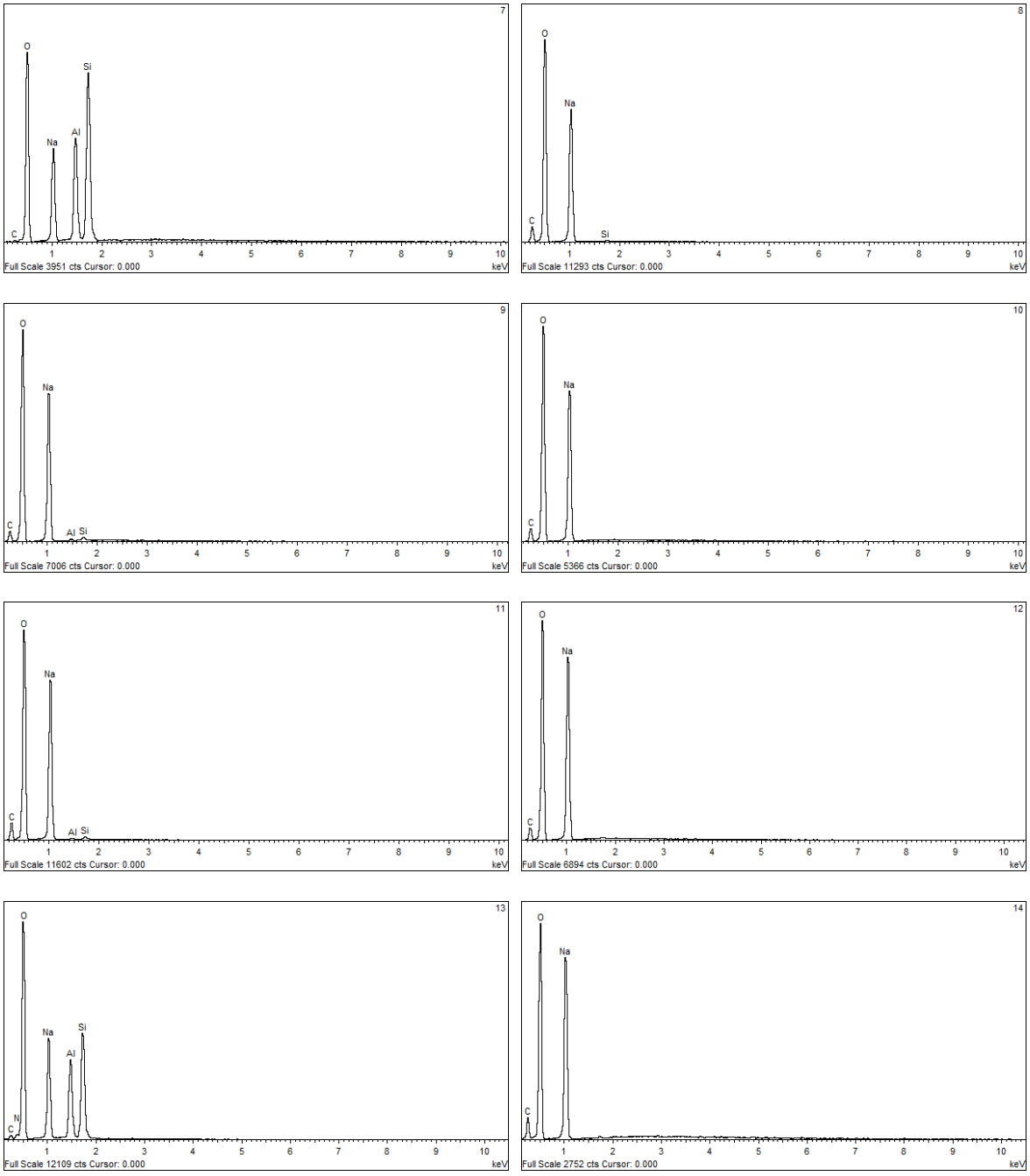

**Figure B-12. Additional XEDS for Figure B-11P**

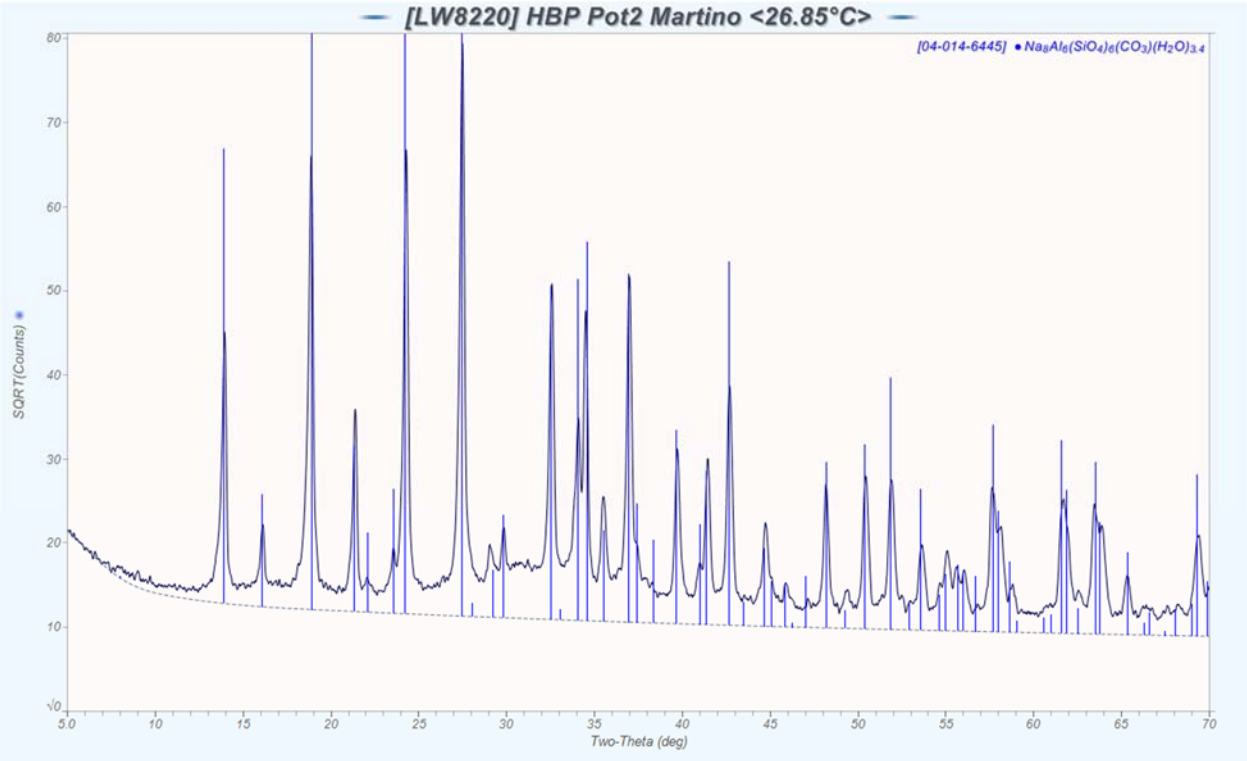


**Figure B-13. XRD of White Solids from the Kettle of HGR Simulant Test**

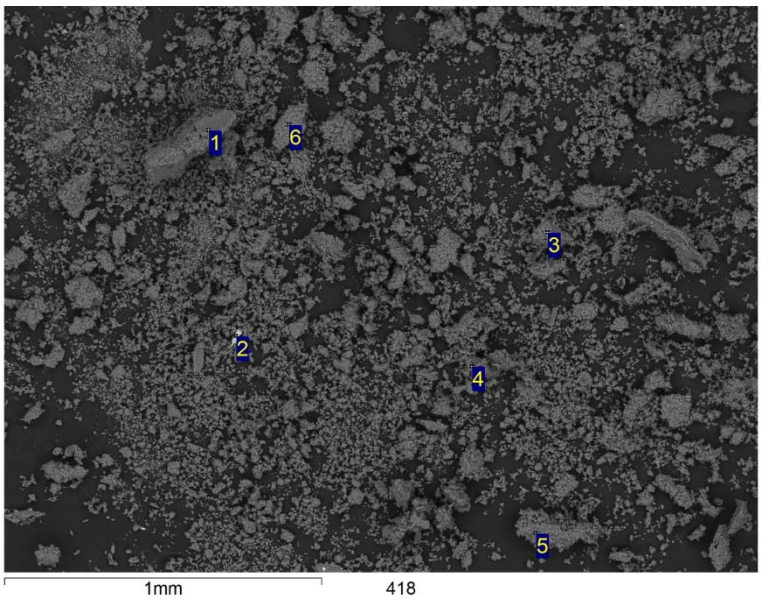
1
6
3
2
4
5
1mm
418

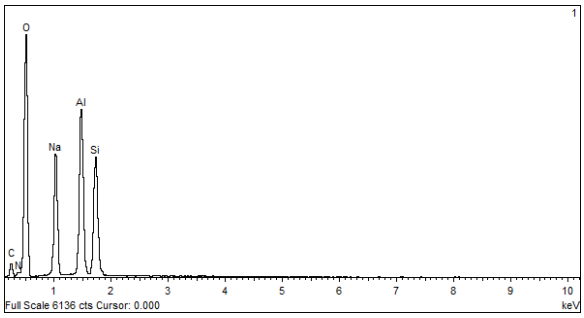
1
O
Na
Al
Si
C
N
Full Scale 6136 cts Cursor: 0.000
keV

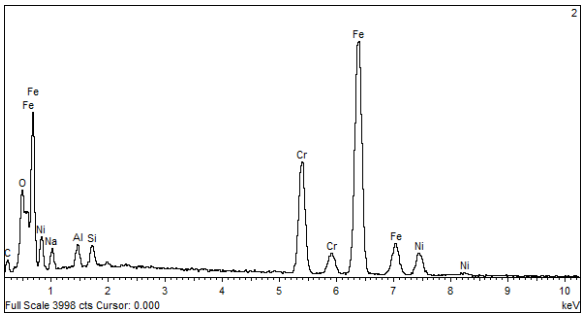
2
Fe
Fe
Fe
O
Cr
Ni
Na
Al
Si
C
Cr
Fe
Ni
Ni
Full Scale 3998 cts Cursor: 0.000
keV

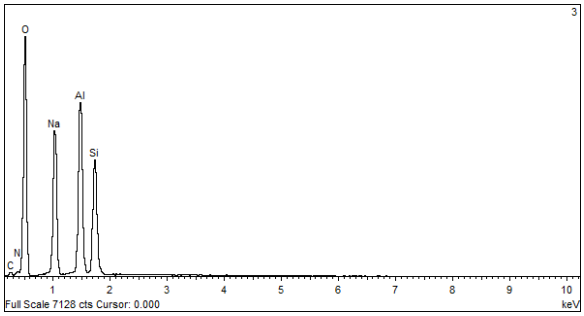
3
O
Na
Al
Si
N
C
Full Scale 7128 cts Cursor: 0.000
keV

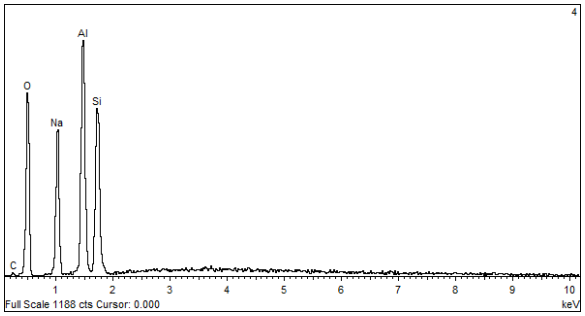
4
Al
O
Na
Si
C
Full Scale 1188 cts Cursor: 0.000
keV

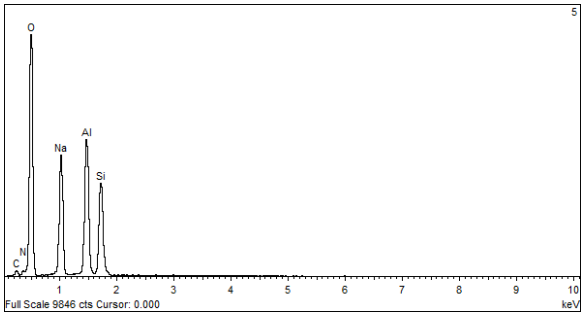
5
O
Na
Al
Si
N
C
Full Scale 9846 cts Cursor: 0.000
keV

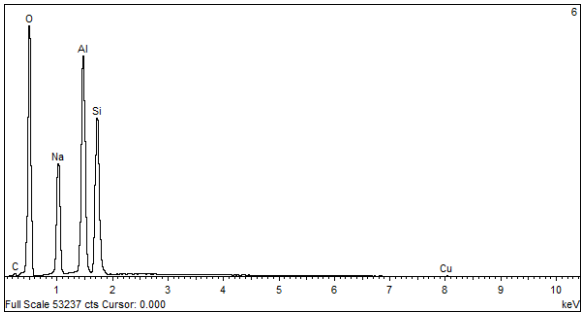
6
O
Al
Si
Na
C
Cu
Full Scale 53237 cts Cursor: 0.000
keV

**Figure B-14. SEM and XEDS of Solids on the Mixer from HGR Simulant Test**

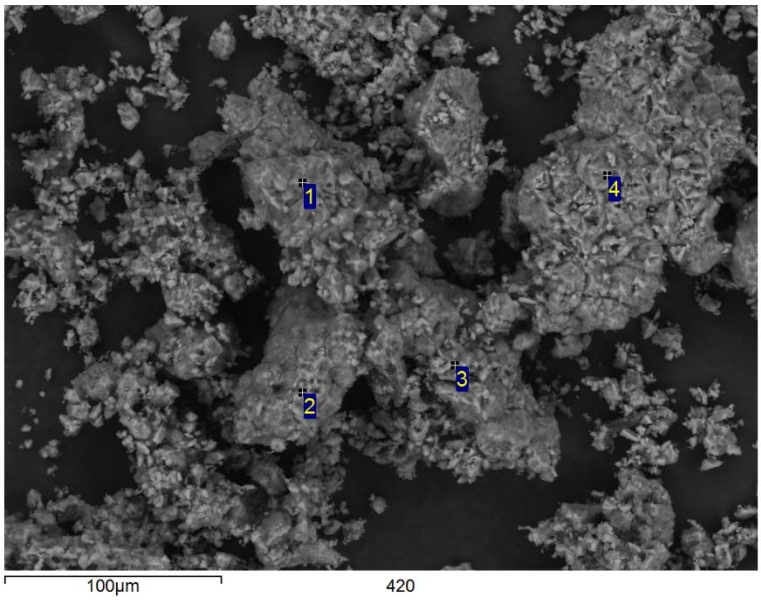


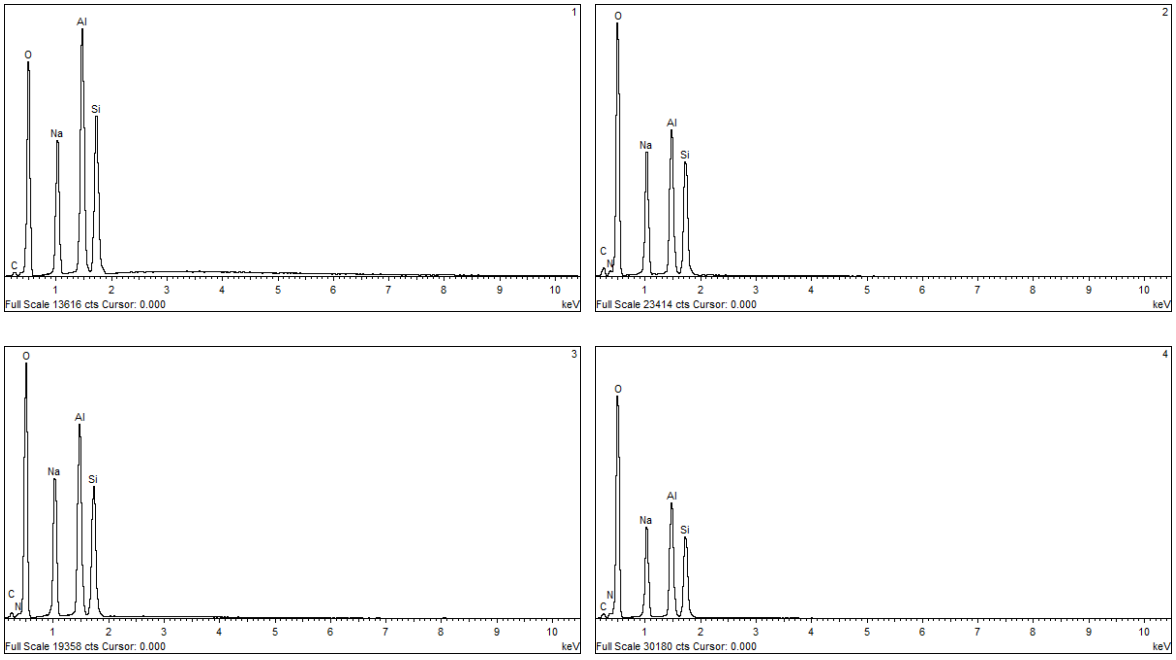


**Figure B-15. SEM and XEDS of Solids on the Mixer from HGR Simulant Test**

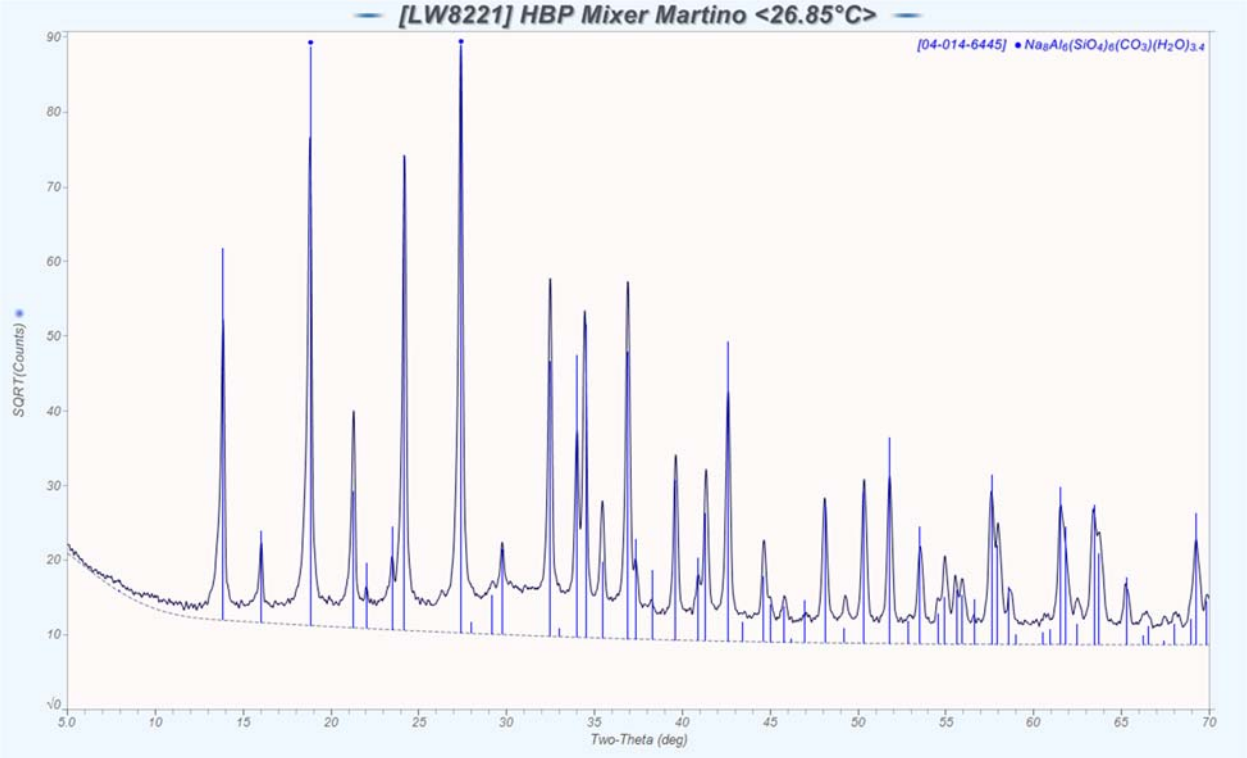


**Figure B-16. XRD of Solids on the Mixer from HGR Simulant Test**

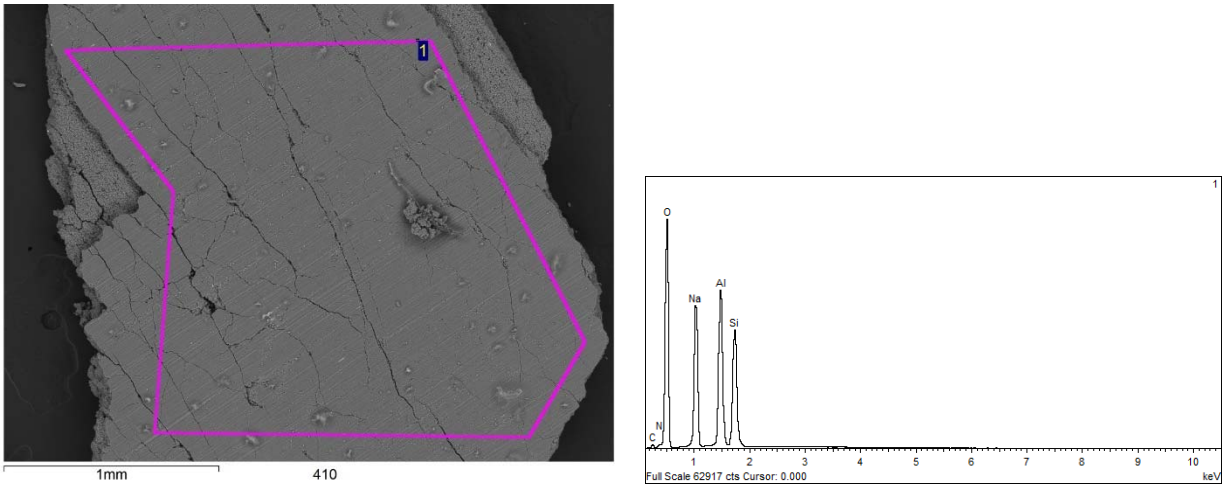


**Figure B-17. SEM and XEDS of Solids on the Heating Rods from HGR Simulant Test**

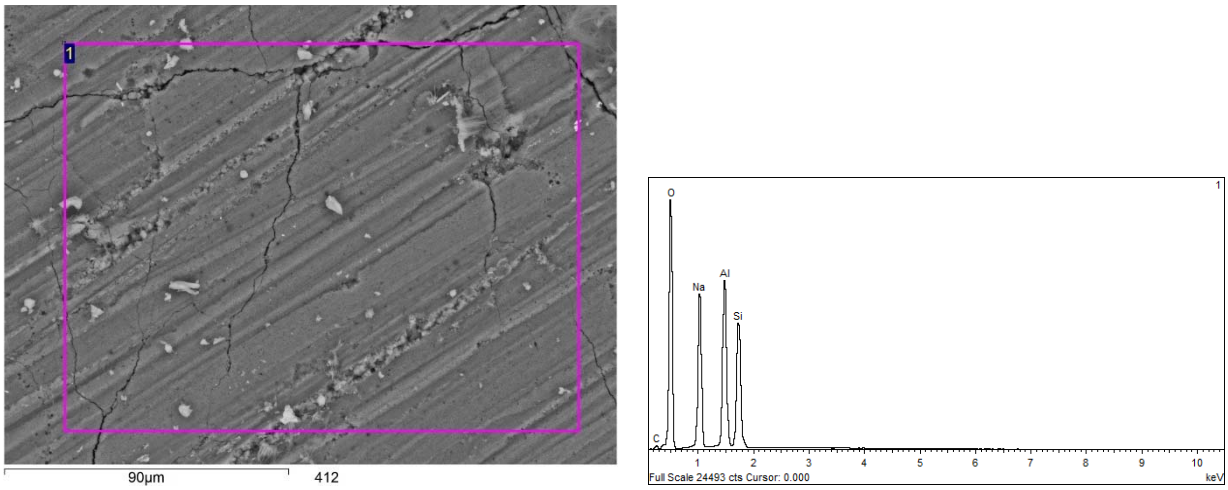


**Figure B-18. SEM and XEDS of Solids on the Heating Rods from HGR Simulant Test**

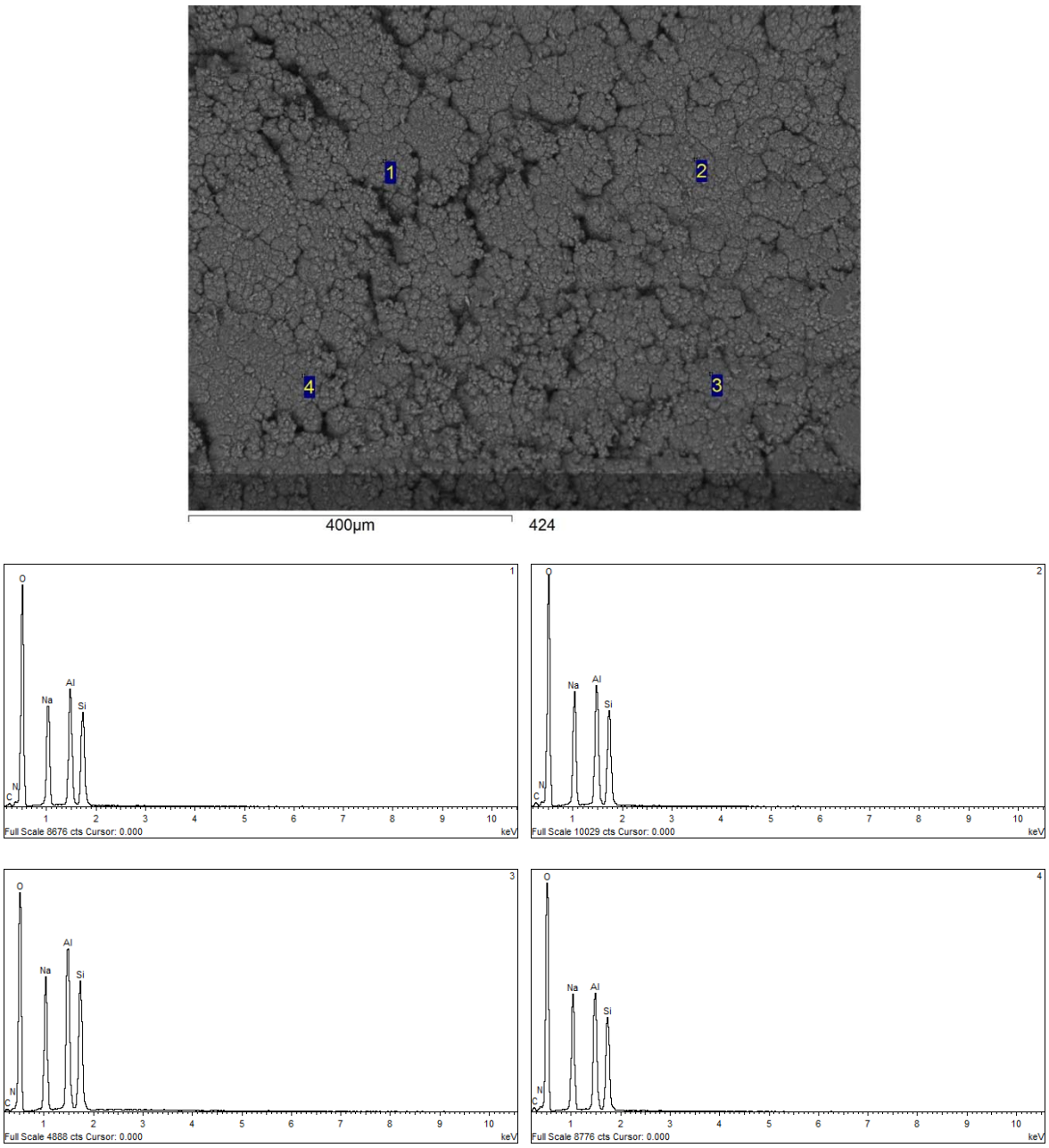


**Figure B-19. SEM and XEDS of Solids on the Heating Rods from HGR Simulant Test**

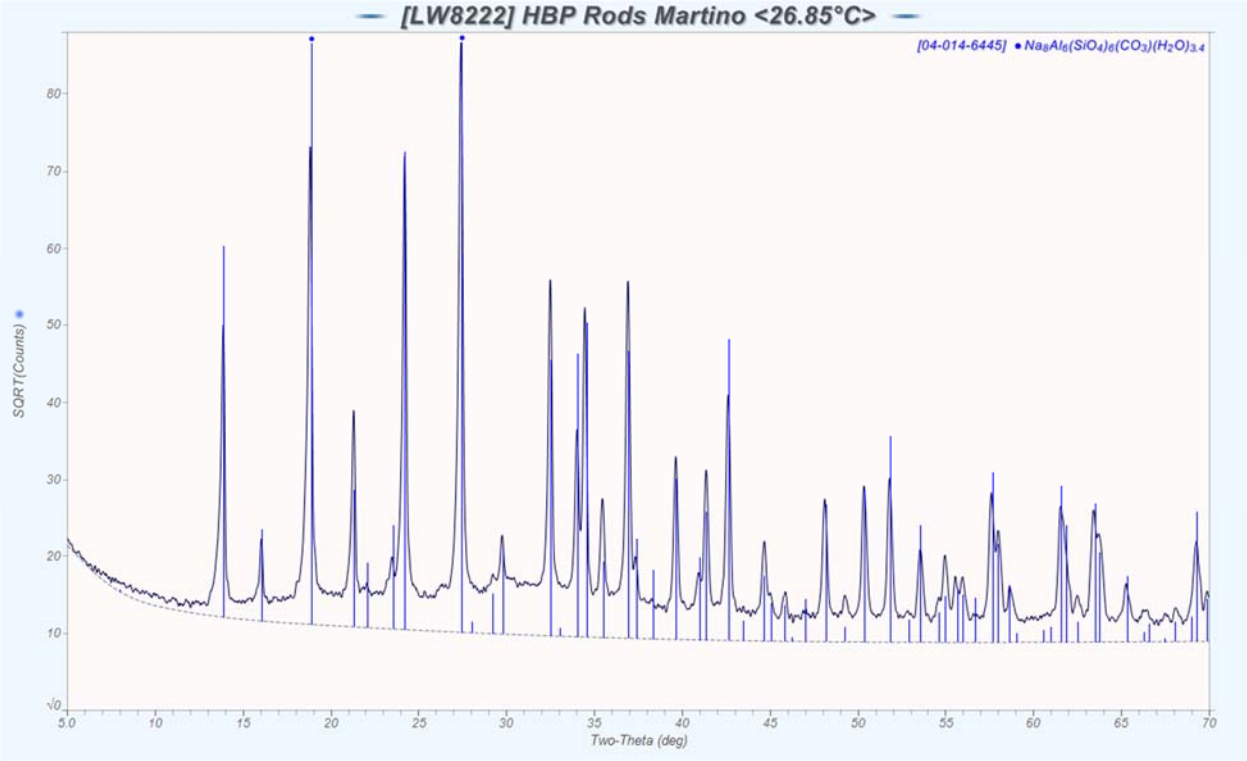


**Figure B-20. XRD of Solids on the Heating Rods from HGR Simulant Test**

**Distribution:**

timothy.brown@srnl.doe.gov
alex.cozzi@srnl.doe.gov
david.crowley@srnl.doe.gov
a.fellinger@srnl.doe.gov
samuel.fink@srnl.doe.gov
nancy.halverson@srnl.doe.gov
erich.hansen@srnl.doe.gov
connie.herman@srnl.doe.gov
john.mayer@srnl.doe.gov
daniel.mccabe@srnl.doe.gov
Gregg.Morgan@srnl.doe.gov
frank.pennebaker@srnl.doe.gov
Amy.Ramsey@srnl.doe.gov
William.Ramsey@SRNL.DOE.gov
luke.reid@srnl.doe.gov
geoffrey.smoland@srnl.doe.gov
michael.stone@srnl.doe.gov
Boyd.Wiedenman@srnl.doe.gov
bill.wilmarth@srnl.doe.gov
Records Administration (EDWS)
jeffrey.crenshaw@srs.gov
james.folk@srs.gov
roberto.gonzalez@srs.gov
tony.polk@srs.gov
patricia.suggs@srs.gov
Austin.Chandler@srs.gov
Kevin.Brotherton@srs.gov
eric.freed@srs.gov
Vijay.Jain@srs.gov
Victoria.Kmiec@srs.gov
kent.rosenberger@srs.gov
aaron.staub@srs.gov
steven.thomas@srs.gov
terri.fellinger@srs.gov
jeffrey.gillam@srs.gov
barbara.hamm@srs.gov
chris.martino@srnl.doe.gov
jeff.ray@srs.gov
paul.ryan@srs.gov
hasmukh.shah@srs.gov
celia.aponte@srs.gov
timothy.baughman@srs.gov
earl.brass@srs.gov
Richard.Edwards@srs.gov
Thomas.Huff@srs.gov
Ryan.McNew@srs.gov
phillip.norris@srs.gov
Christine.Ridgeway@srs.gov
Azadeh.Samadi-Dezfouli@srs.gov
Christie.sudduth@srs.gov
arthur.wiggins@srs.gov
thomas.colleran@srs.gov
bill.holtzscheiter@srs.gov
john.iaukea@srs.gov
Spencer.Isom@srs.gov
MARIA.RIOS-ARMSTRONG@SRS.GOV